Title
The Fisher Droplet Model and Physical Clusters at Liquid-Vapor Phase Coexistence with Implications for the Nuclear Phase Diagram

Author
Lake, Peter Theodore

Publication Date
2014

Peer reviewed|Thesis/dissertation

The Fisher Droplet Model and Physical Clusters at Liquid-Vapor Phase Coexistence with Implications for the Nuclear Phase Diagram

by

Peter Theodore Lake, Jr.

A dissertation submitted in partial satisfaction of the

requirements for the degree of

Doctor of Philosophy

in

Chemistry

in the

Graduate Division

of the

University of California, Berkeley

Committee in charge:

Professor Luciano G. Moretto, Chair
Professor Joseph Cerny
Professor Eric B. Norman

Fall 2014

The Fisher Droplet Model and Physical Clusters at Liquid-Vapor Phase Coexistence with Implications for the Nuclear Phase Diagram

Abstract

The Fisher Droplet Model and Physical Clusters at Liquid-Vapor Phase Coexistence with Implications for the Nuclear Phase Diagram

by

Peter Theodore Lake, Jr.

Doctor of Philosophy in Chemistry

University of California, Berkeley

Professor Luciano G. Moretto, Chair

The nuclear strong force, which binds the nucleons within an atomic nucleus, is a van der Waals force. A consequence of this is that the phenomenon of liquid-vapor phase coexistence occurs in the nuclear system. The experimental means of constructing the nuclear phase diagrams rely heavily on the thermodynamics of cluster theories, theories that historically have not served in many practical applications. In this thesis I explore the validity of the ideal cluster law and the Fisher droplet model in systems where the phase diagrams are known from traditional means.

For molecular fluids, I show that the phase coexistence of a wide variety of systems can be described using the Fisher theory. This study is closely related to the study of an extended principle of corresponding states. These considerations demonstrates the utility of the Fisher droplet model in describing liquid-vapor phase coexistence of van der Waals fluids.

For model systems, I show that the physical clusters of the Lennard-Jones model at coexistence can be used to construct the phase diagrams of the fluid. The connection between the physical clusters and the thermodynamic properties of the vapor are established using the ideal cluster law. Furthermore, the cluster concentrations are well described by the Fisher droplet model. These considerations lead to an alternative construction of the phase diagrams for the Lennard-Jones system.

The success of cluster theories to describe properties of liquid-vapor coexistence that are already well established demonstrates the validity of applying these concepts to construct the nuclear phase diagrams.

I dedicate this thesis to anyone that I have had the privilege to teach something new.
To understand a concept is a personal experience, but to share it is equally important.

Contents

List of Figures

List of Tables

Acknowledgments

Many people have made it possible for me to go from a first year graduate student with only the slightest idea of what would lie ahead to a graduate completing a doctoral thesis. I would like to acknowledge these people.

First, I thank Luciano Moretto. He gave me the opportunity to study a field of science I did not even consider before coming to Berkeley. Furthermore, my perspective of what science is has unquestionably been molded by our many conversations. I have learned much about many aspects of the human experience from his stories, not least of them being nuclear physics.

I also thank Larry Phair. I have relied on Larry in the past years for many facets of the graduate school experience including discussing the science of this thesis, the administration and bureaucracy of science, and life in general. No matter how many times I have darkened his doorway, he has greeted me with a smile and taken time to help me.

I thank Jim Elliott for always being interested in the science I was doing. His work on the Fisher droplet model definitely guided the work I have done here. I regret not being able to get his input for the final product of my work in the group.

The calculations I have performed in this work were done at the Building 88 Computing Center. I thank the entire group that maintained the computers, and specifically name Paul Ellison, Oliver Gothe, Nick Esker, and Joey McLaughlin. Even though the creation of this computing center may have been a thin veiled excuse to have a coffee and socialize in different people's offices, it also allowed me to do the work presented in this thesis.

An aspect of graduate student life I have come to appreciate are the student run practice qualifying examinations. I want to thank all who have invited me to their practice qual, especially the students of Year Awesome and the Nitsche group. It may seem that participating is a favor to the person taking the exam, but these experiences have allowed me to review basic concepts of chemistry and learn the new and exciting science that will become their own theses.

This work would not have been possible without Ellie Browne and her patience she has given me. For every doubt I have had, she has reassured me and has kept me focused.

Beyond the support I have been given to succeed in doing science, I also want to thank everyone who has made everyday life in Berkeley enjoyable. This includes every cup of coffee we talked over, every night in the library we did homework, every Thursday Indian food lunch we ate, every conversation we had when I came home to the apartment, every phone call we had from across the country, every beer we brewed, every board game we played, every softball game we played, every trip to the record store we took. I have cherished these moments and am grateful for the time we shared. You have made this work possible, also.

Chapter 1

Introduction

Recent studies of atomic nuclei have focused on describing the phase transition of nuclear matter, for example [Mor11; Ell13; Gro97; RW01; BR08]. The experiments performed to deduce the phase diagram of nuclear matter consist of accelerating a projectile nucleus to collide with a target nucleus. The resulting nuclear collision produces an excited nucleus that can be described as a hot liquid drop that lowers its energy by evaporating smaller nuclei. These emitted nuclei are physical clusters of neutrons and protons and are the primary measurement in studying thermal nuclear decay. This is in direct contrast to the experimentally accessible observables such as temperature, density, and pressure which are used to measure the phase diagrams of molecular systems. All the same, the phase diagram of nuclear matter can be constructed from these cluster yields.

A large amount of theoretical work has previously been done on cluster theories which not only describe a vapor but also lend insight to liquid-vapor phase coexistence, for example [MM40; Fis67b; Fis67a; Sat03]. The difference between an ideal gas and a real gas is the correlations found between the particles. An intuitive approach to account for this difference is to describe the short range correlations in the real vapor in terms of clusters. These theories proved not to be very practical to study molecular fluids since clusters in a molecular vapor are not readily observed but are crucial in studying the nuclear system.

This present work is a theoretical study to understand liquid-vapor phase coexistence in terms of physical clusters. These considerations demonstrate the validity of using cluster theories to construct the nuclear phase diagram. The three topics of nuclear systems, phase coexistence and cluster theories are first presented to give context to my contributions to the field.

1.1 Atomic Nuclei, Hot and Cold

1.1.1 Cold nuclei as liquid drops

Atomic nuclei are a dense collection of neutrons and protons in their ground state. The force holding these nucleons together is the nuclear strong force as opposed to the Coulomb force that holds molecules together. The structure of nuclei has proven to be relatively simple despite the complicated nature of the strong force. Ultimately, a nucleus is described as a charged, quantum, van der Waals liquid drop.

One piece of experimental evidence that nuclei are liquid drops comes from elastic scattering experiments. Elastic scattering of nuclei is well described as the scattering of two point charges until they come close enough to interact via the short-ranged strong force. This contact is accompanied with a dramatic decrease in the elastic cross section and gives a clear measure for the size of a nucleus. These experiments reveal that all stable nuclei are characterized by the relation

$$R_A = r_0 A^{1/3}, \tag{1.1}$$

where R_A is the nuclear radius, A is the mass number of the nucleus, and r_0 is a constant observed to be $r_0 \simeq 1.2$ fm [RG06]. This relation is consistent with all nuclei having a constant density and indicates that the strong force acts attractively at short distances between nucleons but creates an excluded volume at even smaller distances. Forces of this type are referred to as van der Waals forces and are analogous to the forces in molecular fluids.

The nuclear binding energies are further experimental evidence that nuclei are liquid drops. Weizsacker developed a semi-empirical equation to describe the binding energies B of all nuclei as a function of mass number A and atomic number Z [Wei35],

$$B(A,Z) = a_v A - a_s A^{2/3} - a_c \frac{Z^2}{A^{1/3}} - a_a \frac{(A-2Z)^2}{A} \pm \frac{\delta}{\sqrt{A}}. \tag{1.2}$$

Each of the five terms represent a different aspect of a nucleus as a finite, charged, quantum liquid drop. This equation is known as the liquid-drop model of nuclear binding energies.

The first two terms of Eq. 1.2 are part of the leptodermous expansion. The leptodermous expansion is the series expansion of the binding energy of a finite van der Waals liquid drop in inverse powers of the drop's radius,

$$B(R) = b_v R^3 + b_s R^2 \quad + b_r R \quad + \ldots \tag{1.3a}$$

$$B(A) = a_v A - a_s A^{2/3} - a_r A^{1/3} + \ldots, \tag{1.3b}$$

where the second relation comes from using Eq. 1.1. The first term is the volume term and is a property of the bulk liquid. The second term is the surface term and accounts for the lack of binding at the surface of a drop. The expansion continues onto higher order terms but historically is stopped at the second term for the nuclear case.

The third term in Eq. 1.2 is the named the Coulomb term and is equivalent to the self-energy E_c of a charged sphere,

$$E_c = -\frac{3}{5}\frac{Z^2e^2}{R} = -a_c\frac{Z^2}{A^{1/3}}, \tag{1.4}$$

where e is the fundamental charge. This prediction allows for an independent measure of the nuclear radius and is consistent with the elastic scattering experiments.

The last two terms of Eq. 1.2 are attributed to quantum effects. The fourth term is the asymmetry term and describes the tendency for nuclei to be more stable when symmetric in neutron and proton number. The last term is the pairing energy and accounts for the mass difference between even-even, odd-odd neutron-proton numbers, and odd-A systems.

Fitting the five coefficients to the experimental binding energies yields an equation that is accurate to 1%, or 10 MeV, for all nuclear masses [MS69; Kir08; RG06; Mor12]. This impressive feat emphasizes how a holistic approach to the complicated physics of the strong force is effective as opposed to starting from first principles. The errors are associated with shell structure and can be calculated via the Strutinski procedure to yield errors of 0.1% [Str67]. This concise physical picture of nuclei gives rise to a simple equation for the nuclear masses that has a precision unmatched by more "sophisticated" *ab initio* calculations [GCP09; RS04].

The data of nuclear radii and binding energies indicate that nuclear matter is a van der Waals liquid. Whatever the exact nature of the strong force may be, the net result is an internucleonic potential with a short-range attraction and a repulsive core.

1.1.2 Hot nuclei and thermal emission

Even though the nuclear radii and binding energies are aspects of nuclei in their ground states, the liquid drop nature also has implications in the physics of nuclei at high excitation energies.

Nuclear reactions are the experimental means of studying nuclei in excited states. These collisions consist of a wide range of energies including low energy direct reactions to higher energy compound nuclear reactions and multifragmentation. These latter two types of reactions are characterized by statistical means as opposed to studying the discrete states observed in lower energy reactions.

The difference between compound nuclear reactions and multifragmentation is the energy of the collision. Compound nuclear reactions involve the complete fusion of two nuclei into a highly excited system which subsequently decays. Multifragmentation occurs at higher energies and arises when the two nuclei fuse incompletely and then decay. The process does involve non-equilibrated decay, but the majority of the decay products are produced thermally.

Both processes emit particles stochastically and thermally despite their differences [Mor97]. The decay is stochastic in that the multiplicity of emitted intermediate mass fragments, fragments with proton number $Z > 5$, is described by a Poisson distribution. A binomial distri-

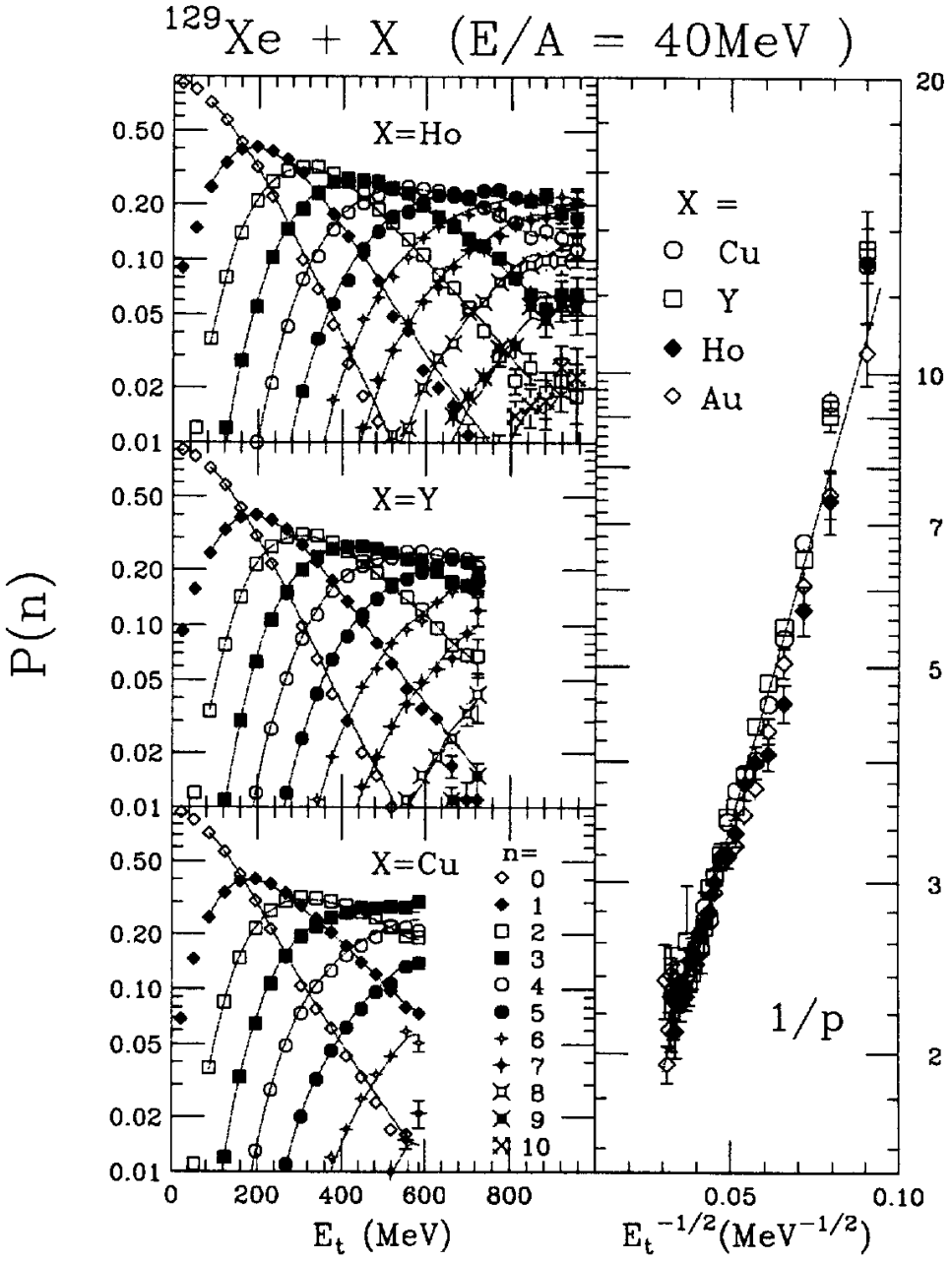

Figure 1.1: The yields of multifragmentation are stochastic and thermal. The plots to the left show the binomial probabilities of emitting a number of intermediate mass fragments, n. The plot on the right is an Arrhenius plot of the inverse single event probability of emitting an intermediate mass fragment as a function of inverse temperature. Adapted from [Mor97].

bution arises when the probability of an event is uncorrelated to the number of times it has happened before. The left panel of Fig. 1.1 plots the probability of the different multiplicities as a function of excitation energy. The lines are the resulting binomial distributions.

The process of particle emission is also thermal. A process is thermal when the probability p of an event is described by an Arrhenius relation

$$p \propto e^{-E^{\dagger}/T}, \tag{1.5}$$

where $E^{\dagger}$ is the activation energy and T is the temperature. The temperature of a collision can be approximated from the Fermi gas prediction that $T \propto \sqrt{E^*}$ for an excitation energy E^*. The right panel of Fig. 1.1 shows the extracted single particle emission probability as a function of $E^{-1/2}$ and shows a clear exponential trend. In this case, the transverse kinetic energy of the decay is used in lieu of the excitation energy, the two being proportional to one another in the case of thermal decay.

The following physical picture is invoked to describe these processes. The object created in a nuclear collision is a hot liquid drop of nucleons. The liquid quickly obtains a well defined temperature and undergoes evaporative cooling whereby small nuclei are emitted from the surface of the liquid.

The description of nuclear collisions decaying through evaporative cooling invokes a direct reference to liquid-vapor phase coexistence. A natural question arises: what is the phase diagram of nuclear matter? Also, how can it be constructed from experimental data? The remainder of this chapter addresses the concepts necessary to do this.

1.2 The Thermodynamics of Phase Coexistence

Liquid-vapor phase coexistence is a ubiquitous aspect of molecular systems, with the nature of the coexistence being similar throughout these systems. The nuclear system is anticipated to be a specific case of this general phenomenon due to the phenomenological similarity of the force between constituents.

1.2.1 The Gibbs phase rule and phase diagrams

Phase coexistence is the situation when a system spontaneously separates into two or more distinct phases and is explained by the Gibbs phase rule.

A generic chemical system can be described as having different components and being separated into different phases. A component is a chemical species that can be varied in quantity relative to the other components. For example, a mixture of ethanol and water is a two component system where the relative amount of the two chemicals can be varied. A phase is a homogeneous state of matter with distinct properties of other phases. Typical phases of matter are solid, liquid, and vapor. The symmetry of the solid makes it distinct from the liquid and vapor and the difference of densities make the liquid and vapor distinct.

Consider a system of C components in P different phases. Thermodynamic equilibrium arises when the entire system has a constant temperature T, the phases have an equal pressure p, and the components have the same chemical potential μ_i throughout all phases. This equivalence of the thermodynamic variables represents a system of equations to be solved simultaneously. The Gibbs phase rule counts the number of degrees of freedom F for this system of equations as

$$F = C - P + 2. \tag{1.6}$$

If $F \geq 0$ then the system is physically possible, otherwise the system of equations is over-specified and there is no solution. Furthermore, F represents the dimensionality of the phase coexistence within the total thermodynamic phase space of the system.

The top plot in Fig. 1.2 is a phase diagram of a typical single component system with solid s, liquid ℓ, and vapor v phases projected onto the pressure-temperature plane. The diagram demonstrates the results of the Gibbs phase rule whereby the lines are the location of two phase coexistence and the intersection of the three branches is the only point where the three phases can coexist.

An attribute of the phase diagram that is not predicted by the Gibbs phase rule is the termination of the liquid-vapor phase coexistence at a critical point. The presence of a critical point attests to the similarity of the liquid and vapor phases, which are collectively named a fluid. Whereas the difference between solid and fluid phases is well defined in terms of symmetry for all temperatures, the distinction between a liquid and vapor disappears above the critical point. Only below the critical point are the two phases distinguished by their differing densities.

Another useful projection of a phase diagram is onto the temperature-density plane as shown in the bottom plot of Fig. 1.2 for a typical system. Coexistence occurs in an area of the phase diagram in this projection as opposed to the line in the pressure-temperature projection. This feature arises from the fact that the relative amount of each phase is not specified in the system of equations dictating equilibrium. The pressure at a given temperature is constant within the region of coexistence and the amount of each phase varies continuously. The boundaries of the diagram are the densities of the respective phases in coexistence. The critical point is where the liquid and vapor densities are equal at coexistence and the labeling of the phases becomes ambiguous.

The Gibbs phase rule offers a means of understanding how phase coexistence can arise through the principles of thermodynamics. It also explains how phase coexistence for a one component system can be mapped in a two dimensional phase diagram. However, it does not reveal any quantitative measure of the coexistence for a specific system.

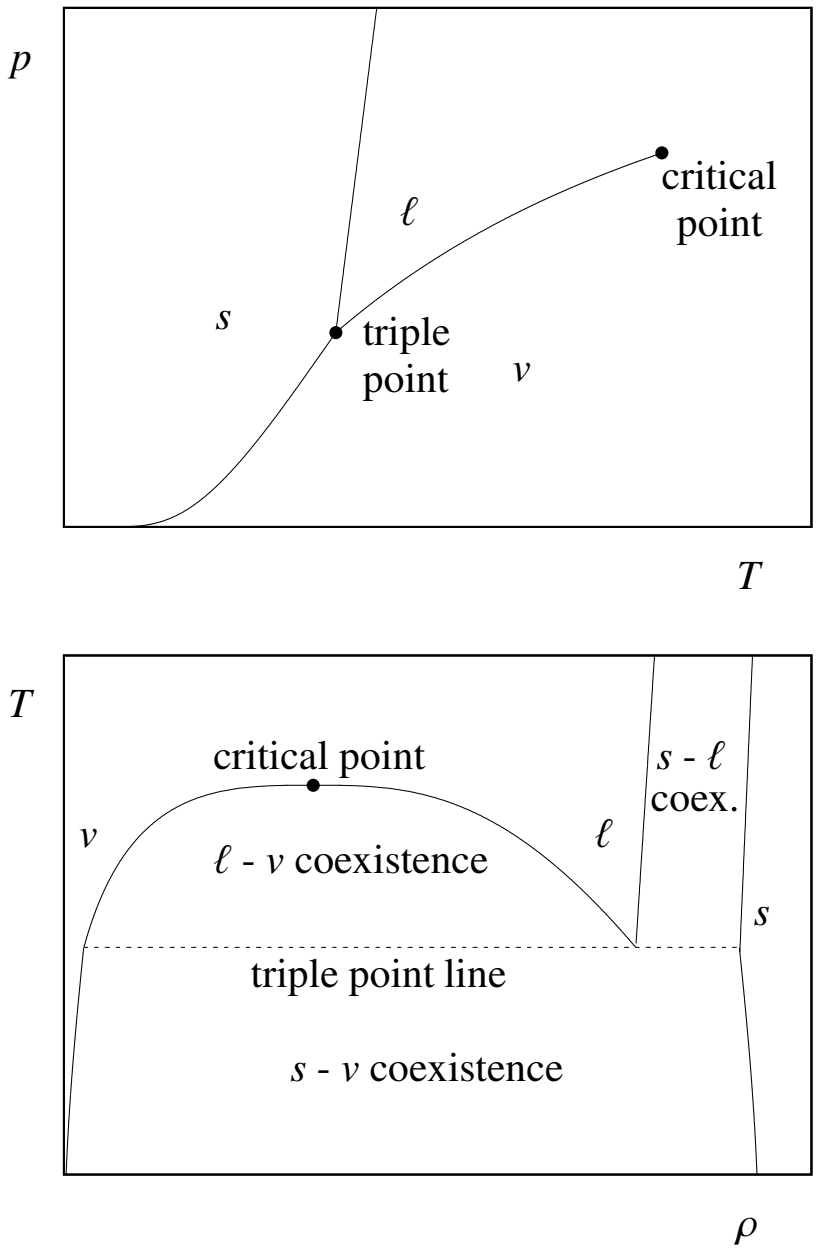

Figure 1.2: Typical phase diagrams of a molecular system which exhibits solid s, liquid ℓ, and vapor v phases. The top diagram is a pressure-temperature phase diagram and the bottom diagram is a temperature-density phase diagram.

1.2.2 The Clausius-Clapeyron relation

Another exact result of phase coexistence is the Clausius-Clapeyron relation. This relation evaluates the change in the coexistence pressure as the temperature is varied,

$$\left.\frac{dp}{dT}\right|_{coex} = \frac{\Delta H}{T\Delta v}, \tag{1.7}$$

where ΔH is the difference in enthalpy per particle between the two phases and Δv is for the difference in volume per particle. Notice how dp/dT is a total differential which attests to the fact that the coexistence is fully specified by one degree of freedom.

The Clausius-Clapeyron equation is applicable to any pair of phases in coexistence but can be exactly integrated with suitable approximations of the two phases. For example, liquid-vapor phase coexistence at low temperatures. The vapor can be considered ideal for sufficiently low densities and the liquid can be approximated as being incompressible and dense enough such that $\Delta v \simeq T/p$. It is also a fair approximation that ΔH is a constant at low temperatures. These approximations lead to an equation for the vapor pressure at coexistence as

$$p = p_0 e^{-\Delta H/T}, \tag{1.8}$$

with p_0 being a system dependent constant of integration.

A surprising aspect of experimental phase diagrams is the validity of Eq. 1.8 over the entire range of liquid-vapor coexistence despite the approximations used to derive this relation being unphysical near the critical point [Gug45; Gug93]. For example, the difference in volume per particle and difference in enthalpy per particle are both zero at the critical point. Regardless, the deviations from the approximations used to derive Eq. 1.8 are empirically seen to cancel one another to make the equation applicable all the way to the critical point.

Whereas the Gibbs phase rule explains the possibility of phase coexistence, the Clausius-Clapeyron equation describes the shape of the phase diagram. Making intuitive approximations for the two phases in coexistence allow for exact integration of the equation to deduce the nature of the coexistence pressure as a function of temperature. This process leads to a reliable expression in the case of liquid-vapor coexistence.

1.2.3 Principle of corresponding states

The equation of state is a complete relation for a pure system's thermodynamic state with the Gibbs phase rule dictating that it is a function of two variables. The thermodynamic functions of different systems are alike phenomenologically alike due to the similarity of the microscopic physics that give rise to the bulk properties. In fact, many equations of state for molecular systems can be scaled to one another when normalized into appropriate units. This is known as the principle of corresponding states.

Guggenheim and Pitzer formulated a series of rules which would make the principle of corresponding states rigorously exact [Pit39; Gug45; Gug93]. These rules suggest that if the only things that differ between molecular systems are the physical size of the molecules and

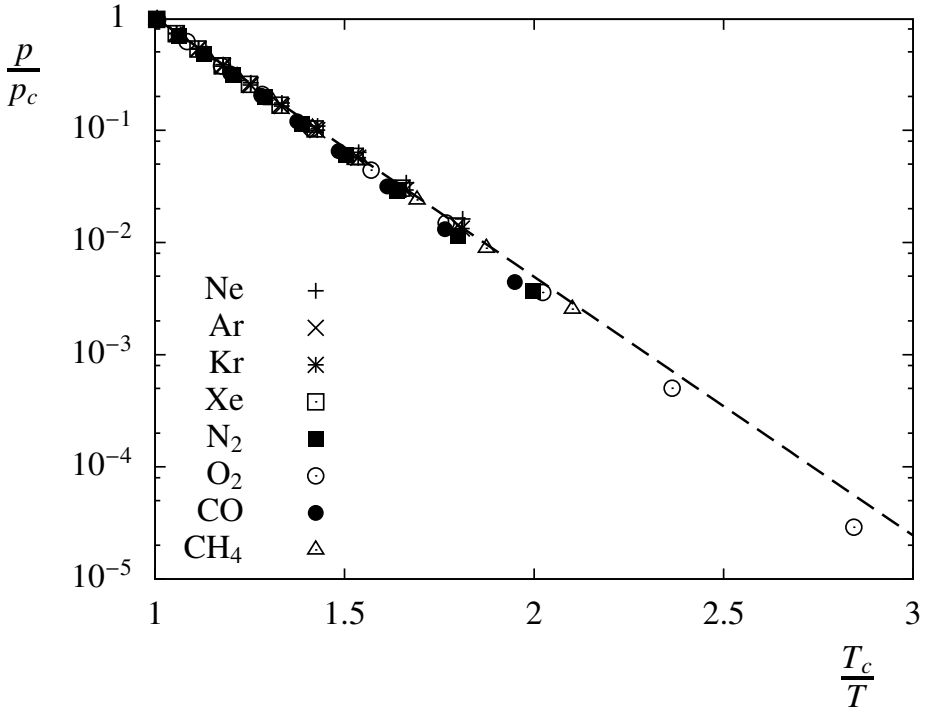

Figure 1.3: Scaling of pressure-temperature phase diagrams in reduced variables and the Guggenheim scaling.

the magnitude of binding then they can all be scaled to one another. The empirical observation of corresponding states in molecular systems indicates the accuracy or lack thereof of these statements.

Phase coexistence represents a subset of the equation of state of a system. Thus, comparing phase diagrams of different systems allows for testing for corresponding states. Furthermore, the uniqueness of the critical point of the liquid-vapor coexistence makes it a good reference point to which different systems can be scaled. The thermodynamic variables divided by their value at the critical point are referred to as reduced variables.

Guggenheim compared the liquid-vapor phase diagrams of Ne, Ar, Kr, Xe, N_2, O_2, CO, and CH_4 to demonstrate the principle of corresponding states [Gug45; Gug93]. For example, Fig. 1.3 displays the reduced pressure-temperature phase diagrams of these eight systems. The results of the Clausius-Clapeyron equation are immediately seen in the linear trend of the data sets. Eq. 1.8 predicts the coexistence pressures to be

$$\frac{p}{p_c} = \exp\left[-\frac{\Delta H}{T_c}\left(\frac{T_c}{T} - 1\right)\right]. \tag{1.9}$$

The fact that all eight data sets fall on the same line suggests that $\Delta H/T_c$ is a constant for all these systems and has the numerical value of $\Delta H/T_c \simeq 5.21$.

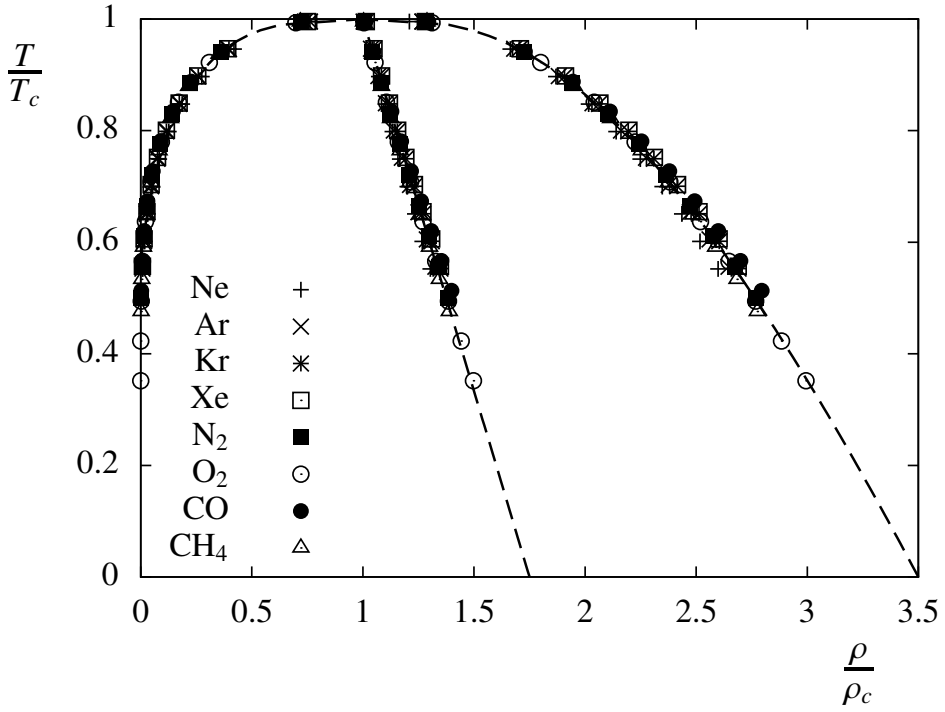

Figure 1.4: Scaling of temperature-density phase diagrams in reduced variables and the Guggenheim scaling.

The temperature-density phase diagram is also used to demonstrate the principle of corresponding states. Fig. 1.4 shows the phase diagrams in reduced units of density and temperature of the same eight systems as in Fig. 1.3. The average of the liquid and vapor densities are also shown and follow a linear trend. Without having a theory that anticipates the shape of the phase diagram in this representation, Guggenheim suggests the following empirical equation [Gug45; Gug93]

$$\frac{\rho_{\ell,v}}{\rho_c} = 1 + b_1 \left(1 - \frac{T}{T_c}\right) \pm b_\beta \left(1 - \frac{T}{T_c}\right)^\beta . \tag{1.10}$$

The upper sign describes the liquid density and the bottom is for the vapor. The phase diagrams of the eight systems considered are well described when the values $\beta = 1/3$, $b_1 = 3/4$, and $b_\beta = 7/4$ are used.

These eight systems were chosen because they are expected to follow the criteria proposed for the principle of corresponding states and as a result the scaling between the systems is good, but many molecular systems are expected to differ from these eight. Fig. 1.5 shows the phase diagrams in reduced units of 73 different molecular fluids whose data are reported in the NIST Chemistry WebBook [LMF11]. A list of the molecules considered is found in

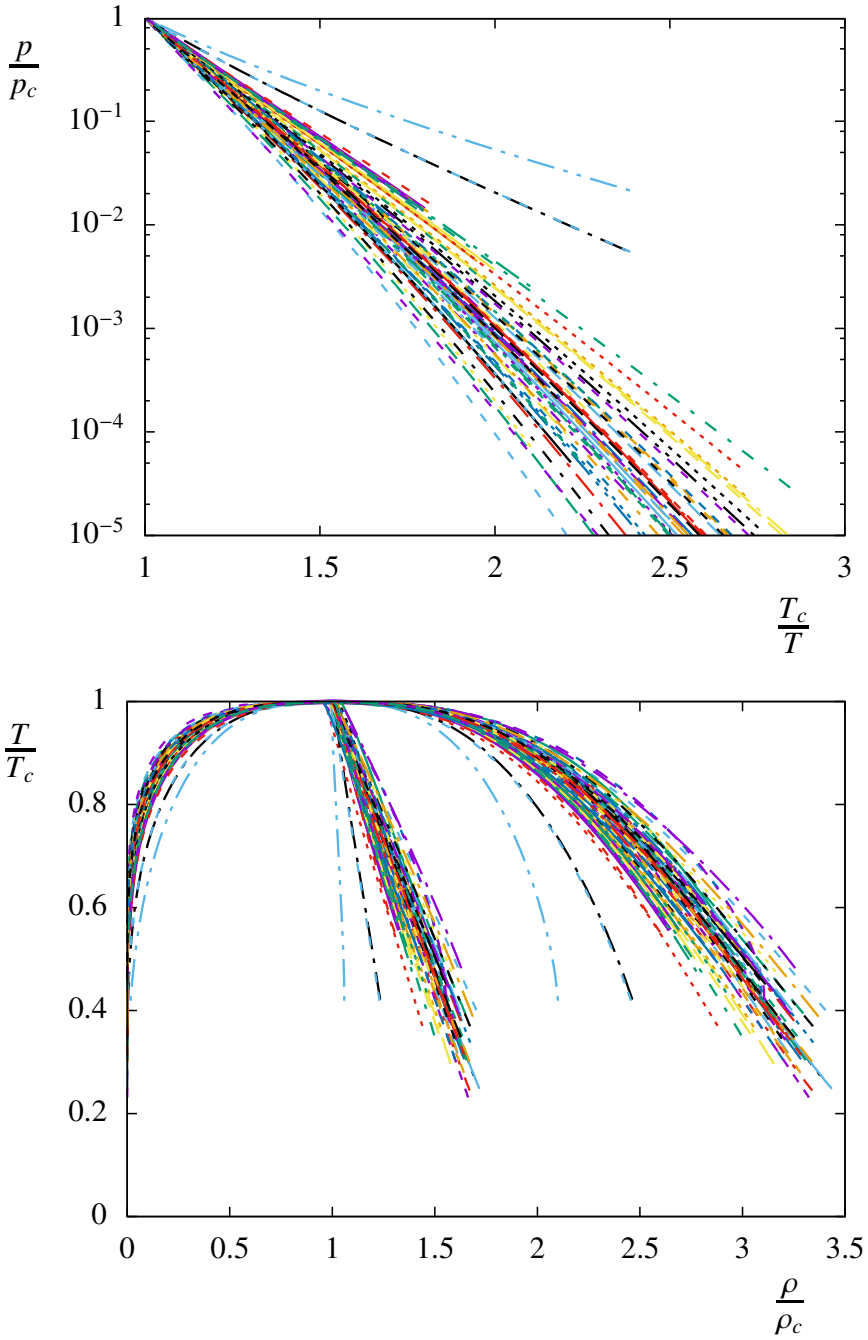

Figure 1.5: The same scaling of the phase diagrams as found in Fig. 1.3 and Fig. 1.4 but with a wider selection of systems.

Appendix 1. Even though the deviations are obvious, they are systematic. A goal of this work is to understand these deviations and find a theory which describes all these systems simultaneously.

1.3 Cluster Theories

The previous section describes what can be anticipated about some aspects of the nuclear phase diagram. For example, the shape of the nuclear phase diagram can be predicted solely on the basis of the Clausius-Clapeyron equation, where the ΔH at low temperatures for nuclear matter is the volume energy coefficient a_v. Also, the principle of corresponding states suggest that the phase diagram is related to those of molecular systems. What these considerations do not tell is the location of the critical point. An experimental determination of the critical point is necessary to complete the phase diagram.

The difficulty is that nuclear matter is not studied the same way as molecular systems. A typical molecular fluid is studied experimentally in the bulk. A phase diagram of a substance is measured by controlling the temperature of a system and measuring the vapor pressure and densities of the two phases at coexistence. There is no such thing as bulk nuclear matter, making a traditional measurement of the phase diagram impossible. Cluster theories provide a novel approach to extract the nuclear phase diagram from nuclear reaction experiments.

The van der Waals force between molecules give rise to short-range correlations in a vapor. These correlations can be understood by considering particles in proximity of each other as being in a cluster. The entire set of particles in a vapor are partitioned thus into clusters. These clusters are ephemeral and are created and destroyed continuously as the system evolves. This definition of clusters is also ambiguous in that the concept of "proximity" is ill-defined. Regardless, the idea is that the observed bulk thermodynamics, including liquid-vapor phase coexistence, can be described in terms of clusters via the physical cluster theory. Below is a description of the physical cluster theory and of different ways that cluster concentrations have been approximated.

1.3.1 Physical clusters

The physical cluster theory considers a vapor to be composed of independent clusters [Sat03]. Clusters may change in size as the system evolves but static equilibrium cluster concentrations are established. A cluster has internal degrees of freedom that are characterized by an energy and an entropy. A cluster partition function q_A is defined for each cluster of size A,

$$q_A = \int g_A(E) e^{-E/T} dE, \tag{1.11}$$

where $g_A(E)$ is the cluster degeneracy of energy E.

The following thermodynamics of the physical clusters are found. Clusters of size A have a chemical potential μ_A and thermodynamic equilibrium gives rise to

$$\mu_A = A\,\mu_1 \equiv A\,\mu. \tag{1.12}$$

The concentration n_A of clusters is

$$n_A = q_A\, e^{A\mu/T} \tag{1.13}$$

Furthermore, the independent nature of these clusters gives rise to a pressure and density of

$$p = T\sum q_A\, e^{A\mu/T} = T\sum n_A \tag{1.14a}$$

$$\rho = \sum A\, q_A\, e^{A\mu/T} = \sum A\, n_A. \tag{1.14b}$$

These equations are named the ideal cluster laws since each cluster size imparts its partial pressure and density independently to the thermodynamics properties.

The physical cluster theory connects the observed clusters to the thermodynamic properties of a system. No description of the clusters is actually given in the theory except for the cluster partition functions q_A, which contain all the information about the clusters and is left as an abstraction. An appropriate approximation of the q_A would provide a means of calculating the equation of state of a vapor in terms of clusters.

1.3.2 The Bilj-Band-Frenkel cluster model

The first theory to approximate the cluster partition function was developed independently by Bilj, Band, and Frenkel [Bij38; Ban39a; Ban39b; Fre39b; Fre39a]. In this theory it is proposed that the clusters are limited in possible shapes and are all spherical. This approximation has two consequences. One is that the entropy of clusters of all sizes is virtually zero. The other consequence is that the energy of the clusters can be approximated with the leptodermous expansion,

$$E_A \simeq -a_v A + a_s A^{2/3}, \tag{1.15}$$

where the coefficients a_v and a_s are temperature dependent.

The resulting cluster partition functions and concentrations are

$$q_A = \exp\left[-\frac{E_A - T\,S_A}{T}\right] = \exp\left[\frac{a_v}{T}A - \frac{a_s}{T}A^{2/3}\right], \tag{1.16a}$$

$$n_A = \exp\left[\frac{a_v + \mu}{T}A - \frac{a_s}{T}A^{2/3}\right]. \tag{1.16b}$$

The equation for cluster concentration explicitly demonstrates how condensation occurs at some limiting chemical potential. When the chemical potential is below a value of $-a_v$ then

the cluster concentrations are asymptotically zero for large clusters. Above the coexistence chemical potential, the term linear in A causes the cluster concentrations to diverge.

The Bilj, Band, Frenkel model of clusters can in principle be used to generate a phase diagram. This is done by combining Eq. 1.16b at a chemical potential of $\mu = -a_v$ with Eq. 1.14. This theory does not predict a critical point nor the temperature dependence of a_s and thus a knowledge of a_s for all temperatures would be needed to construct the phase diagram.

1.3.3 The Fisher droplet model

An extension in approximating the physical cluster concentrations is to add a term for the cluster entropy and was first suggested by Fisher [Fis67b; Fis67a]. The approximation he uses for the entropy is done in such a way to produce an equation consistent with critical scaling.

Fisher writes the leptodermous expansion as

$$E_A = -a_v A + c_0 A^\sigma. \tag{1.17}$$

The term A^σ is proportional to the surface area of a cluster as a function of cluster size and is expected to be 2/3 but is left unspecified in the theory.

In this theory, the entropy of a drop S_A has a similar leptodermous expansion in addition to a logarithmic term,

$$S_A = b_v A + b_s A^\sigma - \tau \ln A + \ln q_0. \tag{1.18}$$

The leptodermous expansion is appropriate because the bulk liquid has a constant entropy per particle b_v and the surface adds more entropy due to the many possible configurations of the surface. The logarithmic term is added to make the theory consistent with known critical scaling.

From this formulation of the cluster energy and entropy, the cluster concentrations are

$$n_A = q_0 A^{-\tau} \exp\left[\left(\frac{\mu + a_v}{T} + b_v\right) A - \left(\frac{c_0}{T} - b_s\right) A^\sigma\right]. \tag{1.19}$$

This equation exhibits the same phenomenon of condensation as the Bilj, Band, Frenkel theory when the chemical potential is $\mu = -a_v - b_v T$, but also predicts the critical point. The cluster concentrations at the coexistence chemical potential are

$$n_A = q_0 A^{-\tau} \exp\left[-\left(\frac{c_0}{T} - b_s\right) A^\sigma\right]. \tag{1.20}$$

When the temperature is larger than c_0/b_s the cluster concentration diverge and there is no coexistence. This limiting value of temperature is distinguished as the critical point. The cluster concentrations are then rewritten in terms of the critical temperature T_c as

$$n_A = q_0 A^{-\tau} \exp\left[-c_0 A^\sigma \left(\frac{1}{T} - \frac{1}{T_c}\right)\right]. \tag{1.21}$$

The constants σ and τ are critical exponents and relate to the cluster size distribution at the critical point. The values of these two exponents fully specify the critical scaling of all other aspects of the system through the concept of hyperscaling. In this way the Fisher droplet model is consistent with the modern concept of critical phenomenon when $\sigma = 0.6395(4)$ and $\tau = 2.2088(2)$ [Cam02; PV02].

A different approach to the Fisher droplet model is that it can be used to generate a phase diagram based on measurements of clusters. The observed cluster concentrations in a vapor at coexistence can be used to predict T_c of a system. Furthermore, the ideal cluster law can be used to calculate the pressure and density of the system over the whole range of coexistence. The possibility that the theory can be used as a predictive theory was previously not recognized and becomes relevant in reference to the nuclear phase diagram.

1.4 The Nuclear Phase Diagram

The observation of thermal emission in nuclear collisions combined with the Fisher droplet model gives a means of generating a nuclear phase diagram [MEP05]. The Arrhenius behavior of nuclear yields is consistent with thermal emission and the Fisher droplet model. Furthermore, the Fisher droplet model predicts that the relative magnitude of different mass fragments are directly related to the critical temperature. Using the ideal cluster law then allows for calculation of the entire liquid-vapor phase diagram of the nuclear system.

This analysis is not without caveats. First, the system for which we want the phase diagram must be specified. The system we are interested in is bulk, uncharged, symmetric nuclear matter. Seeing that nuclei are finite, charged, and not necessarily symmetric, each of these aspects must be considered in turn.

The current study considers nuclear matter in its most stable composition of equal neutron and proton content. There is no physical restriction making it a necessity to study only symmetric nuclear material. The problem is simplified by only considering symmetric nuclear matter because the system can be treated as a single component system. Recalling the Gibbs phase rule, leaving the proton and neutron numbers free to vary would create a more complicated phase diagram.

The Coulomb force in nuclei is accounted for in two ways [MEP03]. First, the liquid drop model accounts for the Coulomb force felt within both the source and the emitted cluster. Second, the Coulomb force felt between clusters is considered. This term is what makes describing the thermodynamics of charged particles inherently difficult. The approximation made here is that only the Coulomb barrier of the cluster at the surface of the hot source is important and is approximated as the energy of two touching spheres. Once emitted, a cluster travels in the vacuum and does not influence the system further. In these ways the Coulomb force is seen to be a perturbation to the strong force in which we are ultimately interested.

Finite size corrections are due to the need of a larger vapor pressure for a liquid drop to be in coexistence compared to the bulk coexistence pressure [RW82]. To see this, consider

the Clausius-Clapeyron equation for the case of a liquid drop of size A_0,

$$\left.\frac{dp}{dT}\right|_{coex} = \frac{\Delta H(A_0)}{T\,\Delta V}. \tag{1.22}$$

The ΔH is different from the bulk value since the binding energy of the liquid drop changes when a particle is emitted. Using the leptodermous expansion and the fact that a monomer has zero binding energy

$$\Delta H(A_0) \simeq \Delta E(A_0) = -a_v(A_0-1) + a_s(A_0-1)^{2/3} + a_v A_0 + a_s A_0^{2/3}, \tag{1.23a}$$

$$\simeq a_v - \frac{2}{3} a_s A_0^{-1/3}. \tag{1.23b}$$

Recall that a_v is a property of the bulk system and is equivalent to the ΔH of the bulk system. Integrating the Clausius-Clapeyron equation with this value of ΔH yields

$$p(A_0) = p_\infty \exp\left[\frac{2a_s(T)}{3TA_0^{1/3}}\right], \tag{1.24}$$

where p_∞ is the coexistence vapor pressure in the bulk. This equation is known as the Kelvin equation, albeit in terms of $A_0^{1/3}$ as opposed to the typical presentation as a function of the radius R of the drop.

Notice how the derivation of Eq. 1.24 is the approximation for the case that the vapor is ideal. The complement correction is a consistent way of finding the finite size correction for clusters of any size [Mor05]. Consider the change in free energy between a liquid drop and a residual liquid drop with a small cluster. The Fisher droplet model suggests that the change in energy and entropy are

$$\Delta E = c_0\left[A^\sigma + (A_0-A)^\sigma - A_0^\sigma\right], \tag{1.25a}$$

$$\Delta S = \frac{c_0}{T_c}\left[A^\sigma + (A_0-A)^\sigma - A_0^\sigma\right] - \tau\log\left[\frac{A(A_0-A)}{A_0}\right] + \log(q_0). \tag{1.25b}$$

The cluster concentrations for the saturated vapor of a liquid drop is predicted to be

$$n_A = q_0\left(\frac{A(A_0-A}{A_0}\right)^{-\tau}\exp\left[-c_0\left(A^\sigma + (A_0-A)^\sigma - A_0^\sigma\right)\left(\frac{1}{T}-\frac{1}{T_c}\right)\right], \tag{1.26a}$$

$$\simeq n_{A\infty}\exp\left[\frac{\sigma c_0 A}{A_0^{1-\sigma}}\left(\frac{1}{T}-\frac{1}{T_c}\right)\right], \tag{1.26b}$$

where $n_{A\infty}$ is the cluster concentration in bulk coexistence. The second equation is a Taylor expansion of the first and is in a form analogous to Eq. 1.24.

The exact details of the analysis of the nuclear data are presented elsewhere [Mor11; Ell13]. The corrections due to the Coulomb force and the finite size effects are just two examples of how the physical system differs from the bulk properties we are interested in.

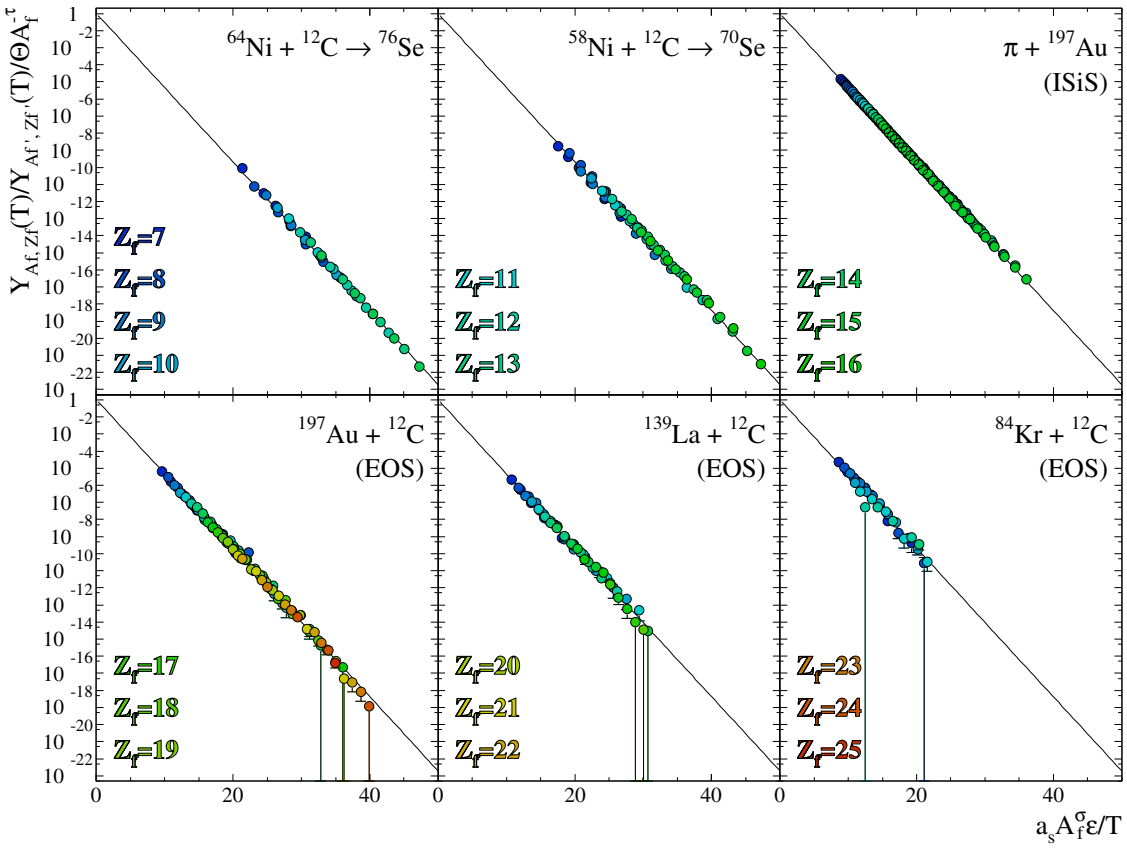

Figure 1.6: The scaled isotopic yields from nuclear collisions. Adapted from [Ell13].

Fig. 1.6 shows the experimental yields of the different masses scaled together from different experiments. The collapse of the data to a single line shows the validity of the Fisher droplet model. The extracted critical temperature from the fit to each of the experiments consistently yields a value of 17.9±0.4 MeV.

The construction of the phase diagram as a function of the reduced variables is accomplished by using the fit parameters and the ideal cluster law. The phase diagram in absolute units requires finding a suitable value of q_0 in the Fisher model. The absolute measure of the coexistence densities are pressures are found through a combination of Guggenheim scaling of the coexistence densities and the known density of ground state nuclei. Guggenheim scaling suggests that the liquid and vapor coexistence densities are related as

$$\rho_{\ell,v} = 1 + b_1 \left(1 - \frac{T}{T_c}\right) \pm b_\beta \left(1 - \frac{T}{T_c}\right)^{\beta}, \tag{1.27}$$

where the upper sign is for the liquid phase and the bottom sign is for the vapor. The reduced vapor density predicted from the Fisher droplet model can be used to determine b_1

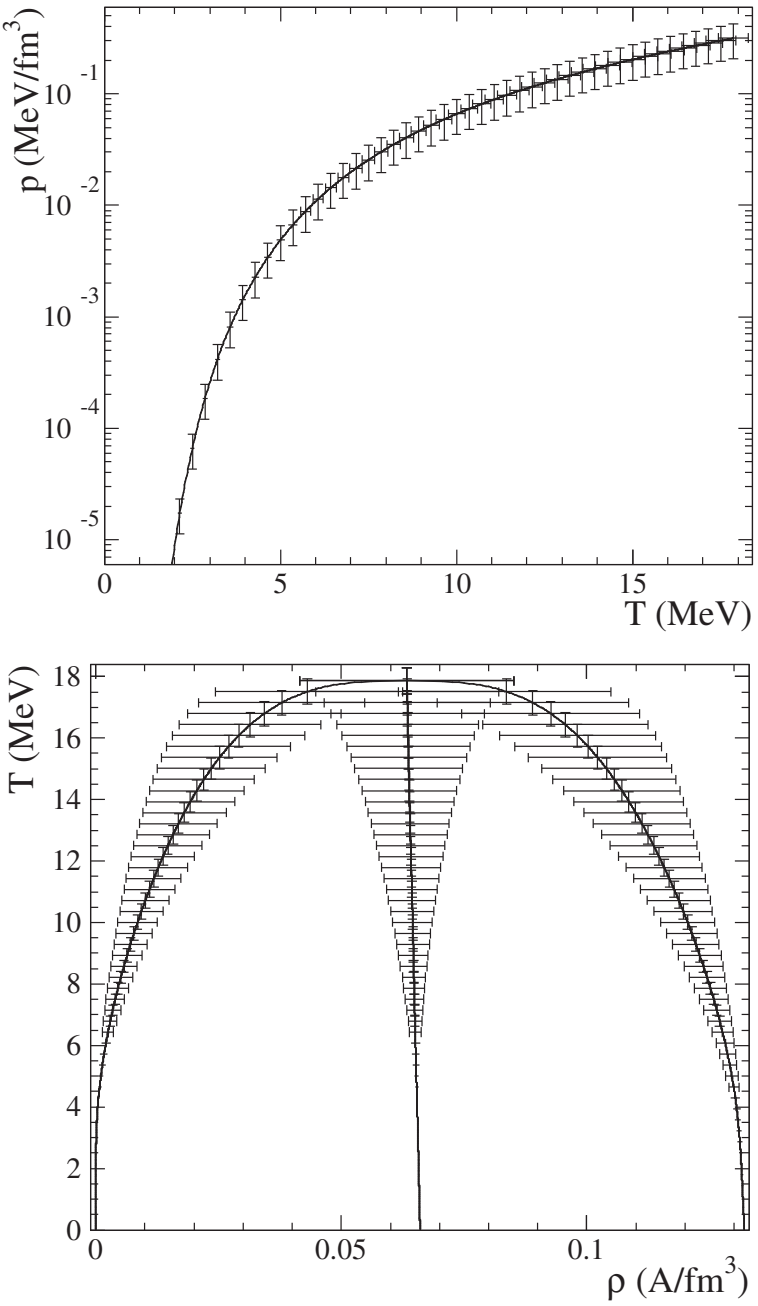

Figure 1.7: The experimental phase diagrams of nuclear matter in absolute units. Adapted from [Ell13].

and b_β. The liquid density is predicted to be

$$\rho_\ell/\rho_c = \rho_v/\rho_c + 2b_\beta \left(1 - \frac{T}{T_c}\right)^\beta . \tag{1.28}$$

The absolute phase diagrams are found by scaling the liquid density at zero temperature to the known value from ground state nuclei.

The phase diagrams of bulk nuclear matter are shown in Fig. 1.7. These plots are the first experimental phase diagrams of nuclear matter. Whereas the liquid drop model describes nuclei in their ground states, these diagrams extend our understanding of nuclei to the regime of finite temperatures. For example, consider the temperature-density phase diagram. At zero temperature, the vapor phase is a vacuum of zero density and the liquid phase is the known saturation density of nuclei. The phase diagram shows the trend of the density as the temperature is increased. The straight line in the middle of the diagram is the average of the two densities at a given temperature. It demonstrates the symmetric nature of the phase diagram relative to other systems such as shown in Fig. 1.4.

Just as the phase diagrams in Fig. 1.7 are constructed from nuclear collision experiments, they also allow for predicting the results of such experiments. The phase coexistence has implications in any study of thermal nuclei, such as studies of the symmetry energy as a function of temperature. Also, to understand the dynamical processes in nuclear collisions, first the thermal properties need to be established to be able to differentiate the two phenomena.

The combination of a concise physical picture of nuclear collisions combined with the Fisher droplet model makes the construction of the nuclear phase diagram possible. One goal of this thesis is to determine the reliability of this novel use of the Fisher droplet model to demonstrate the accuracy of these predictions for the nuclear system.

1.5 Goals of the Project

The purpose of this work is to study the reliability of using cluster theories to construct liquid-vapor phase diagrams, driven by the recent developments in creating an experimental phase diagram of nuclear matter.

To accomplish this goal, first the phase diagrams of molecular systems are considered. The Fisher droplet model represents an equation of state for a vapor below the critical point. This equation of state exhibits an extended principle of corresponding states whereby the systems do not scale solely by their reduced variables. The observation that molecular vapors can be described via this theory emphasizes the physical relevance of cluster theories.

Second, computer simulations of a Lennard-Jones fluid at coexistence are performed to study physical clusters. The configurations generated by the simulation are considered with different cluster definitions. A physically consistent cluster definition leads to ideal clusters that reflect the thermodynamics of the system.

Third, these clusters found in the model system are shown to exhibit Fisher scaling. This allows for the generation of the phase diagram for the system through only considering the physical clusters of the vapor.

The combination of these considerations demonstrate the validity of using the Fisher droplet model to construct a phase diagram of nuclear matter.

Chapter 2

Evidence of the Fisher Droplet Model in Molecular Fluids

The purpose of this chapter is to consider the validity of the Fisher droplet model as the equation of state of a vapor. The goal is to observe the prediction of the Fisher droplet model in the experimental phase diagrams of molecular fluids. Such an analysis requires no reference to the physical clusters that are present in the system.

The equation of state that is derived from the Fisher droplet model demonstrates an extended principle of corresponding states. Phase diagrams of different systems can be scaled in terms of their reduced variables and the system dependent constant c_0 found in the equation for cluster concentrations. The scaled phase diagrams can then be compared to the results of the Fisher droplet model to establish the validity of the model to describe the phase diagrams of real systems.

2.1 Extended Principle of Corresponding States

According to the principle of corresponding states, the equations of state for different molecular systems can be scaled to one another despite having different intermolecular potentials. In particular, the phase diagrams of different systems are the same when the variables are scaled to the critical point values. In this way many molecular systems do scale together, but there is a marked variability between others. The concept of an extended principle of corresponding states is to find additional scaling parameters that explain these differences.

An early example of an extended principle of corresponding states is from Pitzer, which relies on dividing different systems based upon the acentric factor ω [Pit55]. The acentric factor is effectively the slope of the reduced pressure-temperature phase diagram which in turn is dictated by $\Delta H/T_c$ as seen in the Clausius-Clapeyron relation. The acentric factor is defined such that $\omega = 0$ for the original set of systems considered by Guggenheim [Gug45; Gug93] and other systems are predominately $\omega > 0$. Pitzer's interpretation of this variation in the phase diagrams is that polyatomic systems have a non-zero acentric factor because the

center of the attractive force does not coincide with the center of the molecule but rather the center of each atom within the molecule. The theory is that systems with the same acentric factor exhibit the principle of corresponding states.

A more recent approach to an extended principle of corresponding states is suggested by Noro and Frenkel [NF00]. Noro and Frenkel suggest using a reduced form of the second virial coefficient as the third parameter as opposed to Pitzer's acentric factor. The second virial coefficient is a measure of the range of interaction relative to the size of a molecule's repulsive core and thus relates to a microscopic aspect of the system. Despite the fact that different reduced second virial coefficients do give rise to different scalings between systems, this correlation is empirical; there is no theory that predicts the relationship between the microscopic properties of the system and the phase diagram.

The Fisher droplet model is shown to follow an extended principle of corresponding states. As with previous studies of the extend principle of corresponding states, different systems can be divided into different groups which scale by their reduced variables. The Fisher droplet model goes a step further and suggests that the equation of state of these different groups can be scaled together.

2.1.1 The Fisher equation of state

The Fisher droplet model was originally developed to study critical phenomena in the vapor phase in terms of clusters [Fis67b; Fis67a]. The utility of the model has thus historically focused on the vicinity of the critical point. However, the Fisher droplet model, in conjunction with the ideal cluster laws, creates an entire equation of state for a vapor. For example, the pressure p as a function of temperature T and chemical potential μ is

$$p(T,\mu) = T\sum_{A=1}^{\infty} q_0 A^{-\tau} \exp\left[-c_0 A^{\sigma}\left(\frac{1}{T}-\frac{1}{T_c}\right)+\frac{A(\mu-\mu_{coex})}{T}\right], \tag{2.1}$$

where μ_{coex} is the chemical potential at coexistence for the respective temperature.

This equation of state is only valid for the vapor phase below the coexistence chemical potential and below the critical temperature. The term linear in A in the exponential causes the sum in Eq. 2.1 to diverge when the chemical potential is above the coexistence chemical potential. This divergence is related to the inability of the theory to explain the nature of the liquid phase. The argument for why the equation of state is valid only below the critical point is more phenomenological. The value $c_0(1/T - 1/T_c)$ is related to the surface tension of the liquid. The surface tension is zero above the critical temperature leading to the conclusion that this equation of state is unphysical above the critical point even for chemical potentials that produce a convergent sum in Eq. 2.1.

An important aspect the Fisher equation of state is that it exhibits an extended principle of corresponding states where the constants q_0, c_0, and T_c are system dependent and completely determine the nature of the phase coexistence. The exponents τ and σ have the same value for every system due to arguments of universality of critical exponents.

The constant q_0 in the Fisher equation of state has units of inverse volume and is directly related to the critical density of the system. The critical density in the Fisher equation of state is

$$\rho_c = q_0 \sum_{A=1}^{\infty} A^{1-\tau} = q_0 \zeta(\tau - 1), \tag{2.2}$$

where $\zeta(x)$ is the Riemann zeta function.

The two other system dependent constants c_0 and T_c both have units of energy. The Fisher droplet model suggests that these are two independent energy scales within a system that affect the equation of state.

Consider the coexistence pressure and density as a function of temperature, all in reduced units, in the Fisher equation of state

$$\frac{p}{T}\frac{T_c}{p_c} = \frac{1}{\zeta(\tau)} \sum_{A=1}^{\infty} A^{-\tau} \exp\left[\frac{c_0}{T_c} A^{\sigma} \left(\frac{T_c}{T} - 1\right)\right], \tag{2.3a}$$

$$\frac{\rho}{\rho_c} = \frac{1}{\zeta(\tau - 1)} \sum_{A=1}^{\infty} A^{1-\tau} \exp\left[\frac{c_0}{T_c} A^{\sigma} \left(\frac{T_c}{T} - 1\right)\right]. \tag{2.3b}$$

The phase diagrams of different systems are expected to all scale in terms of reduced variables when they have the same value of c_0/T_c. Furthermore, the Fisher theory offers insight into how the equation of state is changed when the ratio of the two energy scales vary, thus going a step further than previous studies of an extended principle of corresponding states.

The Fisher equation of state suggests that the phase diagram of all systems scale if plotted as a function of $c_0(1/T - 1/T_c)$. This scaled and shifted temperature scale takes into account the difference between the two energy scales c_0 and T_c within a system. Notice that the pressure itself does not scale with this parametrization but the pressure divided by the temperature does. For brevity in the remainder of this thesis, phase diagrams including pressure divided by temperature are referred to solely as the pressure. This scaling can be directly tested in real fluids by determining the value of c_0 for different systems and comparing them to the results of the Fisher equation of state.

2.2 Scaled Pressure-Density Phase Diagrams

One method to test the Fisher scaling in real fluids is to consider the pressure-density projection of the phase diagrams. An advantage of using this projection of the phase diagram is that it avoids needing to define c_0 for each system since Eq. 2.3 is a parametric equation of the variable $c_0(1/T - 1/T_c)$.

Fig. 2.1 is a plot of the 73 molecular fluids, listed in Appendix 1, from the NIST Chemistry WebBook graphed as a function of their reduced variables [LMF11]. Also plotted is the equation generated from the Fisher equation of state in Eq. 2.3. All of these phase diagrams scale nicely to each other, indicating the accuracy of the Fisher equation of state.

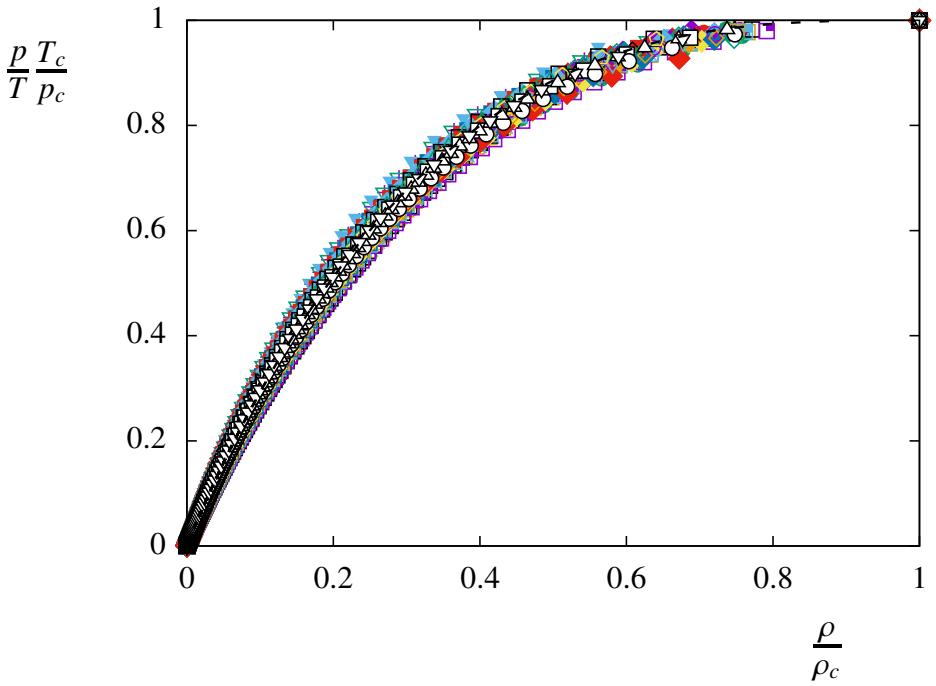

Figure 2.1: The reduced pressure-density phase diagrams of molecular fluids. Amongst the points is a line showing the prediction from the Fisher equation of state.

The scaling at low temperatures is indicative of the critical compressibility Z_c being constant for all the systems, where

$$Z_c = \frac{p_c}{T_c \rho_c}. \tag{2.4}$$

At low temperatures, the coexistence vapor is nearly ideal and the compressibility approaches $Z = 1$. As a result, the low temperature scaling of the reduced phase diagrams is predicted to be

$$\frac{p}{T\rho} = 1 \tag{2.5a}$$

$$\implies \frac{p}{T}\frac{T_c}{p_c} = \left(\frac{\rho}{\rho_c}\right)\left(\frac{\rho_c T_c}{p_c}\right). \tag{2.5b}$$

The Fisher equation of state predicts the slope of the phase diagrams at low temperatures to be

$$\frac{\rho_c T_c}{p_c} = \frac{\zeta(\tau - 1)}{\zeta(\tau)} \simeq 3.607, \tag{2.6}$$

using the nominal value of $\tau = 2.2088(2)$ [Cam02; PV02]. Fig. 2.2 shows the values of Z_c for the molecular fluids. The trend of increasing Z_c with T_c is beyond the theory presented here but is a small perturbation to the constant value.

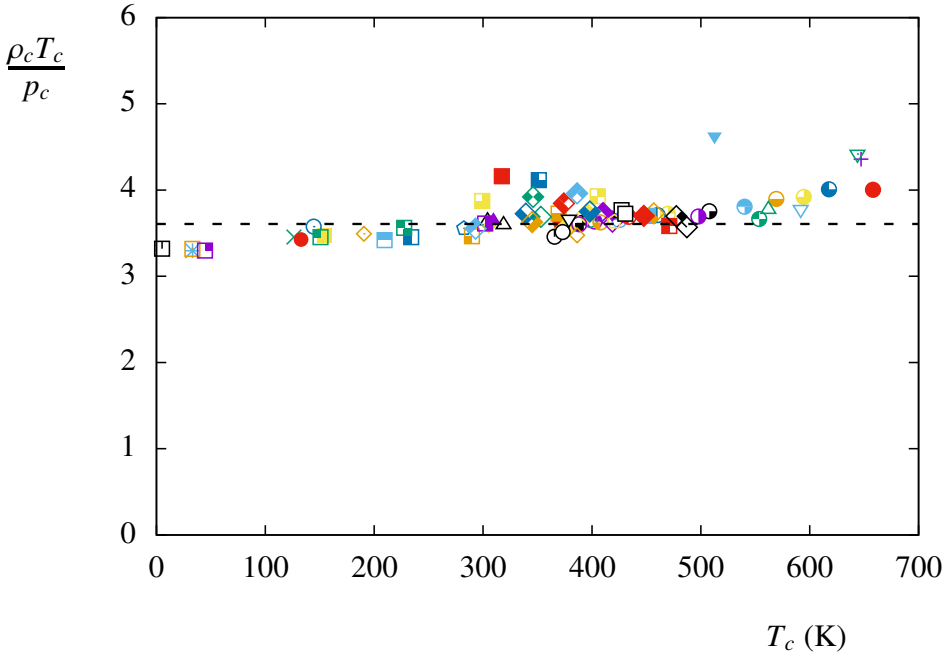

Figure 2.2: The inverse of the critical compressibility for molecular fluids. The line is the value predicted from the Fisher equation of state.

The scaling at high temperature is consistent with critical scaling where the the pressure and density scale as

$$1 - \frac{p}{T}\frac{T_c}{p_c} \sim \left(1 - \frac{\rho}{\rho_c}\right)^{1/\beta}, \tag{2.7}$$

where β is a critical exponent with the value $\beta = 0.3265(3)$. This scaling is emphasized in a logarithmic plot showing the asymptotic trend as the system approaches the critical point, as in Fig. 2.3. Not only is the critical exponent consistent, the prefactor is the same for all the systems when plotted in this reduced form. Furthermore, the observed scaling is predicted by the Fisher equation of state.

The pressure-density projection also allows for comparing how the liquid phase scales using this parametrization. Fig. 2.4 is the phase diagram consisting of both the vapor and liquid phases. The left part of the curve shows the consistency of the vapor phase as discussed. To the right are the liquid densities. The pleasing scaling observed in the vapor phase is not present in the liquid phase. In part, this lack of scaling is not surprising since the Fisher equation of state only describes the vapor phase. The aspect that is not immediately clear is how the vapor phase at coexistence can be determined with no information about the liquid phase.

The pressure-density phase diagram is a convenient projection to test the Fisher equation

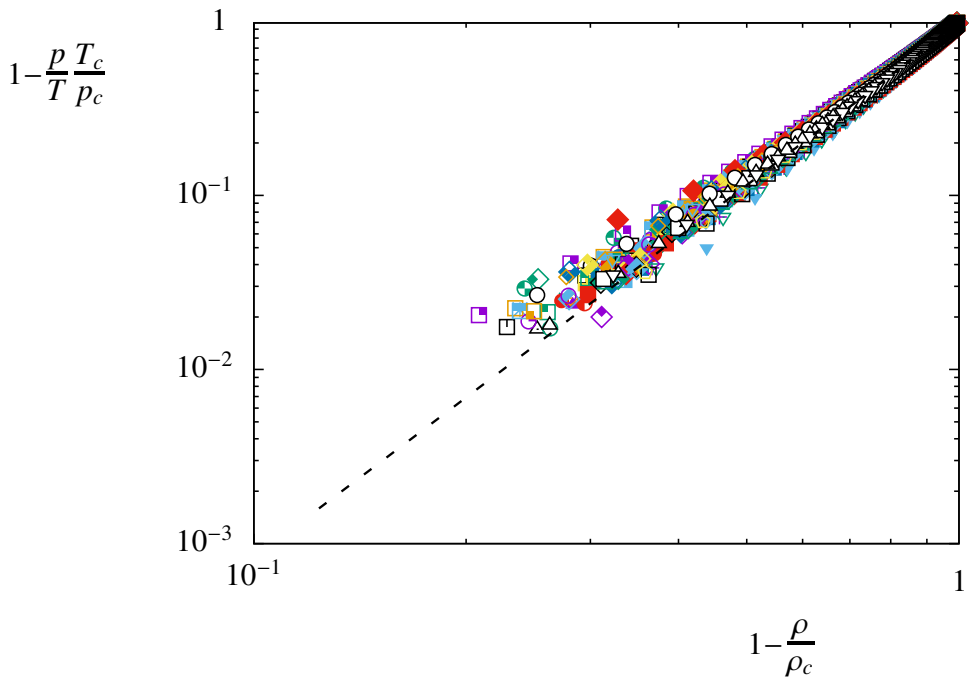

Figure 2.3: The reduced pressure-density phase diagrams of molecular fluids plotted logarithmic scale to show the critical scaling. The line shows the prediction from the Fisher equation of state.

of state since it avoids defining c_0 for a system. The resulting reduced phase diagrams are all described by the Fisher equation of state and supports the validity of the Fisher theory throughout the entire range of liquid-vapor phase coexistence.

2.3 A Working Definition of c_0

The value of c_0 for a system must be defined to test the temperature dependence of the Fisher equation of state. The correspondence between the Fisher theory and the Clausius-Clapeyron relation suggests that c_0 is related to ΔH of evaporation whereas the derivation of the Fisher droplet model suggest that c_0 is related to the surface tension. This connection between the volume and surface energies is not necessarily consistent and makes a concrete definition of c_0 elusive.

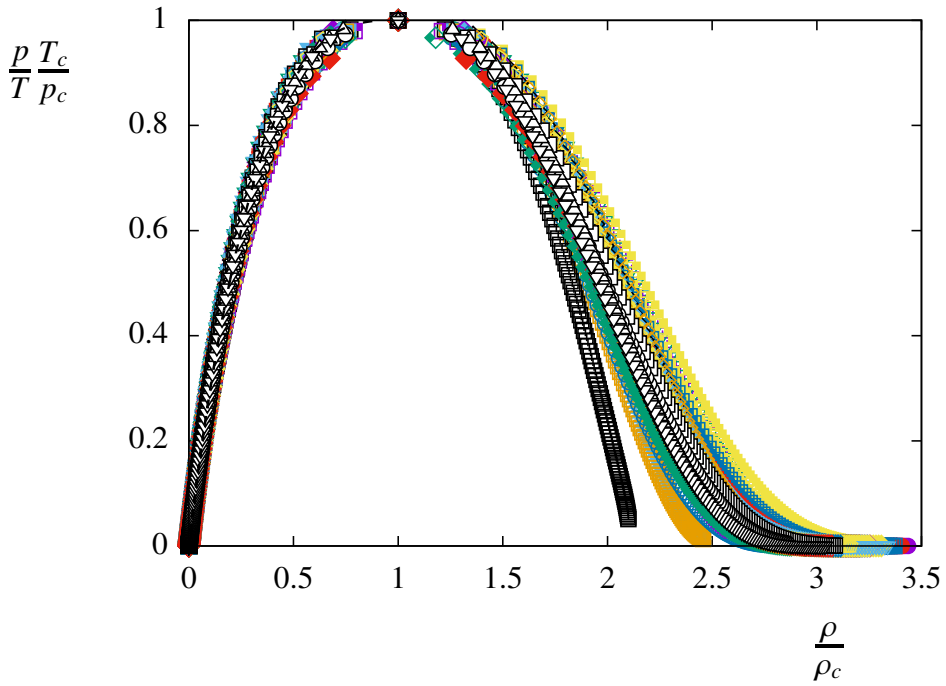

Figure 2.4: The reduced pressure-density phase diagrams of molecular fluids including the liquid branch of the coexistence.

2.3.1 Fisher equation of state and the Clausius-Clapeyron relation

One interpretation of c_0 of the Fisher droplet model comes from comparing the Fisher equation of state with the Clausius-Clapeyron relation, where the enthalpy of evaporation ΔH at low temperatures relates directly to c_0. The typical assumption used with the Clausius-Clapeyron relation is that the vapor is ideal and the liquid has a volume per particle that is negligible compared to that of the vapor. The change in enthalpy between the two phases is also approximated as being constant. The resulting coexistence pressure is

$$p = p_0 e^{-\Delta H/T}, \tag{2.8}$$

where p_0 is a system dependent constant.

The low density limit for a real vapor as an ideal gas corresponds to a system of only monomers in cluster theories. The pressure predicted at low temperatures in the Fisher equation of state is

$$p = T\, q_0 \, \exp\left[-c_0\left(\frac{1}{T} - \frac{1}{T_c}\right)\right], \tag{2.9a}$$

$$= p_0' T e^{-c_0/T}, \tag{2.9b}$$

where all the temperature independent constants are collected into p_0'.

Comparing Eq. 2.8 and Eq. 2.9b shows that the two approximations yield slightly different mathematical forms of the coexistence pressure. Namely, there is a factor of T in the Fisher theory that is not in the equation derived through the Clausius-Clapeyron relation.

A small change in the approximations used in the Clausius-Clapeyron relation yields an equation for the vapor pressure identical to the Fisher equation of state. Instead of assuming that ΔH is constant, the change in energy $\Delta E = \Delta H - p\Delta v$ is assumed to be constant. Integrating the Clausius-Clapeyron equation with this approximation yields

$$p = Tp_0' e^{-\Delta E/T}, \tag{2.10}$$

just as in Eq. 2.9b. The Fisher droplet model predicts the numerical value for p_0', which is not predicted in the Clausius-Clapeyron relation. The accidental agreement of experimental phase diagrams with Eq. 2.8 has historically motivated the argument that ΔH is constant whereas the Fisher equation of state is consistent with ΔE being constant. The practical application of using the enthalpy of evaporation to approximate the phase diagram is not highly changed since $\Delta H \simeq \Delta E$ at low temperatures.

Eq. 2.9b and Eq. 2.10 are equivalent when $c_0 = \Delta E$. It is interesting to note that c_0 in the Fisher droplet model is interpreted as a surface energy but ΔE is the volume energy.

2.3.2 The surface and volume energy coefficients

There is a precedent for the correspondence between the surface and volume energy coefficients of the leptodermous expansion. A dense system will have the surface and volume coefficients be of the same order of magnitude. This phenomenon is a result of the geometric origin of the two terms of the leptodermous expansion. Furthermore, a system in its ground state empirically has the two coefficients being exactly the same.

The nuclear system is an example. The liquid drop model in its traditional form predicts $a_v \simeq 16$ MeV and $a_s \simeq 18$ MeV [MS69; RG06]. These values may not be equivalent but they are relatively close. A recent study has extended the number of terms in the leptodermous expansion for the nuclear system to include a curvature term and yields fits with $a_v = a_s$ to within error [Mor12].

A simple model system that also has $a_v = a_s$ is a system of sticky cubes. Consider a set of A cubic particles that do not interact except for when they are in direct contact and bond together with an energy of $-\epsilon$. The lowest energy configuration for a collection of these particles is itself a larger cube with a binding energy B_A of

$$B_A = 3\epsilon A - 3\epsilon A^{2/3}. \tag{2.11}$$

Thus, the surface and volume energy coefficients are $a_s = a_v = 3\epsilon$.

The equivalence of the surface and volume energy coefficients at low temperatures is also seen in molecular systems. Since the liquid phase becomes metastable below the triple point temperature compared to the vapor and solid phases, the properties of the liquid at the

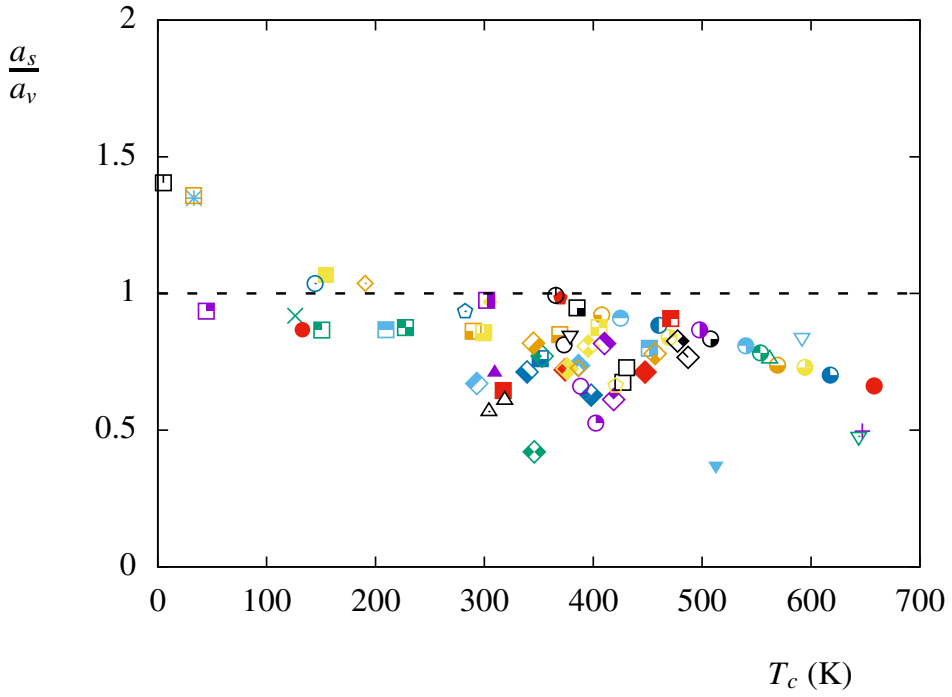

Figure 2.5: Ratio of the surface tension and the enthalpy of evaporation of molecular fluids expressed as the coefficients of the leptodermous expansion. The line is the result if the two terms in the expansion are equivalent.

triple point are used as a low temperature limit. The volume energy at the triple point can be approximated as the energy of evaporation per particle and the surface energy coefficient can be approximated as the surface tension γ. Appropriate units of energy per $A^{2/3}$ are used for the surface energy coefficient and, presuming the liquid drop is spherical, is related to the surface tension as

$$a_s = \gamma \left[\frac{36\pi}{\rho_\ell^2} \right]^{1/3} . \tag{2.12}$$

Fig. 2.5 shows the ratio of these two values for the 73 molecular systems considered. All of the systems have the two energies within the same order of magnitude and all but four of the systems have values within a factor of two. The difference can be explained in that the triple point may not be a low enough temperature to be considered as a low temperature limit.

The sticky cube model is considered again to demonstrate that the surface and volume energy coefficients differ at non-zero temperatures. A collection of sticky cubes at a low, non-zero temperature will be at a higher energy than the cubic ground state by creating holes within the volume of the cube. The holes can be approximated as uncorrelated and

evenly dispersed throughout the volume. The volume energy E_v is

$$E_v = -3\rho\epsilon A, \tag{2.13}$$

where the density ρ is the probability that any given cell is occupied. The surface energy E_s is half the energy required to cut a block of length ℓ out of a bulk sample,

$$E_s = \frac{1}{2}\, 6\ell^2\, \rho, \tag{2.14}$$

where $6\ell^2$ is the surface area of the removed section. The density is used to convert E_s into a function of $A^{2/3}$ and results in a leptodermous expansion of

$$B_A = 3\rho\epsilon A - 3\rho^{2/3}\epsilon A^{2/3}. \tag{2.15}$$

The differing ρ dependence of the surface and volume energy coefficients makes $a_v = a_s$ occur only at the most dense state.

2.3.3 A low temperature definition of c_0

The equivalence of the surface and volume energy coefficients support using the enthalpy of evaporation at low temperatures as a possible measure of c_0. Using this value of c_0 generates the scaled phase diagrams in Fig. 2.6. The scaling does not effectively describe all the systems simultaneously but does demonstrate this value of c_0 is of the right magnitude.

The effect of this scaling is to make the low temperature portion of the phase diagrams all parallel. In general, the second derivative of the phase diagrams at the triple point are not zero. This feature suggests that the triple point is too high in temperature to use the approximation that $a_s = a_v$. Furthermore, using the triple point as a reference temperature is inconsistent since it occurs at different values of the scaled temperature.

A c_0 defined by a low temperature property does not scale the phase diagrams of molecular systems effectively, despite the predictions of the Fisher theory. Some combination of not having a sufficiently low temperature for the system and inaccuracies of the Fisher theory to describe low temperature makes this approach of defining c_0 insufficient.

2.3.4 Relation of c_0 and the surface tension

The surface tension itself can be used as a measure of c_0 in the Fisher droplet model. The surface tension is the Helmholtz free-energy per unit surface area of a bulk surface. Upon inspection of the Fisher droplet model, the temperature dependence of the surface free-energy F_s for large A is

$$F_s = \gamma S_A = c_0 A^\sigma \left(1 - \frac{T}{T_c}\right), \tag{2.16}$$

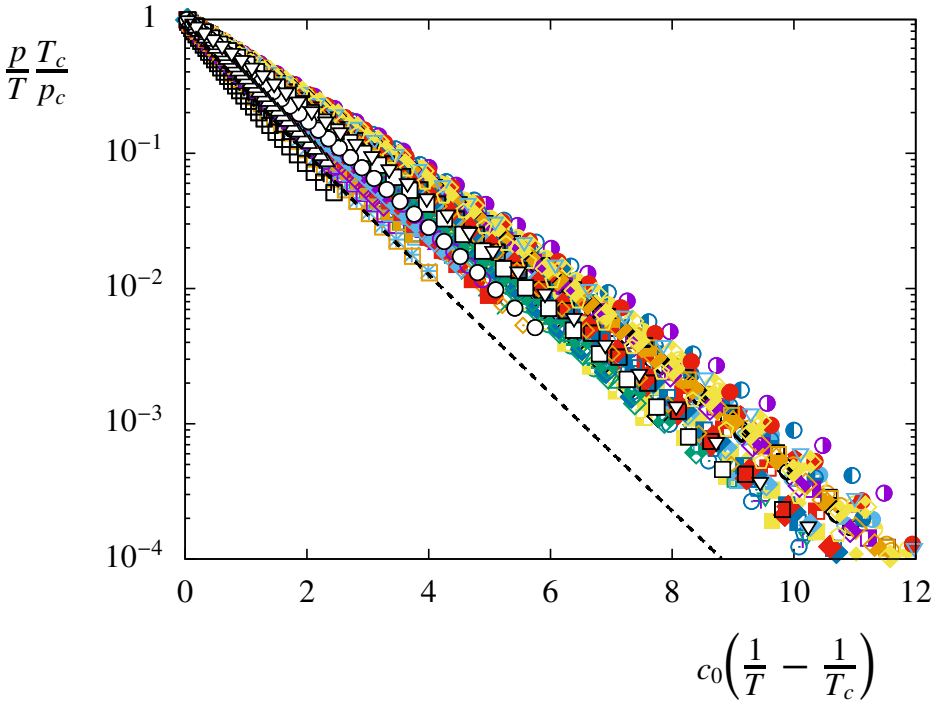

Figure 2.6: The reduced pressure-temperature phase diagrams of molecular fluids using the enthalpy of evaporation at the triple point as the value of c_0. The line is the result of the Fisher equation of state.

where γ is the surface tension and S_A is the surface area of a droplet. This relation suggests a linear relation of the surface tension as a function of temperature as the critical point is approached. Empirically, the critical scaling of the surface tension is

$$\gamma \sim \left(1-\frac{T}{T_c}\right)^{2\nu}, \tag{2.17}$$

where the critical exponent ν describes the limiting behavior of the correlation length and is $\nu = 0.63012(16)$ [Cam02; PV02]. Despite this discrepancy of the critical scaling, the surface tension is roughly linear over a large temperature range away from the critical point.

An alternative approach to scale the phase diagrams of molecular fluids is to plot the pressure as a function of the surface tension directly, instead of as a function of $c_0(1/T-1/T_c)$. The conversion of the surface tension into the surface energy coefficient requires the relation of the surface and volume of a drop as a function of A as in Eq. 2.12 for the case of a spherical cluster. The expected result for Fisher droplets is unclear since the clusters are distinctively non-spherical with $\sigma \neq 2/3$.

Fig. 2.7 is a plot of the scaled pressure-surface tension phase diagram for the molecular systems along with the result from the Fisher equation of state. There is a decent amount of

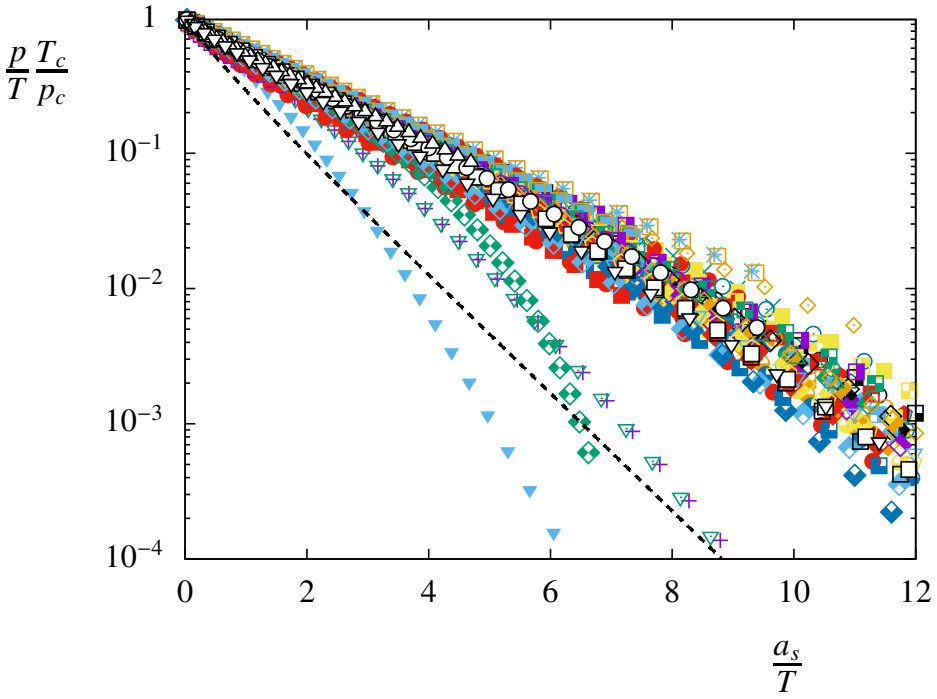

Figure 2.7: The reduced pressure-surface tension phase diagrams of molecular fluids. The surface tension is converted into units of the surface energy coefficient from the leptodermous expansion. The line is the prediction of the Fisher equation of state.

scatter in the scaling of the systems. The largest deviations come from methanol, water and heavy water, fluids that form hydrogen bonds. The presence of hydrogen bonding gives rise to anomalous physics for these systems compared to the majority of molecular fluids. The fourth system with pronounced deviations is 1,1,1-trifluoroethane. This fluid is observed to have an uncharacteristic maximum in its surface tension above the triple point temperature.

Beyond the scatter between the phase diagrams of molecular systems, the prediction from the Fisher theory has a much larger slope than the observed trends in the molecular fluids. These observations call into question the interpretation of the Fisher droplet model being motivated by an empirical description of the surface tension and eschews finding a physical interpretation of the constant c_0 in the Fisher droplet model.

2.3.5 Consistent scaling at the critical point

Using the physical properties of fluids is seen to be insufficient in consistently scaling the phase diagrams of molecular fluids. This observation does not imply that the Fisher equation of state is incorrect. Rather, the approximations and interpretations of the constants in the Fisher model are not accurate.

A direct comparison of the Fisher equation of state to the observed phase diagrams allows for a sufficient scaling of all systems. This goal is accomplished by considering the Fisher equation of state in the limit of the critical temperature. For example, the slope of the reduced pressure-temperature phase diagram as a function of inverse temperature is expected to be finite at the critical point,

$$\lim_{T \to T_c} \frac{d}{d\, 1/T} \left(\frac{p}{T} \frac{T_c}{p_c} \right) = -c_0 \frac{\zeta(\tau - \sigma)}{\zeta(\tau)}. \tag{2.18}$$

The slope at the critical point is proportional to c_0 and the proportionality constant is $\zeta(\tau - \sigma)/\zeta(\tau) \simeq 1.598$. Scaling the phase diagrams to this empirical value of c_0 scales the systems at the critical point. What is not trivial is how consistent the scaling is away from the critical point.

Fig. 2.8 is a plot of the reduced pressure-temperature phase diagrams scaled using a fitted value of c_0 near the critical temperature. Not only do the phase diagrams all scale near the critical point, they scale together over the entire temperature range.

The notable exceptions are helium, hydrogen, and para-hydrogen. It is curious to note that despite helium not scaling with the other molecular systems, the Fisher equation of state does describe its entire phase coexistence. It is difficult to tell if this trend is physically significant or coincidental without a concept of why real systems are not well described by the Fisher equation of state.

By definition, the Fisher equation of state describes the scaling at the critical point well using this definition of c_0. However, the Fisher equation of state has different scaling at low temperatures. The fact that this value of c_0 consistently scales all the real fluids over the whole temperature range indicates that it is physically significant. Unfortunately, the mathematical form of this scaling is not described by the Fisher equation of state at low temperatures.

2.4 Scaled Temperature-Density Phase Diagram

In principle, the scaling of the vapor branch temperature-density phase diagram is ensured by the previously demonstrated scaling of the density-pressure and pressure-temperature phase diagrams. Nevertheless, the scaling of the phase diagrams in this projection is important in context of previous studies of phase coexistence. In particular, the Guggenheim scaling and the law of rectilinear diameter can be discussed in the context of the Fisher equation of state.

Fig. 2.9 demonstrates the scaling of the vapor branch temperature-density phase diagrams of molecular fluids using the same definition of c_0 as in the previous section. The top plot of the figure is the density on a logarithmic scale as a function of inverse temperature, analogous to to the typical representation of the pressure-temperature phase diagram. The bottom plot shows the consistency of the scaling at the critical point.

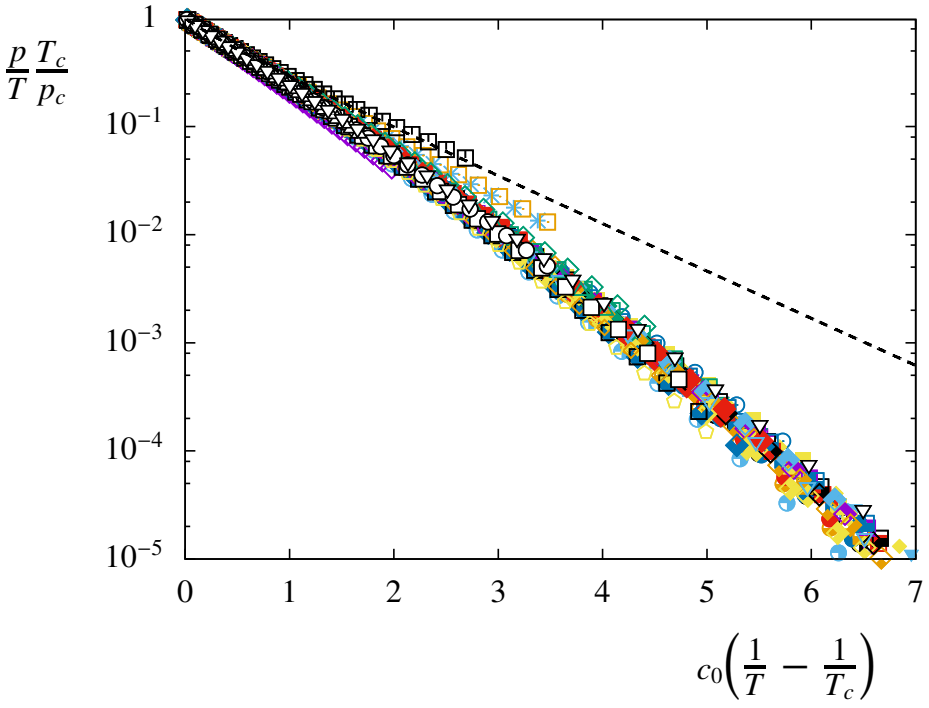

Figure 2.8: The reduced pressure-temperature phase diagrams of molecular fluids using a value of c_0 to consistently scale the systems at the critical point. The line is the result of the Fisher equation of state.

The observed deviations in the scaling and the Fisher equation of state are analogous to the deviations found in the pressure-temperature projection. The similarity of the deviations are anticipated due to the ideal nature of the gas at low temperatures.

What is more impressive is the consistency of the scaling at the critical point. The critical scaling in the pressure-temperature projection is ensured since the definition of c_0 was based upon this scaling. The consistency of the density-temperature phase diagram at the critical point demonstrates how the Fisher equation of state can simultaneously describe the pressure and the density as a function of temperature.

2.4.1 The Fisher equation of state and Guggenheim scaling

Guggenheim's work on the principle of corresponding states produced an approximation for the reduced coexistence densities as a function of reduced temperature [Gug45; Gug93]. The coexistence densities are proposed to be

$$\frac{\rho_{\ell,v}}{\rho_c} = 1 + b_1\left(1-\frac{T}{T_c}\right) \pm b_\beta\left(1-\frac{T}{T_c}\right)^\beta, \tag{2.19}$$

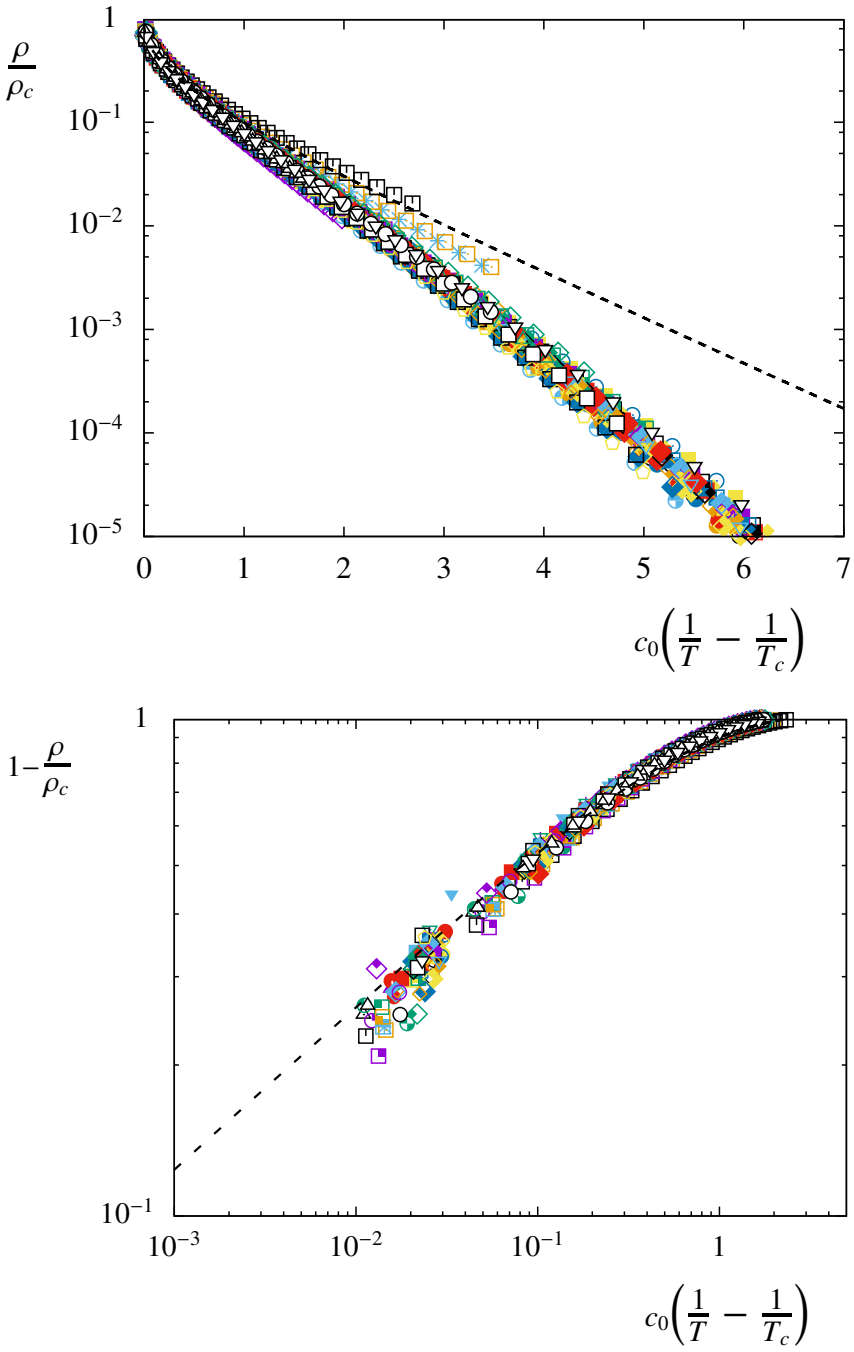

Figure 2.9: The reduced temperature-density phase diagrams of molecular fluids. The line is the result of the Fisher equation of state. The two plots are different representations of the same data to emphasize the scaling at low temperatures (top) and temperatures near the critical point (bottom).

where b_1 and b_β are system dependent constants. The upper sign is for the liquid phase and the lower sign is for the vapor. The original scaling proposed by Guggenheim has $\beta = 1/3$, $b_1 = 3/4$, and $b_\beta = 7/4$. In light of the fact that not all systems follow the principle of corresponding states, the equation suggested by Guggenheim is generalized to have b_1 and b_β be any value. The exponent β is a critical exponent and is kept constant for all systems as $\beta = 0.3265(3)$.

This equation for the Guggenheim scaling should be treated as a form of critical scaling since the low temperature limit of Eq. 2.19 is unphysical. For example, the original values of b_1 and b_β produce an equation that predicts negative vapor densities. These negative densities occur below the typical triple point temperatures of molecular fluids and thus this unphysical prediction is not a major concern in comparing the equation to experimental data.

An accurate description of the vapor density at low temperatures can be predicted using its ideal nature and the Clausius-Clapeyron relation. These approximations are consistent with the low temperature limit of the Fisher equation of state,

$$\lim_{T\to 0} \rho_v \sim q_0 \exp\left[-c_0\left(\frac{1}{T} - \frac{1}{T_c}\right)\right], \tag{2.20a}$$

$$\sim \rho_0 e^{-c_0/T}, \tag{2.20b}$$

where ρ_0 contains the temperature-independent constants. This equation is in contrast to the less accurate form of the Guggenheim scaling at low temperatures.

The Fisher equation of state can be expanded at the critical point into the same form as Eq. 2.19. The analytic behavior of the Fisher equation of state is deduced by approximating the sum over all cluster concentrations by an integral. Care must be taken to convert a sum into an integral to avoid introducing unnecessary errors to the result.

One example of inappropriately converting a sum into an integral is in calculating the critical density. Consider the exact value and the respective integrated value of ρ_c,

$$\rho_c = q_0 \sum_{A=1}^{\infty} A^{1-\tau} = q_0 \zeta(\tau - 1), \tag{2.21a}$$

$$\simeq q_0 \int_1^{\infty} A^{1-\tau}\, dA = \frac{q_0}{\tau - 2}. \tag{2.21b}$$

The nature of the zeta function makes this approximation inappropriate for values of τ close to 2. For example, there is an 11% difference in the two values for the value $\tau = 2.2088(2)$. To avoid this incongruity, the value $\rho_c - \rho$ is considered,

$$\rho_c - \rho_v = q_0 \sum A^{1-\tau}\left(1 - e^{-c\,A^\sigma}\right), \tag{2.22a}$$

$$\simeq q_0 \int A^{1-\tau}\left(1 - e^{-c\,A^\sigma}\right) dA, \tag{2.22b}$$

where the temperature dependence is rewritten as $c \equiv c_0(1/T - 1/T_c)$ to simplify the expressions.

The difference between a sum and the corresponding integral is found in the Euler-Maclaurin relation

$$\sum_{i=a}^{b} f(i) = \int_a^b f(x)\,dx - \frac{f(a)-f(b)}{2} - \sum_{k=1}^{\infty} \frac{B_{2k}}{(2k)!}\left[f^{(2k-1)}(a) - f^{(2k-1)}(b)\right] + R, \qquad (2.23)$$

where B_{2k} are the Bernoulli numbers and R is a small, function dependent error. This relation shows that the properties of f at the initial and final values of the sum are the source of error in approximating a sum as an integral.

The values of the cluster concentration and all derivatives are zero in the limit of large A and there are no errors associated with the upper limit of the sum in converting the Fisher sum into an integral. This is not true for $A = 1$, and the sum can be further modified by making the first term in the sum equal to zero to lessen this error

$$\rho_c - \rho_v = q_0\left(1 - e^{-c}\right)\sum_{A=1}^{\infty} A^{1-\tau} + q_0 e^{-c_0}\sum_{A=1}^{\infty} A^{1-\tau}\left(1 - e^{-c(A^\sigma - 1)}\right), \qquad (2.24a)$$

$$\simeq q_0\zeta(\tau-1)\left(1-e^{-c}\right) + q_0 e^{-c_0}\int_1^{\infty} A^{1-\tau}\left(1 - e^{-c(A^\sigma-1)}\right)\,dA. \qquad (2.24b)$$

This integral is analytical and produces the following approximation for the vapor density

$$\rho_c - \rho_v \simeq q_0\zeta(\tau-1)(1-e^{-c}) + \frac{c^\beta}{\beta\sigma}\Gamma(1-\beta, c), \qquad (2.25)$$

where $\beta = (\tau - 2)/\sigma$ and $\Gamma(s, x)$ is the incomplete gamma function. This equation of $\rho_c - \rho_v$ is found to be accurate to within less than a percent of the numerical summation over the entire temperature range. It is less accurate when compared to the density itself due to differing asymptotic behavior at low temperatures.* The study here is concerned with the critical scaling so this deviation is inconsequential.

The asymptotic behavior of Eq. 2.25 at the critical point is equivalent to the Guggenheim expression. The constants b_β and b_1 can be predicted using the parameters in the Fisher model

$$b_\beta = \frac{\Gamma(1-\beta)}{\beta\sigma\zeta(\tau-1)}\left(\frac{c_0}{T_c}\right)^\beta \simeq 1.196\left(\frac{c_0}{T_c}\right)^\beta, \qquad (2.26a)$$

$$b_1 = \left(\frac{1}{\sigma\beta(1-\beta)\zeta(\tau-1)} - 1\right)\left(\frac{c_0}{T_c}\right) \simeq 0.324\left(\frac{c_0}{T_c}\right). \qquad (2.26b)$$

*A precise equation can be produced by keeping the first term of the sum separate and taking the integral starting at $A = 2$ using the technique already described. This ensures the low temperature asymptotic behavior is consistent and the density is correct to within one percent over the entire temperature range.

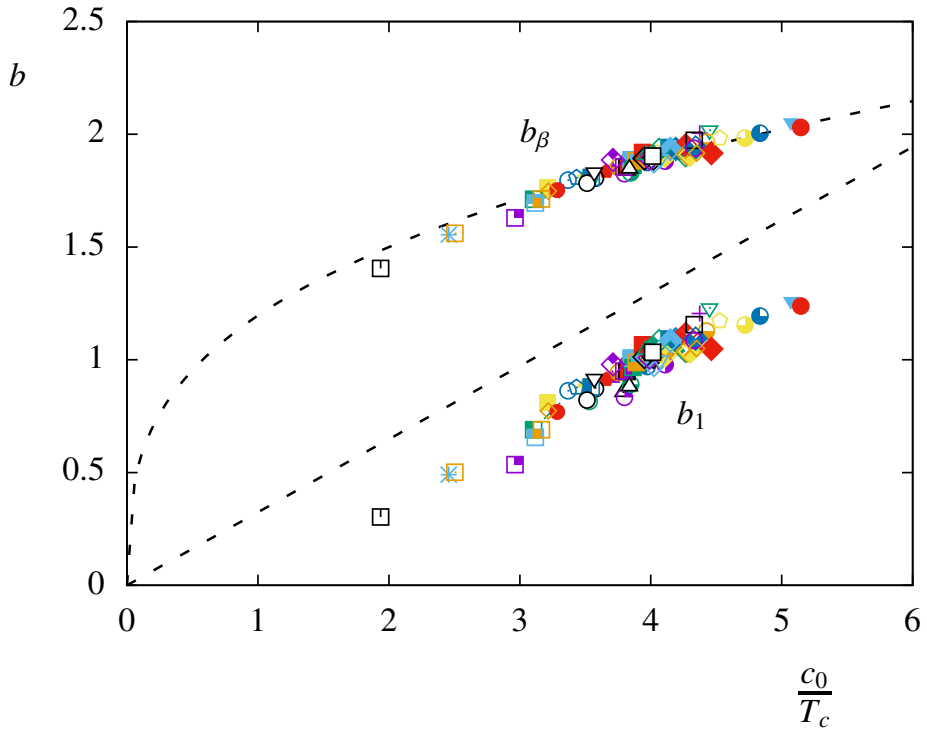

Figure 2.10: The fit parameters of the Guggenheim scaling for the molecular vapors. The lines represent the predicted values from the Fisher theory critical scaling.

It should be noted that the value for b_β is exact but the term for b_1 is not due to higher order terms in the Euler-Maclaurin expansion of the sum. Comparison to numerical values of the sum indicate that the error in b_1 is about 2%. The only system dependent variable that affects the Guggenheim scaling is the ratio c_0/T_c, where the constants to the left are composed solely of critical exponents and are constant for all systems. Furthermore, these equations predict that b_β and b_1 are not independent.

The results of equation Eq. 2.26 can be tested by fitting the Guggenheim scaling relation in Eq. 2.19 to the molecular phase diagrams. There are several ways that Eq. 2.19 can be fit to the data. A typical way is to fit the sum and difference of the liquid and vapor densities and presume that the values of b_1 and b_β are the same for the two phases. The focus of the Fisher equation of state is only the vapor phase and as such only the vapor densities are used to fit the Guggenheim scaling in this case. The liquid density is considered separately.

Fig. 2.10 is a plot of the fitted values of b_1 and b_β as a function of c_0/T_c for the molecular fluids with the lines corresponding to the prediction found in Eq. 2.26. The values of b_β are well described by this prediction. The value of b_1 are less clearly related to the prediction but are correlated with c_0/T_c with a linear dependence.

Equations of the form $b_1 = \alpha_1(c_0/T_c)$ and $b_\beta = \alpha_\beta(c_0/T_c)^\beta$ can be fit to the extracted

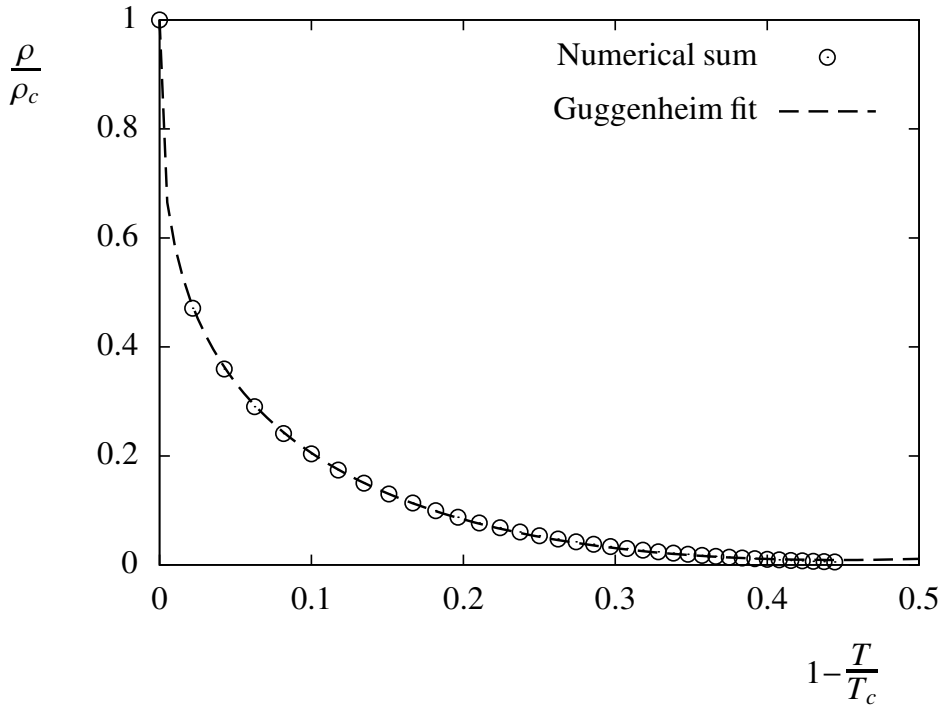

Figure 2.11: The predicted phase diagram from the Fisher equation of state as a function of $(1-T/T_c)$ with $c_0/T_c = 4.5$. The line is a fit of the Guggenheim scaling with $b_1 = 0.25(c_0/T_c)$ and $b_\beta = 1.20(c_0/T_c)^\beta$.

values of b_1 and b_β for the molecular systems. This yields $\alpha_\beta = 1.20$, consistent with the predicted value from the Fisher theory, and $\alpha_1 = 0.25$, which is significantly smaller than the predicted value.

The difference in slopes is due to fitting Eq. 2.19 to the data versus extracting the critical scaling directly. The equation for the Guggenheim scaling can be fit to the predicted Fisher phase diagram to demonstrate that the observed values of b_1 are consistent with the Fisher theory. The relation between $(1 - T/T_c)$ and $c_0(1/T - 1/T_c)$ requires a definite value of c_0/T_c and $c_0/T_c = 4.5$ is used to represent a typical value from the molecular fluids. Also, only values of $(1 - T/T_c) < 0.45$ are considered to imitate the presence of a triple point. The result is shown in Fig. 2.11 and the fit parameters are found to be $b_1 = 0.25(c_0/T_c)$ and $b_\beta = 1.20(c_0/T_c)^\beta$. These values are unchanged upon varying the value of c_0/T_c and are consistent with the values from the molecular systems.

The Fisher equation of state effectively explains the observed Guggenheim scaling of the vapor densities at coexistence. Furthermore, the two constants b_1 and b_β are related to each other, a result which is empirically observed in molecular fluids. What remains to be seen is how this scaling relates to the liquid phase.

2.5 Evidence of the Fisher Equation of State in the Liquid Phase

The Guggenheim scaling of the temperature-density phase diagram implies a connection between the nature of the liquid and vapor densities at coexistence. The constants b_1 and b_β are assumed to be equal for the two phases in Eq. 2.19 and the only difference in the equation is the change of sign for the term proportional to $(1 - T/T_c)^\beta$. This connection between the two phases would allow to evaluate the liquid coexistence densities from the Fisher equation of state.

The validity of the Guggenheim scaling can be tested by fitting Eq. 2.19 separately to each phase. The plots in Fig. 2.12 show the correlation found in the fit parameters of the two phases. The values of b_β are approximately equal between the two phases but the values of b_1 differ.

Consider the agreement of b_β in the two phases. The equivalence of b_β in the two phases gives rise to the empirical law of rectilinear diameter. If b_β differed in the two phases then the average of the liquid and vapor densities is

$$\frac{\rho_\ell + \rho_v}{2\rho_c} = 1 + \frac{1}{2}(b_1^\ell + b_1^v)\left(1 - \frac{T}{T_c}\right) + \frac{1}{2}(b_\beta^\ell - b_\beta^v)\left(1 - \frac{T}{T_c}\right)^\beta. \tag{2.27}$$

The limiting critical behavior of the diameter would have a critical exponent of β. Even though the limiting behavior of the diameter is debated [ZM72; SP90], the critical exponent associated with this phenomenon is indisputably not β. Having the value of b_β equal in the two phases is consistent with the critical scaling of the temperature-density phase diagram.

There is no analogous arguments for the values of b_1 to be the same in the two phases. The difference in the liquid and vapor densities with differing values of b_1 is

$$\frac{\rho_\ell - \rho_v}{\rho_c} = (b_1^\ell - b_1^v)\left(1 - \frac{T}{T_c}\right) + (b_\beta^\ell + b_\beta^v)\left(1 - \frac{T}{T_c}\right)^\beta. \tag{2.28}$$

The limiting critical behavior is unchanged by the addition of a linear term in the above equation. This equation is physically possible and is a reminder that critical scaling typically does not consider higher order terms.

Unfortunately, the possibility of b_1 being different for the two phases makes it more difficult than suggested by the Guggenheim scaling to determine the liquid density based only upon the vapor density. There may be some relation between the value for the two phases, as seen in Fig. 2.12, but it is unclear what it is.

The value $\frac{1}{2}(b_1^\ell + b_1^v)$ is referred to as the asymmetry in the temperature-density phase diagram. Each system has a different liquid density at low temperatures determined by this asymmetry. Fig. 2.13 is a plot of the reduced phase diagram including the liquid phases to show the variety of limiting densities between the different fluids. The differences in the limiting liquid densities makes scaling the liquid densities in the same fashion as the vapor densities impossible.

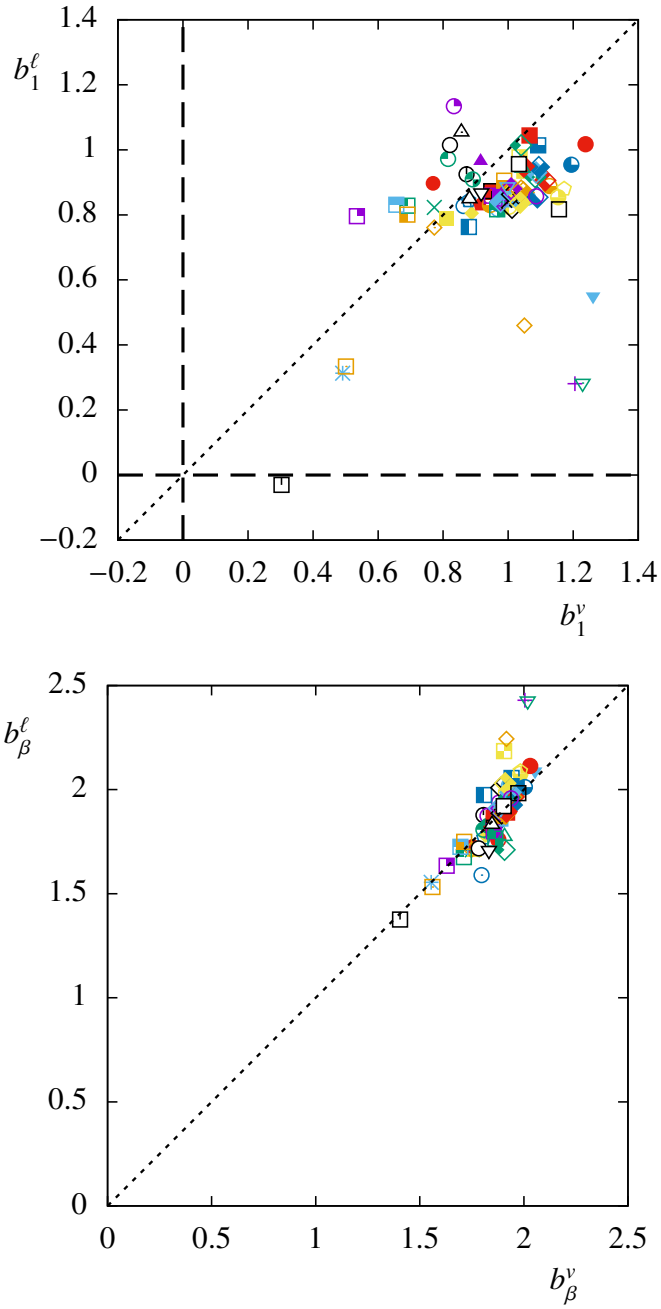

Figure 2.12: The fit parameters for the Guggenheim scaling of the temperature-density phase diagram with the two phases fit independently. The line represents when the fit parameters are equal.

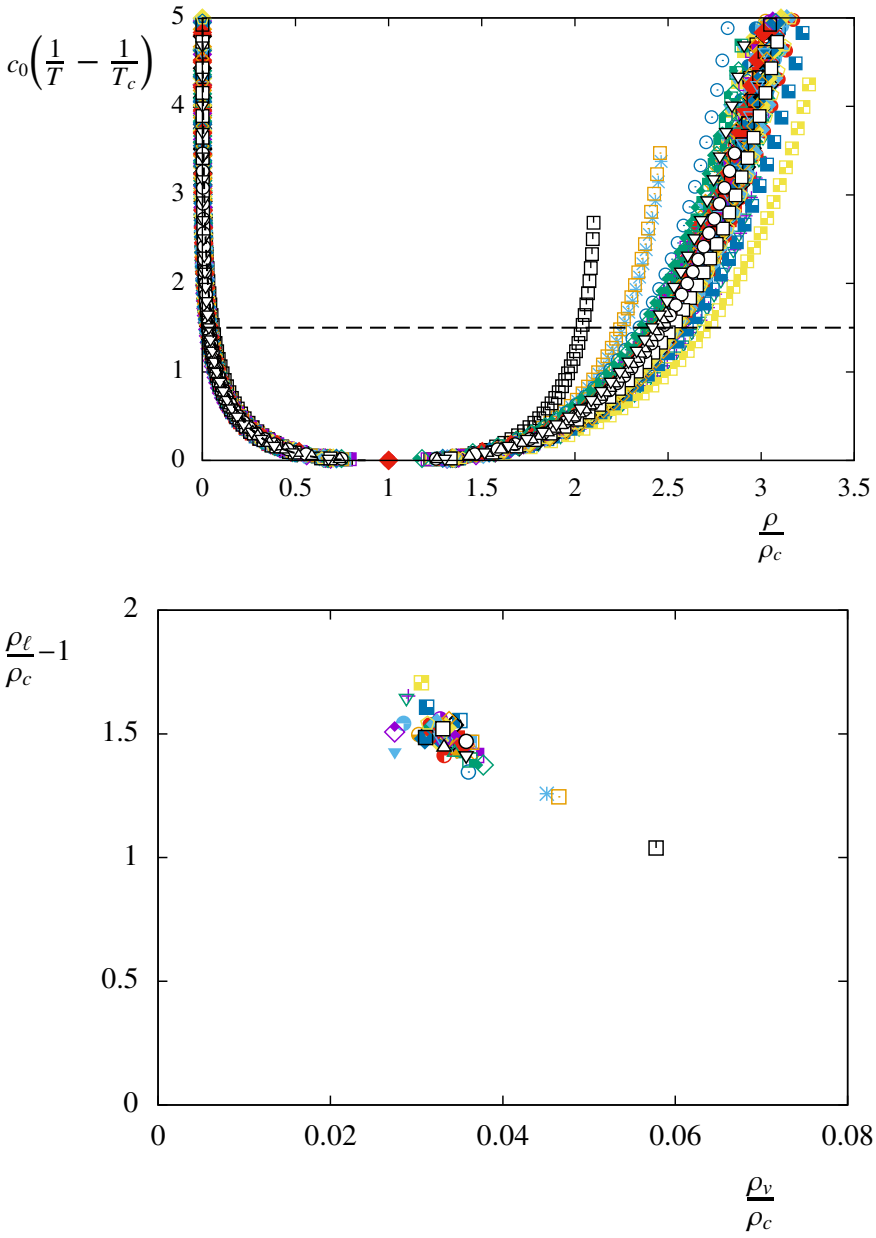

Figure 2.13: Top: The scaled temperature-density phase diagrams of the molecular fluids also showing the lack of scaling found in the liquid densities. Bottom: The liquid and vapor densities of the fluids at a constant value of $c_0(1/T - 1/T_c) = 1.5$, as indicated by the horizontal line in the top figure.

Instead of trying to scale systems of different c_0/T_c simultaneously, consider the weaker statement of the extended principle of corresponding states that systems with different c_0/T_c do not scale together. The arguments made thus far are consistent with all systems having the same critical behavior when scaled appropriately. At lower temperatures the scaling is not consistent for systems of different c_0/T_c. The bottom portion of Fig. 2.13 is a plot of the reduced liquid and vapor densities from a constant value of $c_0(1/T-1/T_c) = 1.5$, as indicated with the horizontal line in the top plot. The variability of the vapor densities correlating with the liquid densities suggest that the nature of the liquid phase can be deduced from knowing the vapor densities, but is beyond the physics of the Fisher equation of state.

2.6 Conclusion

The Fisher droplet model constitutes an equation of state for a vapor that is quantitatively consistent with the experimental phase diagrams of molecular fluids. Despite cluster analysis being an impractical way to study real fluids, the physics of clusters is still detectable in the thermodynamics of phase coexistence. It is necessary that such signals are found in real fluids for the Fisher droplet model to be a predictive theory.

The Fisher equation of state demonstrates an extended principle of corresponding states. There are three system dependent parameters that fully specify the nature of the fluid's phase coexistence. Two of these parameters account for the variability in size and depth of the intermolecular potential as in the original principle of corresponding states. The third parameter accounts for the variability observed in the phase diagrams of the molecular systems plotted as a function of their reduced variables. Furthermore, the Fisher equation of state suggests that the phase diagrams can all be consistently scaled as a function of a reduced and shifted temperature, $c_0(1/T - 1/T_c)$.

The validity of the theory is demonstrated in comparing the phase diagrams of 73 different molecular systems. The variability in these systems makes finding a consistent description ambitious. The systems included vary from small to large molecules, such as methane versus dodecane, systems with weak van der Waals forces to strong hydrogen bonding, such as neon versus water, and highly quantal systems to heavy systems with indisputably classic behavior, such as helium versus xenon. Different projections of these phase diagrams reveal different aspects of the liquid-vapor phase coexistence.

The consistency of the scaling in the reduced density-pressure projection shows the validity of the Fisher theory without a need of defining c_0 for each system. The fact that the critical compressibility is constant for all the systems is immediately demonstrated in this projection. Furthermore, the critical scaling of the density and pressure are simultaneously described by the theory.

The reduced pressure-temperature projection allows for studying the physical origin of the parameter c_0. At low temperatures, the Fisher theory is consistent with the Clausius-Clapeyron relation when c_0 is interpreted as a volume energy as opposed to a surface energy. The correspondence of the surface and volume energy coefficients is a general feature of

leptodermous systems. At higher temperatures, the relation of c_0 as being the surface tension is unreliable. Ultimately, a consistent definition of c_0 is found by describing the critical scaling of the pressure-temperature phase diagram. The resulting scaling consistently scales the phase diagrams of molecular fluids, albeit not consistently with the Fisher theory at low temperatures.

The scaling observed in the temperature-density projection demonstrates the consistency of defining c_0 from the pressure-temperature projection. The Fisher equation of state offers insight to the Guggenheim scaling of the temperature-density phase diagram. The coefficients of this scaling, b_1 and b_β, are predicted to be directly related to the parameter c_0/T_c, which is observed in the molecular systems. This scaling is reliable in describing the vapor densities but the ability of predicting the liquid densities using the Guggenheim scaling is less reliable.

The Fisher droplet model offers many insights to the nature of liquid-vapor phase coexistence. Ultimately, the Fisher equation of state does not completely describe all the properties of coexistence. Nevertheless, it is impressive how the theory leads to a consistent scaling of the phase diagrams of such a diverse set of molecular fluids. These observations validate the predictive power of the Fisher droplet model to predict the liquid-vapor phase coexistence of a fluid.

Chapter 3

Physical Clusters in the Lennard-Jones Model

The purpose of this chapter is to consider the clusters found in molecular simulations of the Lennard-Jones model. Different cluster definitions are considered to find clusters that are consistent with our perception of what a cluster is. Furthermore, the ideal cluster law is tested with these physical clusters, establishing their physical relevance. The intentions of using the Fisher droplet model to build a phase diagram are predicated on these basic properties of physical clusters.

3.1 Molecular Simulations

3.1.1 General overview

Molecular simulations consider a collection of particles interacting through a model potential. The number of particles modeled is small compared to most experimental situations, but large enough such that the thermodynamic limit is sufficiently obtained. Average values of observables are then related to the thermodynamic properties of a bulk system.

There are two classes of molecular simulations: molecular dynamics and Monte Carlo. The Newtonian equations of motion are integrated in discrete time steps in molecular dynamics simulations whereas small changes of the system are randomly created in the Monte Carlo simulations. Both type of simulations satisfy detailed balance and generate the same distribution of microstates.

Ensemble averages of a molecular simulation are performed as follows. An initial configuration of the particles is generated and small changes are sequentially applied to the system. After one iteration the system is highly correlated with the initial state and the small changes are applied until the system is sufficiently uncorrelated. Statistics of the system are then collected at this correlation time scale to determine ensemble averages which are directly related to the thermodynamics.

Model systems are used in simulations because they are simple compared to the first principle physics of real systems but produce analogous phenomena. This study considers particles interacting via the pairwise Lennard-Jones potential

$$u_{LJ}(r) = -4\epsilon \left[\left(\frac{\sigma}{r}\right)^6 - \left(\frac{\sigma}{r}\right)^{12} \right], \tag{3.1}$$

where r is the distance between two particles. The system dependent constants ϵ and σ define the minimum energy of the potential and the distance of zero binding, respectively. This potential is analogous to intermolecular potentials, as well as internucleonic potentials, having a repulsive core and a diffuse attractive force at larger distances. This similarity on the microscopic level gives rise to similar thermodynamics of real systems including the presence of liquid-vapor coexistence. Furthermore, extensive work has previously been done on the thermodynamics of the Lennard-Jones model and the nature of its phase coexistence is well characterized, for example [JZG93; MP07; Nat12; PP98; Smi92].

3.1.2 Modeling a coexisting vapor

Any vapor can be studied in terms of physical clusters. The ideal cluster theory is predicted to hold for a vapor at any pressure and is not restricted to the study of coexistence. The overarching goal of this work is to use the Fisher droplet model to describe a vapor at coexistence. For this reason, the simulations in this work are restricted to modeling the Lennard-Jones system at liquid-vapor coexistence.

A technique known as the Gibbs ensemble Monte Carlo method is an efficient algorithm to study a system in two phase coexistence [Pan87; Pan88]. This algorithm relies upon the fact that the two phases do not need to be in physical contact to be in coexistence. The only requirement of coexistence is that the two phases have the same temperature, pressure and chemical potential.

In this algorithm, two separate volumes are used to contain each phase. The system is changed by three separate Monte Carlo algorithms: particles are displaced within the same container, the volume of the containers are changed such that the entire volume of the system is constant, and particles are moved from one container to the other.

The temperature is an input parameter to the calculation. The pressure of the two containers is equilibrated by the exchange of volume between the containers and the chemical potential is equilibrated by the exchange of particles. The Gibbs phase rule explains why the system will evolve towards a unique pressure and chemical potential whereby a system in two phase coexistence is fully specified by defining the temperature. An example of a configuration of particles generated in this simulation is shown in Fig. 3.1.

The purpose of this work is to study the clusters found in the vapor phase, but the Gibbs ensemble Monte Carlo simulation generates both the vapor and liquid phases. Simulating a liquid is computationally more difficult than simulating a vapor and is unnecessary in the present study. As such, the Gibbs ensemble Monte Carlo technique is used as a means to measure the coexistence vapor density and a more efficient canonical Monte Carlo algorithm

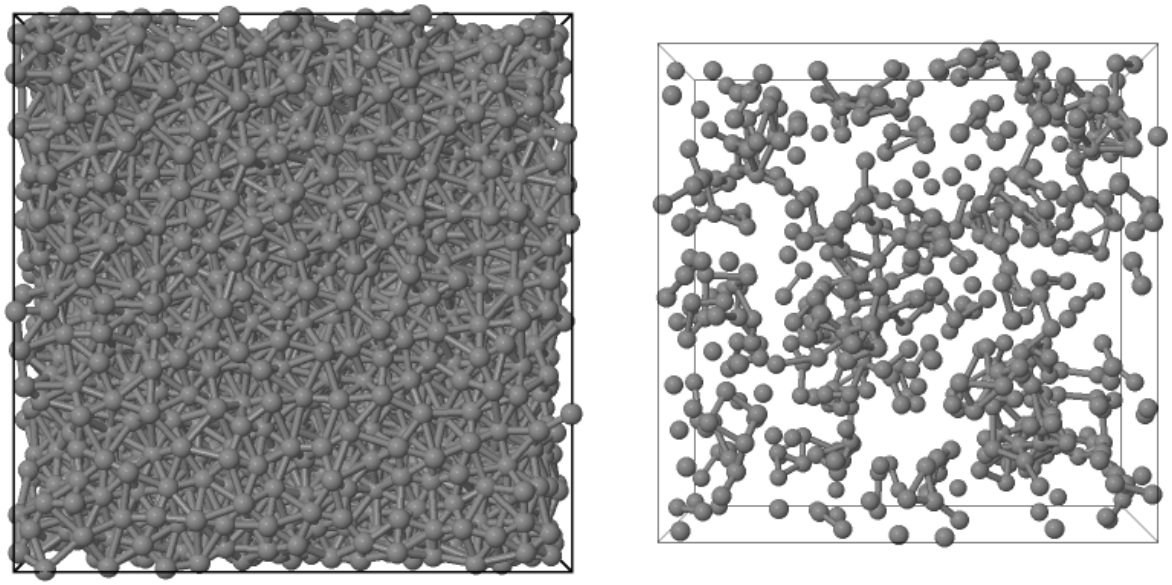

Figure 3.1: An example configuration generated by the Gibbs ensemble Monte Carlo method at a temperature of $T = 1.15\epsilon$. The bonds are to show proximity of particles and have no physical significance.

Table 3.1: Details of the Gibbs ensemble Monte Carlo calculations. The values on the left of the line are parameters of the calculation and to the right are derived quantities and previously reported values.

Simulation details				This work		Previous work [Nat12]	
T (ϵ)	N	V_{tot} (σ^3)	N_{sim}	ρ_v (σ^{-3})	ρ_ℓ (σ^{-3})	ρ_v (σ^{-3})	ρ_ℓ (σ^{-3})
1.00	4800	1.317×10^4	2437	0.02942(5)	0.69951(9)	0.029569(7)	0.70102(10)
1.05	4800	1.350×10^4	3402	0.04046(5)	0.67071(8)	0.040655(9)	0.67215(11)
1.10	4800	1.381×10^4	3709	0.05478(6)	0.63911(9)	0.055077(9)	0.64080(12)
1.15	4800	1.419×10^4	3291	0.07365(9)	0.60364(11)	0.074118(9)	0.60520(9)
1.20	4800	1.454×10^4	3664	0.09881(11)	0.56120(13)	0.10034(3)	0.56316(5)
1.25	4800	1.514×10^4	4668	0.13495(14)	0.50586(17)	-	-

Table 3.2: Details of the canonical ensemble calculations. The values on the left of the line are parameters of the calculation and to the right are derived quantities.

Simulation details				This work		Previous work [Nat12]	
T (ϵ)	N	V (σ^3)	N_{sim}	p (ϵ/σ^3)	log(z)	p (ϵ/σ^3)	log(z)
1.00	1885	6.4×10^4	10000	0.024891(8)	-3.8357(2)	0.024958(5)	-3.83428(11)
1.05	2590	6.4×10^4	10000	0.034266(11)	-3.5966(2)	0.034360(7)	-3.59507(10)
1.10	3507	6.4×10^4	10000	0.045894(16)	-3.3853(2)	0.046020(7)	-3.38410(7)
1.15	4715	6.4×10^4	10000	0.06007(2)	-3.1976(2)	0.060211(7)	-3.19707(6)
1.20	6326	6.4×10^4	10000	0.07693(3)	-3.0322(2)	0.077225(14)	-3.03072(8)
1.25	8617	6.4×10^4	10000	0.09670(4)	-2.8850(2)	-	-

is then used to model only the vapor phase. This method produces more statistics to better study the cluster concentrations.

A common practice in molecular simulations is to use a cut-off parameter in the pair potential. This implementation makes calculations faster by only having to consider the interactions of nearby pairs of $r < 3\sigma$. Studies have shown that using a cut-off parameter affects the measured coexistence properties, most notably near the critical point [Smi92]. It is standard practice when using a cut-off potential to apply long range corrections to the observed averages. The calculations herein do not use a cut-off parameter to ensure that the observed clusters are a property of the true potential. The size of the container creates a natural cut-off of interaction giving rise to a distance greater than 10σ, causing minimal effects to the system.

The temperatures studied are from $T = 1.00\epsilon$ to $T = 1.25\epsilon$ in 0.05ϵ intervals, compared to the triple point temperature of $T_t \simeq 0.684\epsilon$ [MP07] and critical temperature $T_c = 1.3120(7)\epsilon$ [PP98]. The considered temperatures are large enough to have an appreciable vapor pressure and low enough to have a clear differentiation between the liquid and vapor phases.

A summary of the Gibbs ensemble Monte Carlo calculations are presented in Tab. 3.1 including the values for the temperatures T, number of particles N, volume V, and number of uncorrelated realizations N_{sim}. The measured coexistence densities and values reported in previous studies are also listed [Nat12]. The values are not within error, but are consistent. The differences arise from the different techniques used, including the algorithm of finding coexistence and the corrections for using a cut-off parameter.

The same simulation details as reported for the Gibbs ensemble Monte Carlo simulations are shown for the canonical simulations in Tab. 3.2. The measured pressures and chemical potentials are reported and compared to the values of previous studies. The chemical potential is reported in terms of the fugacity z

$$z = \Lambda^{-3} e^{\mu/T}. \tag{3.2}$$

The values agree within the same precision as the coexistence densities.

Molecular simulations allow the study of model systems on a microscopic basis. Gibbs ensemble Monte Carlo simulations are an efficient way to establish coexistence properties. Given the vapor density, a canonical calculation of the vapor allows for collecting a large number of statistics to study physical clusters.

3.2 Cluster Definitions

Defining clusters from simulation realizations is distinct from the cluster theories that give predictions about a system's thermodynamics. For example, the ideal cluster theory could be read as "there exists a partition of the system such that the generated clusters are related to the thermodynamic functions," but offers no insight into what partition gives rise to this relation. The partitioning of a system into clusters has no effect on the simulation itself. Rather, the clustering is only an interpretation of the generated configurations.

The most important aspect of a cluster is the geometric proximity of the particles, and a simple formulation of clusters is to just consider the proximity of particle pairs. Two particles are bound together in the same cluster if they are within a certain distance. An ambiguity arises in this type of cluster definition: How far apart can two particles be to be considered bound? For the Lennard-Jones model, the force between particles is attractive for all distances of $r > \sigma$ and asymptotically goes to zero at large distances. It is obvious that two particles on opposite sides of a container are uncorrelated, but assigning a value to the cut-off is ambiguous.

Previous studies of lattice systems give insight into this problem. One choice for a cluster definition in the Ising model is to have all neighboring particles be of the same cluster [SG76; Bre05]. This is a logical choice since the only particles which interact in the model are neighboring particles but it produces unphysical clusters despite its simplicity. One way that these clusters are unphysical is in the way that the pressure predicted from the temperature weighted sum of the cluster concentrations is lower than the observed pressure [Bre05].

For clusters on a lattice to behave as an ideal cluster gas a bond breaking probability is introduced [CK80]. Each pair of neighboring particles are bonded with the probability

$$p_{CK} = 1 - e^{-\epsilon/2T}. \tag{3.3}$$

The resulting clusters are named Coniglio-Klein clusters and have the desired properties of physical clusters. An analogous algorithm of breaking bonds is anticipated in continuous systems. The goal is to find clusters that are both physically consistent and also demonstrate the ideal cluster law.

3.2.1 Hill clusters

One definition of clusters in a continuous system is based on the concept of stable clusters. Consider two particles at the minimum of their interaction potential. If the relative velocity between the two particles has a kinetic energy greater than this binding it can be expected that these two particles are not in the same cluster. This stability is related to whether a cluster is stable to particle emission for some finite time if left in a vacuum.

Stable clusters are also important in the dynamics of a liquid drop decaying in a vacuum. Previous studies show that the final clusters found in the decay of a liquid drop in a vacuum can be identified early in the evolution of the system as the stable clusters [DR93]. This highlights the importance of stable clusters in the dynamics of the process.

The coupling of the momentum phase space with the geometric phase space has the same effect as the Coniglio-Klein algorithm in the lattice system. In both cases the partitioning of the particles is based on considering bonds between all pairs and breaking them with some probability. This is done stochastically in the Ising model and based on the particles momenta in the continuous system. Unfortunately, using stability as a criterion for clustering is still ambiguous.

One example of a cluster definition considers the relative momentum of all pairs of particles. A pair of particles is considered to be bound if their relative momentum has a kinetic energy less than the potential energy binding the two. These are named Hill clusters and constitute a unique partition given the position and momenta of a collection of particles [Hil55]. Some cutoff distance of pairs is also introduced to remove spurious bonds between particles greatly removed in physical space with the same momentum. The benefits of such a partitioning is in that it is unique and efficient to calculate.

Another cluster definition using stable clusters considers the most stable partition [DR93]. The stability of a given partition is calculated as follows. The potential energy between each pair within a cluster is calculated, but not without. Also, the kinetic energy of the internal degrees of freedom within the cluster is counted, but not the kinetic energy of the center of mass velocity. The partition which has the lowest energy calculated this way is considered to be the most stable. There is no precise prescription to find such a minimum except for an exhaustive search. There are ways to find a local minimum, but the non-ergodic nature of the problem makes finding the global minimum non-trivial. These algorithm are time consuming compared to the pairwise considerations of the Hill clusters.

Ultimately, it is the faster, more simple algorithm which is employed in this work. This decision is motivated by the philosophy that different partitioning methods should yield qualitatively the same results as long as the choice is sensible, and both algorithms are sensible in considering cluster stability.

3.2.2 Probabilistic clusters

A different approach to finding a cluster partition is to disregard the particle momenta. The Coniglio-Klein algorithm for lattice systems is an example of this type of clusters where the

property of two particles being in the same cluster is probabilistic.

The definition of the Hill clusters motivates an algorithm whereby the probability of two particles at a given distance will be bound is equal to the probability that they would be bound using the Hill algorithm. The equation for the bond probability comes from integrating the Boltzmann distribution over the momenta that result in a bond and is

$$p_{Hill}(r,T) = \frac{\Gamma(3/2, -u(r)/T)}{\Gamma(3/2)}, \tag{3.4}$$

where $\Gamma(n,x)$ is the lower incomplete gamma function. A partition of the system is made by considering a bond between each pair of particles with the above probability.

The difference between this cluster definition and the Coniglio-Klein definition is in the functional form of the bond probability. The similarity between the two definitions has been noted before but the physical connection is still unclear [Sat03]. The Coniglio-Klein definition is a mathematical result completely divorced from the concept of stable clusters. It is also interesting to note that using the momentum space to define clusters is sensitive to the dimensionality of the system. Contrarily, the results leading to the Coniglio-Klein clusters show that the bond breaking probability is the same for systems in any dimensional space.

3.2.3 Comparing cluster definitions

It is expected as a first order approximation that the cluster concentrations generated by the Hill and probabilistic algorithms are the same. This similarity is due to the equipartition theorem. The canonical partition function can be separated into the independent momentum space and Cartesian space and implies that the probability of finding a set of momenta is independent of the location of the particles. Assigning random momenta to each particle weighted by the Boltzmann distribution yields the same cluster distributions as using the measured momenta. In effect, this is what the probabilistic cluster algorithm does.

Fig. 3.2 shows the difference in cluster concentrations of the two algorithms for clusters up to size 5. There are statistically significant differences in the two cluster yields originating from a subtle difference in the two definitions. A random number is drawn for each pair of particles in the probabilistic algorithm. This is contradictory insofar as the definition of Hill clusters are concerned because it implies a random momentum is drawn for a given particle for each bond it can form. For example, a fast moving particle is less likely to be bound with any other particle using the Hill algorithm, but this correlation is not captured in the probabilistic algorithm.

The monomer concentrations and the sum of cluster concentrations are important in establishing the ideal cluster law. These two values vary little between the two cluster definitions and thus lead to similar predictions of the thermodynamic properties. The trend for larger clusters is more complicated, where it is temperature dependent which algorithm produces more clusters of a given size. The discrepancies become more pronounced for larger clusters.

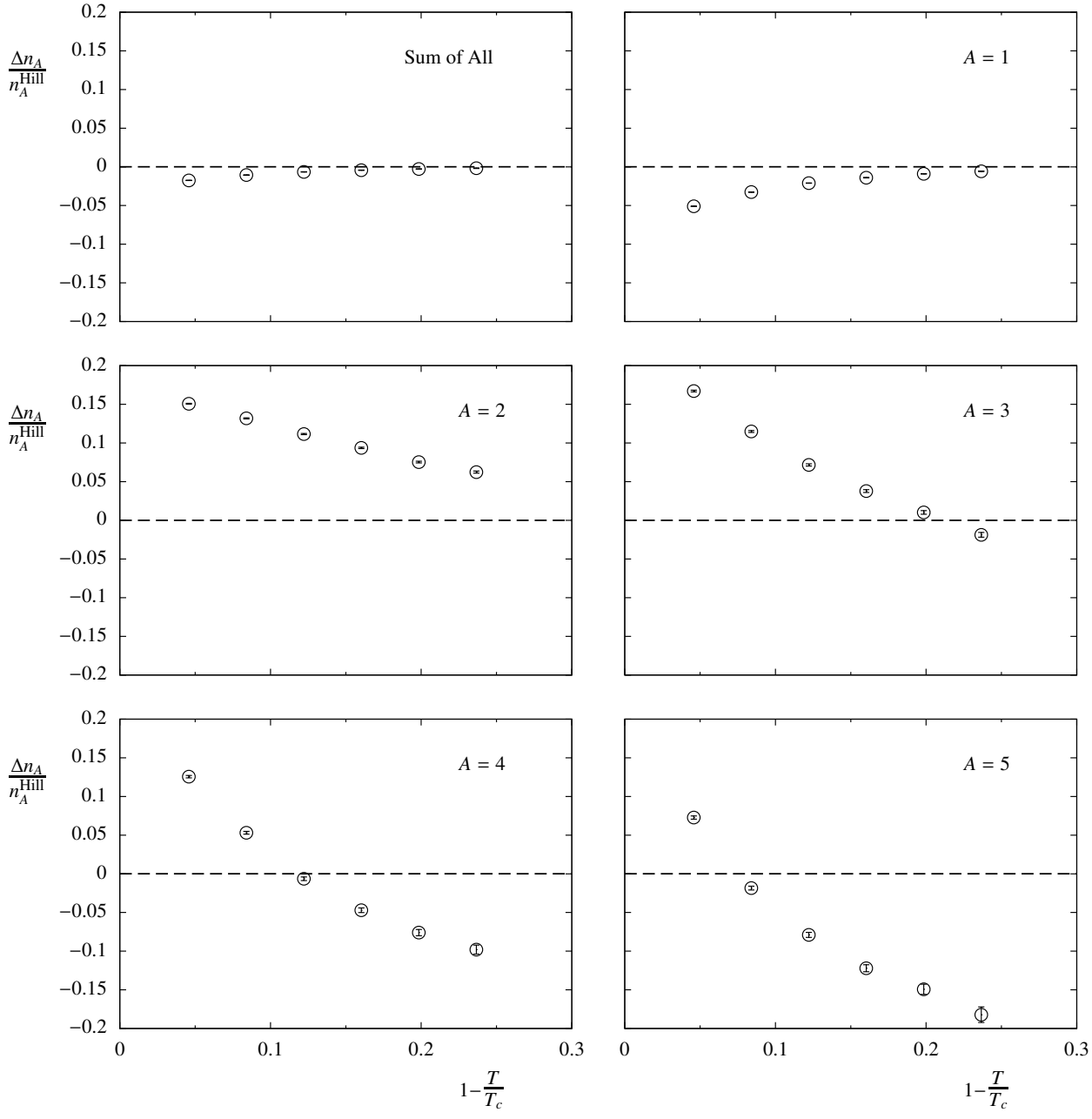

Figure 3.2: The difference in cluster concentrations from the two cluster algorithms. The value Δn_A is the difference between the Hill and probabilistic clusters, $n_A^{Hill} - n_A^{prob}$.

There are reasons to prefer the probabilistic clusters despite the fact that they do not form stable clusters. There are unphysical properties associated with the Hill clusters which then questions the utility of using stable clusters as the physically relevant partition.

The anomalous behavior of stable clusters can be summarized in the phrase "a hot gas of cold clusters" [Sat00]. The act of binding pairs of particles with a slow relative momentum results in clusters not having a kinetic energy characterized by a Boltzmann distribution. The internal degrees of freedom are colder. If the kinetic energy of the internal degrees of freedom are relatively cold to the physical temperature, then the kinetic energy of the cluster's center of mass momentum will be hotter to conserve the total kinetic energy of the system. This is in direct contrast to the probabilistic clusters where the kinetic energy of all the degrees of freedom within a cluster are thermal with the thermodynamic temperature, by construction.

The total kinetic energy of a cluster can be divided into the energy of the normal modes to demonstrate this effect in stable clusters. There are $3A$ normal modes of a cluster of size A which are divided into three types: translational, rotational, and vibrational. Three of the degrees of freedom are associated with the center of mass translational momentum. Another three degrees of freedom, for systems of $A > 2$, are associated with rotational momentum and the kinetic energy of this motion is found by diagonalizing the inertia tensor of the cluster. The remainder of the kinetic energy is associated with the vibrational degrees of freedom.

A thermal system has an energy distribution in a set of d modes as

$$P(E)dE = \frac{1}{T\,\Gamma(d/2)} \left(\frac{E}{T}\right)^{d/2-1} e^{-E/T}\, dE. \tag{3.5}$$

Plotting the energy distribution as

$$F(E)dE \equiv T\,\Gamma(d/2) \left(\frac{T}{E}\right)^{d/2-1} P(E)dE \tag{3.6}$$

produces the same exponential trend for all the distributions. Fig. 3.3 demonstrates the difference of kinetic energy distributions from clusters generated by the two algorithms. The results show that all the kinetic energies of the probabilistic clusters follow the expected trend, but the trends found for the Hill clusters do not follow a Boltzmann distribution of any temperature. For example, the translational motion follows the correct trend at high energies, but there is a deficiency of clusters at lower energies. The smaller clusters, in effect, are colder than the larger clusters in their internal degrees of motion. This is opposed to the probabilistic clusters which follow the physical intuition of thermodynamic equilibrium.

The potential energy of the clusters are also considered. The potential energy is divided into two parts; one part is the binding energy of the cluster and the other is the potential energy associated with the residual cluster-cluster interactions. Fig. 3.4 gives an example of the average potential energies of the clusters showing the qualitative attributes are consistent between the different cluster types. The residual energy per particle is constant for all cluster

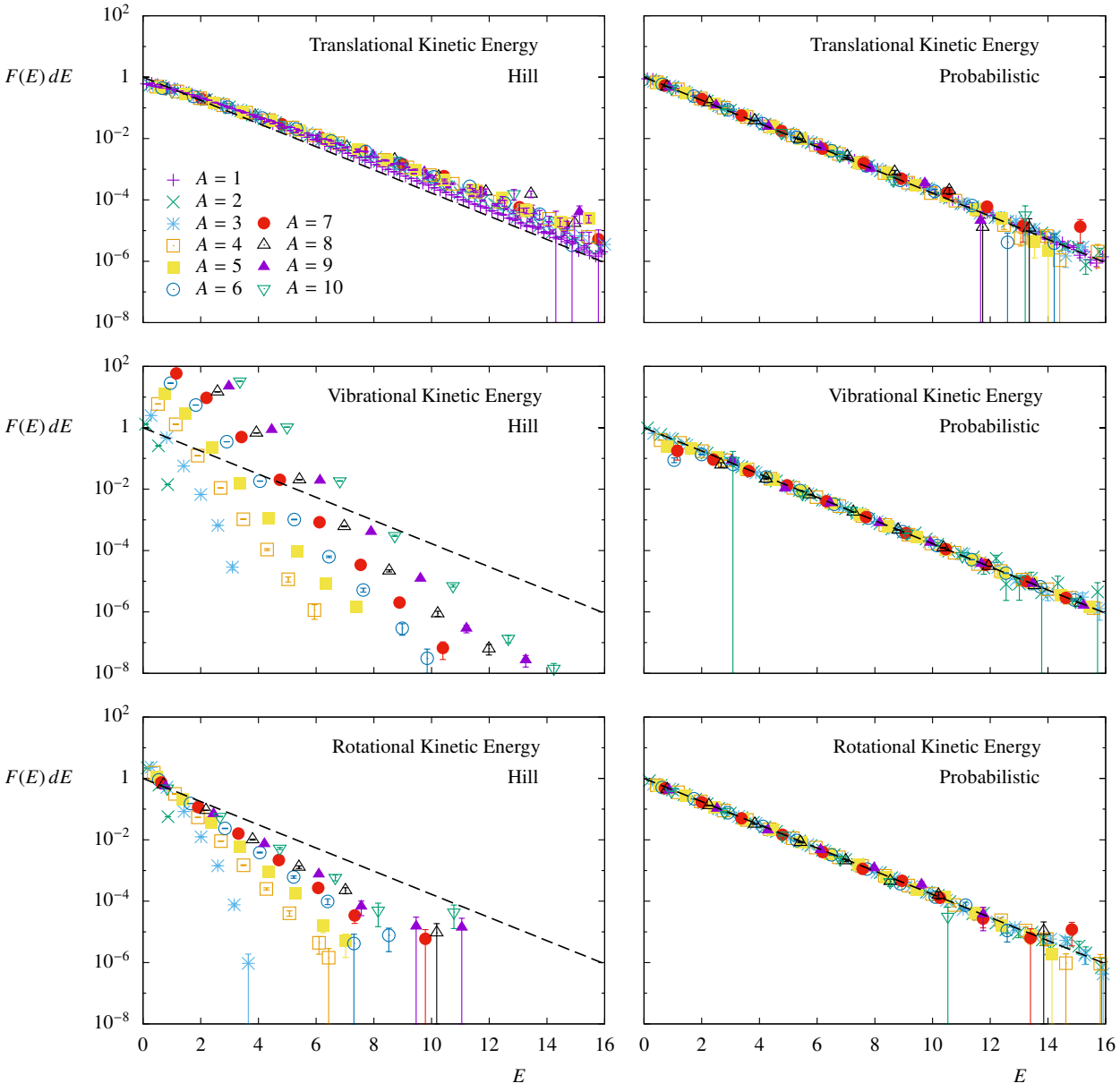

Figure 3.3: The distribution of kinetic energy of clusters divided into different degrees of freedom for $T = 1.15\epsilon$.

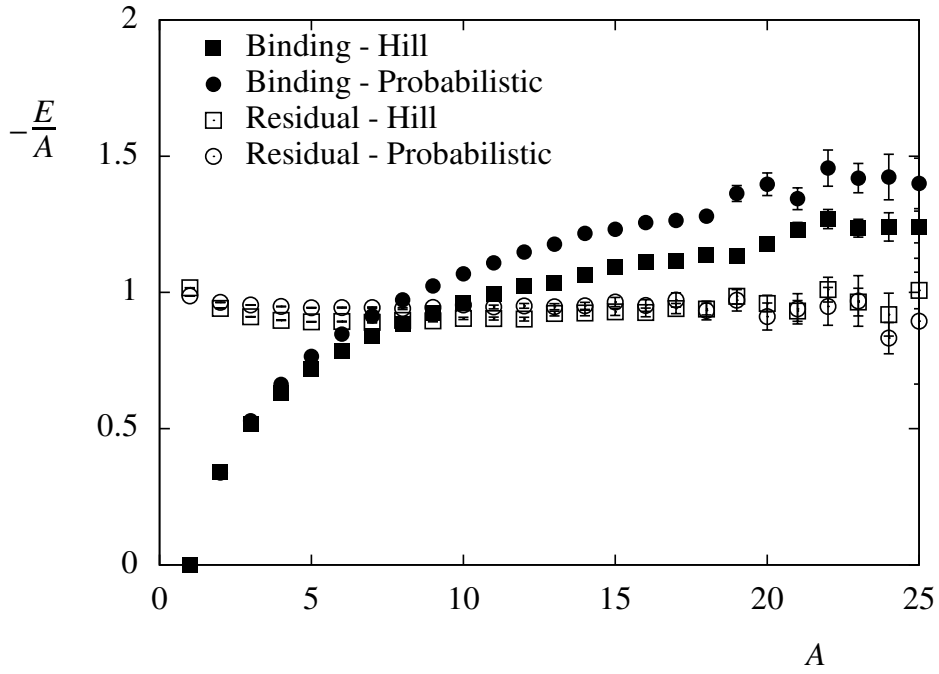

Figure 3.4: The average potential energy of the two cluster definitions for $T = 1.15\epsilon$. The filled points are the binding energy of the clusters and the unfilled points are the energies of the cluster-cluster interactions.

sizes and equal in the two cluster definitions. The Hill clusters have less binding energy on average than the probabilistic clusters. This is surprising in that the Hill clusters are colder in their internal kinetic energy yet have a higher potential energy.

The presence of a system being described with more than one temperature is discomforting. A system in equilibrium is completely described by a single temperature. This directly leads to the question of the physical significance of stable clusters, especially in consideration of the ideal gas properties hoped for these clusters. If the center of mass velocities is what gives rise to the pressure of the system, then the pressure would be too high from stable clusters.

The idea of using stable clusters as physical clusters is misleading. It implies that the clusters are well formed and persist for a measurable time in the system. At low temperatures this may be true, but the correlations at high temperatures are fleeting. There is nothing contradictory in considering a fast moving particle as a part of a cluster, even if it has little spacial correlation to the rest of the cluster a moment later.

The concentrations generated by the two cluster algorithms are similar, which is important in the context of a liquid drop decaying in a vacuum. Previous studies indicate that the clusters found at large times can be identified as the stable clusters at short times of a

hot liquid drop being placed in a vacuum [DR93]. Even though the physical significance of these clusters in reference to the system's thermodynamics is questionable, they correctly represent the concentrations of the physically consistent probabilistic clusters.

3.3 Clusters as an Ideal Gas

The ideal cluster law suggests that the physical clusters of a system are related to the bulk properties of the vapor. One way to test the ideal cluster law is to compare the temperature weighted sums of the concentrations to the mechanical pressure of the system. The ideal cluster law predicts

$$p = T \sum_{A=1}^{\infty} n_A. \tag{3.7}$$

Another way to test the ideality of the clusters is to consider the monomer concentrations compared to the system's chemical potential. The monomer concentration is predicted to be

$$n_1 = q_1 e^{\mu/T} = z, \tag{3.8}$$

where $q_1 = \Lambda^{-3}$, since monomers have no internal structure. Both the pressure and the chemical potential can be measured in the simulations and directly compared to the cluster concentrations.

The pressure of a simulation is calculated using the virial theorem. The pressure is related to the average force $\mathbf{F}$ felt upon the particles

$$p = \rho T - \frac{1}{3V} \left\langle \sum_{i=1}^{N} \mathbf{r}_i \cdot \mathbf{F}_i \right\rangle \tag{3.9a}$$

$$= \rho T - \frac{1}{3V} \left\langle \sum_{i=1}^{N-1} \sum_{j=i+1}^{N} r_{ij} \left. \frac{d\,u(r)}{d\,r} \right|_{r=r_{ij}} \right\rangle. \tag{3.9b}$$

The virial of each configuration is measured and averaged to determine the pressure.

Fig. 3.5 shows a comparison of the temperature weighted sums of the cluster concentrations versus the pressure of the system. The sum of cluster concentrations are close to the same for the two cluster definitions and data from only the probabilistic clusters are shown. Also plotted is the pressure of the system using the ideal gas law, $p = \rho T$, showing the extent that clustering changes the pressure of the system. A majority of the non-ideality is accounted for in the clustering, and the resulting temperature weighted sums approximate the actual pressure within 25% for the highest pressure and is more accurate for lower temperatures.

The chemical potential of a system is measured via the Widom insertion method [Wid63]. The fugacity is related to the following ensemble average involving the change in energy ΔE upon the addition of a particle at a random location

$$z = \Lambda^{-3} e^{\mu/T} = \rho \left\langle e^{-\Delta E/T} \right\rangle^{-1}. \tag{3.10}$$

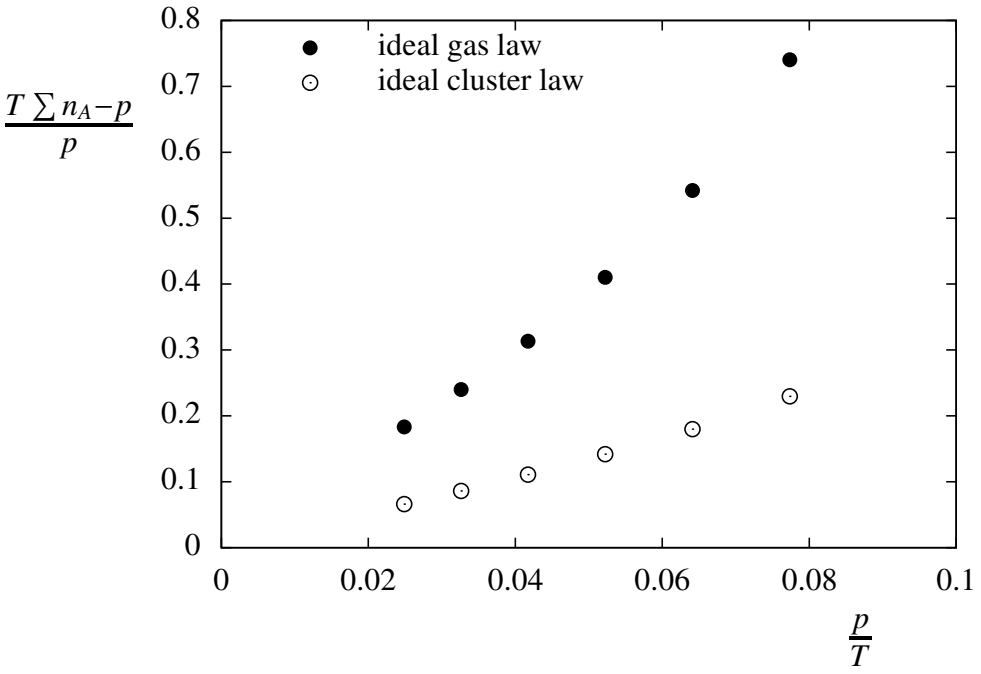

Figure 3.5: The difference between the thermodynamic pressure and the temperature weighted sums of cluster concentrations. The filled points represent the pressure of the system if it were an ideal gas. The unfilled points are the predicted pressures using the ideal cluster gas.

Fig. 3.6 presents the results of comparing the monomer concentrations to the measured fugacity. Also shown is the fugacity that would be observed for each system if the vapor were ideal, $\Lambda^{-3}e^{\mu/T} = \rho$. This comparison gives a sense of the effect clustering has on the system. The same general trend is seen in the chemical potential as in the pressure.

These two tests of the ideal cluster theory show the success of the clustering algorithms used to produce a physically relevant partition. The observed clusters are well described by the ideal cluster law and account for most of the non-ideality of the vapor. The discrepancies represent a source of error in predicting the bulk properties of the vapor using clusters. Perhaps a different cluster algorithm could produce more ideal clusters but the current algorithm is accurate enough to relate physical clusters to the thermodynamics of a vapor.

3.4 Conclusion

The connection between physical clusters to the bulk properties of a vapor is not trivial. Molecular simulations allow the study of clusters in the Lennard-Jones model to test the ideal cluster theory.

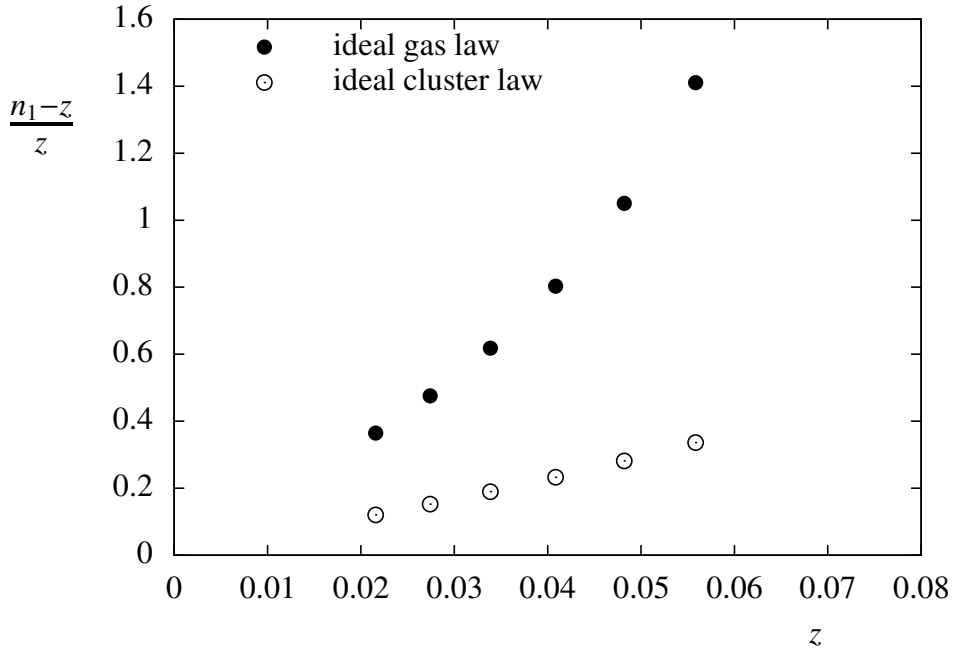

Figure 3.6: The difference between the thermodynamic fugacity and the monomer concentration. The filled points represent the chemical potential of the system if it were an ideal gas. The unfilled points are the predicted chemical potentials using the ideal cluster gas.

Stable clusters are an intuitive approach to partitioning the system into clusters. These clusters are seen to have properties contradictory to the concept of thermal equilibrium despite their simplicity. Probabilistic clusters are physically consistent and are favored for this reason. The similarity in cluster concentrations found in the two cluster algorithms makes this choice superficial in the context of testing the ideal cluster theory.

The ideal cluster theory is tested by comparing the cluster concentrations to the bulk properties of the Lennard-Jones vapor. Namely, the sum of cluster concentrations are related to the pressure and the monomer concentrations are related to the chemical potential. The relations are not exact but nevertheless establish the connection between the clusters and the bulk properties.

Chapter 4

From Fisher Scaling to Phase Diagrams

The purpose of this chapter is to demonstrate the predictive power of the Fisher droplet model in the Lennard-Jones system. Here, the ideas discussed in Chapter 2, the validity of the Fisher equation of state, and Chapter 3, the relevance of physical clusters, are combined to generate the phase diagram of the Lennard-Jones model.

An analogous analysis as done with the molecular systems in Chapter 2 is done for the Lennard-Jones model to establish the relevance of the Fisher equation of state for the system. Then, Fisher scaling is shown to be observed in the physical cluster concentrations discussed in Chapter 3. The fitted parameters of this scaling is then used to extrapolate the phase diagrams for all temperatures.

4.1 The Fisher Equation of State and the Lennard-Jones Model

As established in Chapter 2, the Fisher equation of state effectively describes molecular vapors. Given that the Lennard-Jones fluid is phenomenologically similar to molecular fluids, the Fisher equation of state is anticipated to be a valid representation of the equation of state for the system.

The Fisher equation of state is parametrized by five constants, τ, σ, q_0, c_0, and T_c, as found in the equation that describes the cluster concentrations, n_A [Fis67a; Fis67b],

$$n_A(T) = q_0 \, A^{-\tau} \, \exp\left[-c_0 \, A^{\sigma} \left(\frac{1}{T} - \frac{1}{T_c}\right)\right]. \tag{4.1}$$

As is done in Chapter 2 for molecular fluids, nominal values of these five parameters can be established by considering the observed phase coexistence of the fluid.

The constants τ and σ are critical exponents and are the same for all fluids and have nominal values of 2.2088(2) and 0.6395(4), respectively [PV02; Cam02].

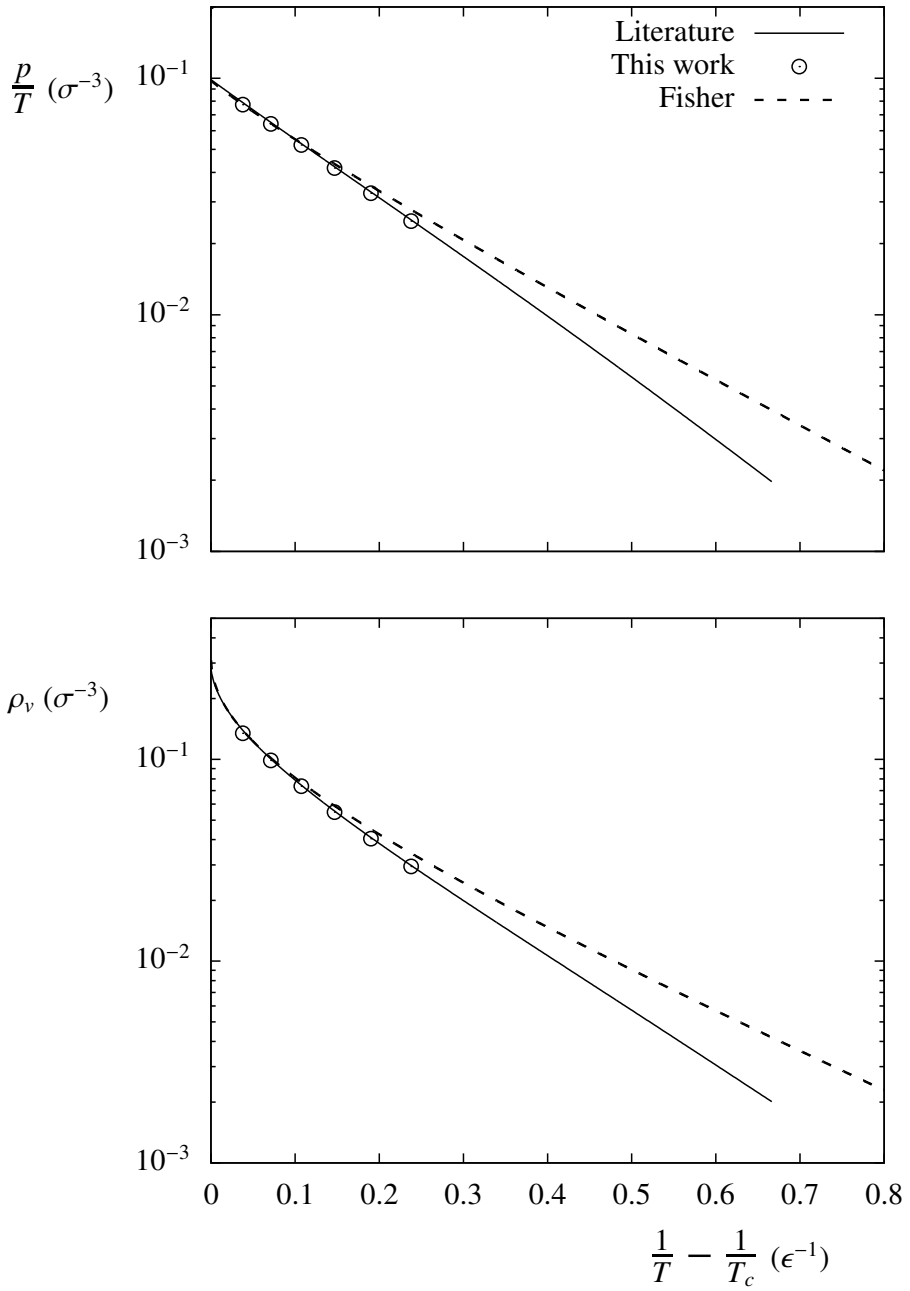

Figure 4.1: Phase diagrams of the Lennard-Jones fluid. The solid line is the phase coexistence reported in the literature [Nat12; JZG93], with the points from the measurements made in this work. The dashed line is the predicted phase coexistence using the nominal values of the parameters in the Fisher equation of state.

The values of T_c and q_0 are established by the critical point properties of the fluid. The critical temperature for the Lennard-Jones model is $T_c = 1.3120(7)\epsilon$ [PP98] and the value of q_0 is predicted from either the critical density or the critical pressure,

$$\rho_c = q_0\zeta(\tau - 1) \tag{4.2a}$$

$$\frac{p_c}{T_c} = q_0\zeta(\tau). \tag{4.2b}$$

The Lennard-Jones model has a critical density of $\rho_c = 0.316(1)\sigma^{-3}$ and critical pressure of $p_c = 0.1279(6)\epsilon/\sigma^3$ [PP98]. Two slightly different values for q_0 are predicted using the above equations. These two values are within 10% of each other and the value suggested by the critical pressure is $q_0 = 0.0657(3)$.

As described in Chapter 2, the value of c_0 in the Fisher theory has no clear thermodynamic interpretation. The slope of the pressure-temperature phase diagram at the critical point produces a consistent value of c_0 for molecular fluids, where

$$\lim_{T\to T_c} \frac{d}{d\,1/T}\left(\frac{p}{T}\frac{T_c}{p_c}\right) \sim -\frac{\zeta(\tau-\sigma)}{\zeta(\tau)}c_0. \tag{4.3}$$

The expected value of c_0 for the Lennard-Jones model is $c_0 \simeq 4.29\epsilon$. Systems with the same value of c_0/T_c demonstrate the principle of corresponding states. The above value of c_0 corresponds to $c_0/T_c \simeq 3.27$ and is comparable to the values associated with the noble gases, $c_0/T_c \simeq 3.1$.

In Fig. 4.1, the predicted phase diagrams using these five nominal values in the Fisher equation of state are compared to the measured phase diagrams of the Lennard-Jones fluid [Nat12; JZG93]. As with the experimental phase diagrams of molecular fluids, the Fisher equation of state correctly predicts the phase coexistence near the critical point but is less reliable in describing the trend at lower temperatures.

These evaluations of the Fisher theory parameters are determined by thermodynamic properties. Next, the relation of the physical clusters to this form of the equation of state is established.

4.2 Fisher Scaling of Physical Clusters

Chapter 3 shows how the physical clusters observed in molecular simulations relate to thermodynamic properties, independent of the mathematical description of the cluster concentrations as a function of size and temperature. Here, the size distribution is studied in light of the Fisher droplet model.

To give context to the cluster concentrations as a function of inverse temperature, Fig. 4.2 shows the concentrations for clusters of up to size 10. The Arrhenius nature of the concentrations is revealed by the linear trends as a function of $1/T$. The lines in Fig. 4.2 are the linear fits done independently for each cluster size and are plotted to guide the eye.

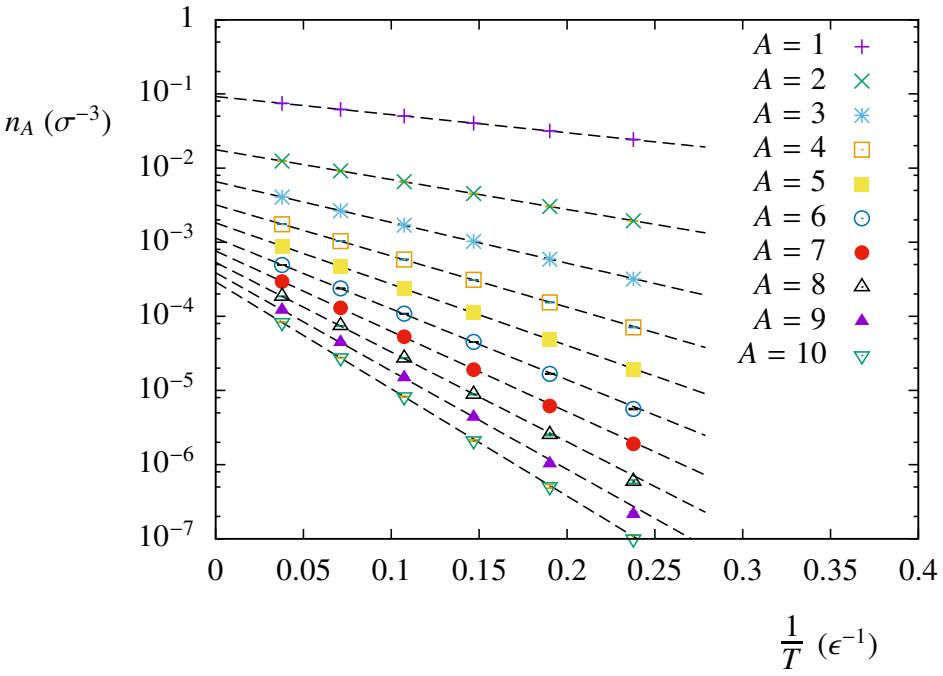

Figure 4.2: The physical cluster concentrations of the Lennard-Jones model for clusters up to size $A = 10$.

An effective way to demonstrate Fisher scaling of the cluster concentrations is to scale the concentrations and temperature for each cluster size such that all the data falls on a single trend. Rearranging the Fisher equation for the cluster concentrations yields

$$\frac{n_A}{q_0\, A^{-\tau}} = \exp\left[-c_0\, A^{\sigma}\left(\frac{1}{T} - \frac{1}{T_c}\right)\right], \tag{4.4}$$

showing that all the cluster concentrations collapse onto a single linear trend when the concentrations scaled by $q_0 A^{-\tau}$ are plotted as a function of $c_0\, A^{\sigma}(1/T - 1/T_c)$.

A first attempt of scaling the cluster concentrations is to use the nominal values of the five parameters as discussed in the previous section and is shown in the top panel of Fig. 4.3. The data do collapse relative to the unscaled concentrations but do not completely follow a single trend. This result is not completely surprising when considering the success of the Fisher equation of state to reproduce the coexistence in the temperature range considered, as seen in Fig. 4.1.

A better scaling of the data is obtained by fitting the five parameters to the measured cluster concentrations. The bottom panel of Fig. 4.3 shows the results and the fitted parameters are reported in Tab. 4.1. The data collapse is visually pleasing and effectively described by a single trend. Despite this visual agreement, the reduced chi-squared of the

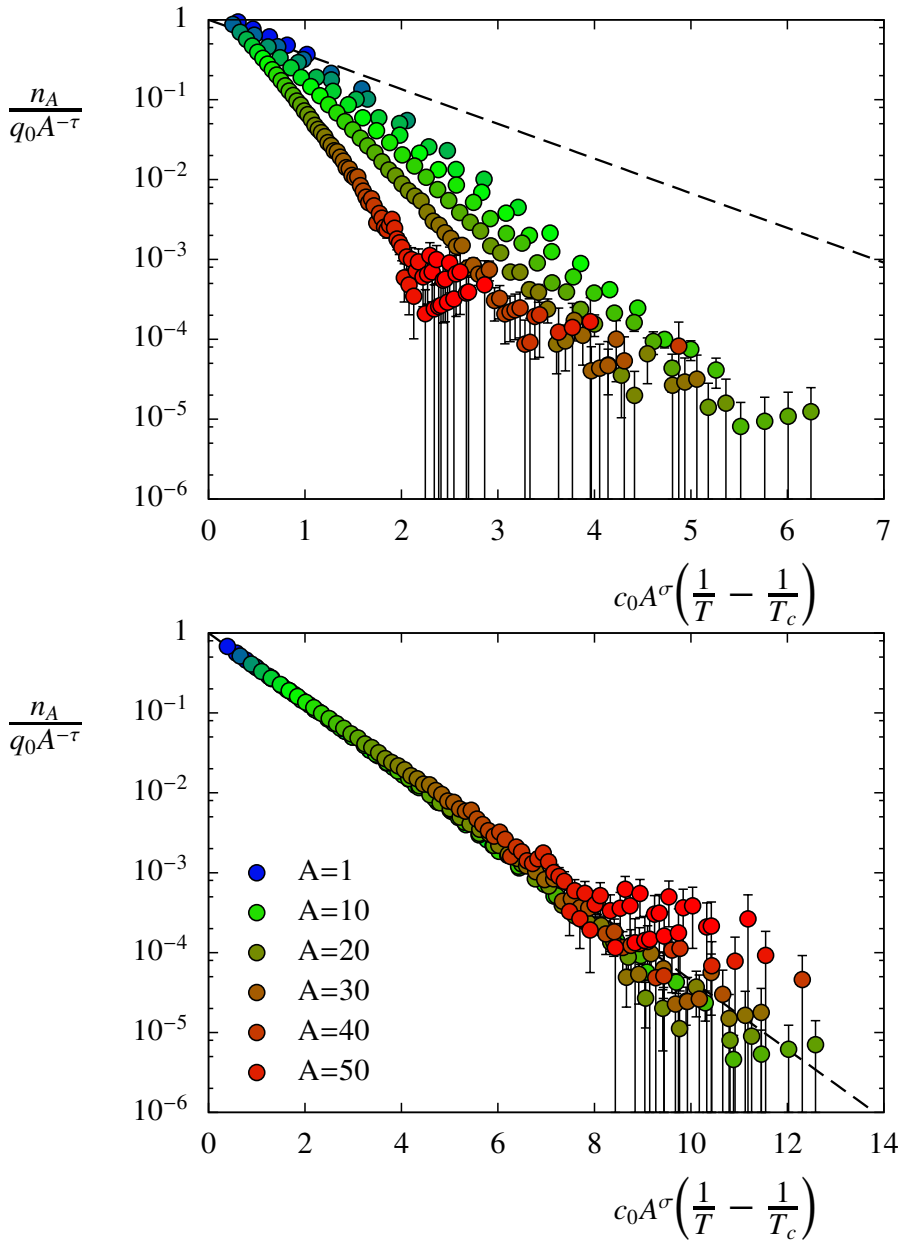

Figure 4.3: Fisher scaling of the physical clusters in the Lennard-Jones model. The top plot uses the nominal parameters and the bottom uses the fitted parameters of the Fisher equation.

Table 4.1: A summary of the five parameters of the Fisher theory. The nominal values are deduced from thermodynamic properties of the fluid and the fit values are from fitting Eq. 4.4 to the cluster concentrations.

Parameter	Nominal Value	Fit Value
τ	2.2088(2)	2.190(4)
σ	0.6395(4)	0.748(2)
T_c (ϵ)	1.3120(7)	1.3689(14)
q_0 (σ^{-3})	0.0657(3)	0.1100(5)
c_0 (ϵ)	$\simeq$4.29	5.614(7)

fit is $\widetilde{\chi}^2 = 28.6$ indicating that the fit is not statistically accurate. Furthermore, the values of the fit parameters are also questionable compared to the nominal values.

First, consider the critical exponents. The extracted value of τ is within 1% of the nominal value. This indicates that the cluster concentrations extrapolate to the anticipated power law at the critical point. This is in contrast to the extracted value of σ, which is 17% percent larger than the nominal value. The implication is that the surface of a cluster is not spherical and compact, but rather are of a smaller fractal dimension.

The extracted critical temperature is within 5% of the nominal value despite the discrepancies of some of the fit parameters. This observation suggests that the critical point can be sufficiently deduced from cluster concentrations away from the critical point.

The same cannot be said of the critical pressure or density which depends on the constant q_0. The extracted value of q_0 is almost double the nominal value and leads to a similar doubling of the predicted critical density and pressure. Furthermore, the nature of the zeta function magnifies the error found in τ, especially in calculating the critical density. The smaller value of τ leads to even larger predictions of the critical density and pressure.

The elusive nature of c_0 makes it difficult to compare the extracted value to the nominal value. The value of c_0 is dictated by the monomer concentrations due to the overwhelming statistics associated with the smaller clusters. Differences between the measured phase diagrams and those predicted from the Fisher theory in Fig. 4.1 give rise to the extracted c_0 to be larger than the nominal value. This observation is reflected in the fitted value.

In summary, the Fisher droplet model can be used to effectively describe the concentrations of physical clusters in the Lennard-Jones model. Not all of the fitted parameters match with the nominal values; some of these differences can be explained at this level of study but others require a more thorough study of the clusters. Regardless of these incongruences, it is emphasized that the measure of the critical temperature is accurate and is effectively found from a fit to the cluster concentrations away from the critical point.

4.3 A Further Look Into Fisher Scaling

The Fisher droplet model makes several approximations to arrive at a succinct formulation of the cluster concentrations. Some of these approximations may differ from the actual cluster concentrations observed in a simulation. Examples of these approximations are the Arrhenius nature of the cluster concentrations, the simplification of the cluster surface energy, and the relation between the surface energy and the surface entropy.

The Arrhenius nature of the cluster concentrations can be exploited to investigate the cluster energy and entropy independently. The general form of the cluster concentrations in terms of the surface energy E_s and surface entropy S_s is

$$\log n_A = -\frac{E_s(A)}{T} + S_s(A). \tag{4.5}$$

It is assumed in the derivation of the Fisher droplet model that E_s and S_s are temperature independent. If this is true, E_s and S_s for each cluster size can be found by fitting the above equation to the respective concentrations and can be compared to the predictions of the Fisher theory.

Another assumption of the Fisher theory is in the definition of the surface energy of the clusters as $E_s = c_0 A^\sigma$. This assumption is predicted to be inaccurate due to the difference between the fitted and nominal values of σ. The extracted values of E_s from the fits to Eq. 4.5 allow for a direct study of this assumption.

A third assumption of the Fisher model is in the direct relation of the surface entropy with the surface energy and critical temperature. If the assumed surface energy term is inaccurate, how does that affect the surface entropy? The relations between E_s, S_s, and T_c are significant aspects of the Fisher theory and need to be better understood.

These three assumptions are considered in turn.

4.3.1 Arrhenius trends of cluster concentrations

Up to this point the Arrhenius trend of the cluster concentrations has been assumed to be correct. Here the validity of this assumption is considered. The validity of using the Arrhenius theory is found through considering the reduced chi-squared values when fitting Eq. 4.5 to the cluster concentrations for different cluster sizes. The fits of the equation for the first ten cluster sizes are seen in Fig. 4.2. The $\widetilde{\chi}^2$ of the fits as a function of cluster size are shown in Fig. 4.4. Cluster sizes up to $A = 33$ are studied, corresponding to clusters that were observed in at least three of the modeled temperatures. A $\widetilde{\chi}^2$ value near 1 indicates that the theory is statistically consistent with the data.

It is observed that the large cluster sizes have a $\widetilde{\chi}^2$ value near 1 and the Arrhenius theory statistically describes the data. On the contrary, the $\widetilde{\chi}^2$ for $A < 10$ are larger than 5, indicating that the Arrhenius theory is not exact. This observation is consistent with the idea that the Arrhenius trend is a first order approximation for the cluster concentrations. The success of the Arrhenius theory is predicated upon the values of E_s and S_s being constant

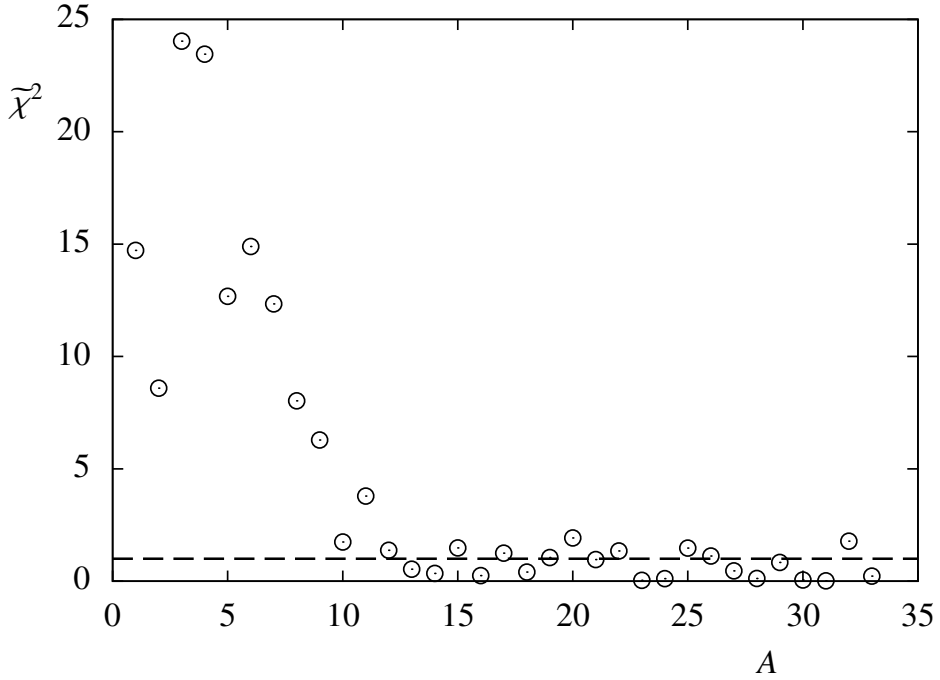

Figure 4.4: The $\widetilde{\chi}^2$ of fitting the Arrhenius equation, Eq. 4.5, to the cluster concentrations.

as a function of temperature. The large statistics for the smaller cluster sizes give rise to measurements with enough precision that higher order terms accounting for the change in E_s and S_s become measurable..

The Arrhenius theory is observed to be accurate in describing the cluster concentrations at coexistence. The level of accuracy is higher than what is observed in using the Fisher equations.

4.3.2 Cluster surface energy

The validity of the Arrhenius theory indicates that the cluster surface energy is constant as a function of temperature. The A dependence of the surface energy is studied by considering the slopes of the Arrhenius trends as shown in Fig. 4.5. The top plot shows the result of fitting the whole range of cluster sizes using the surface energy found in the Fisher droplet model, $E_s = c_0 A^\sigma$. The fitted parameters are consistent with those found from fitting all cluster sizes simultaneously with the Fisher equation, with $c_0 = 5.614(12)$ and $\sigma = 0.748(3)$. As discussed previously, this value of σ is significantly larger than the nominal value of 0.6395(4). As evidenced by a chi-squared of $\widetilde{\chi}^2 = 111$, this parametrization of the surface energy is insufficient to describe the cluster concentrations.

The Fisher droplet model was initially derived to describe the concentrations of large

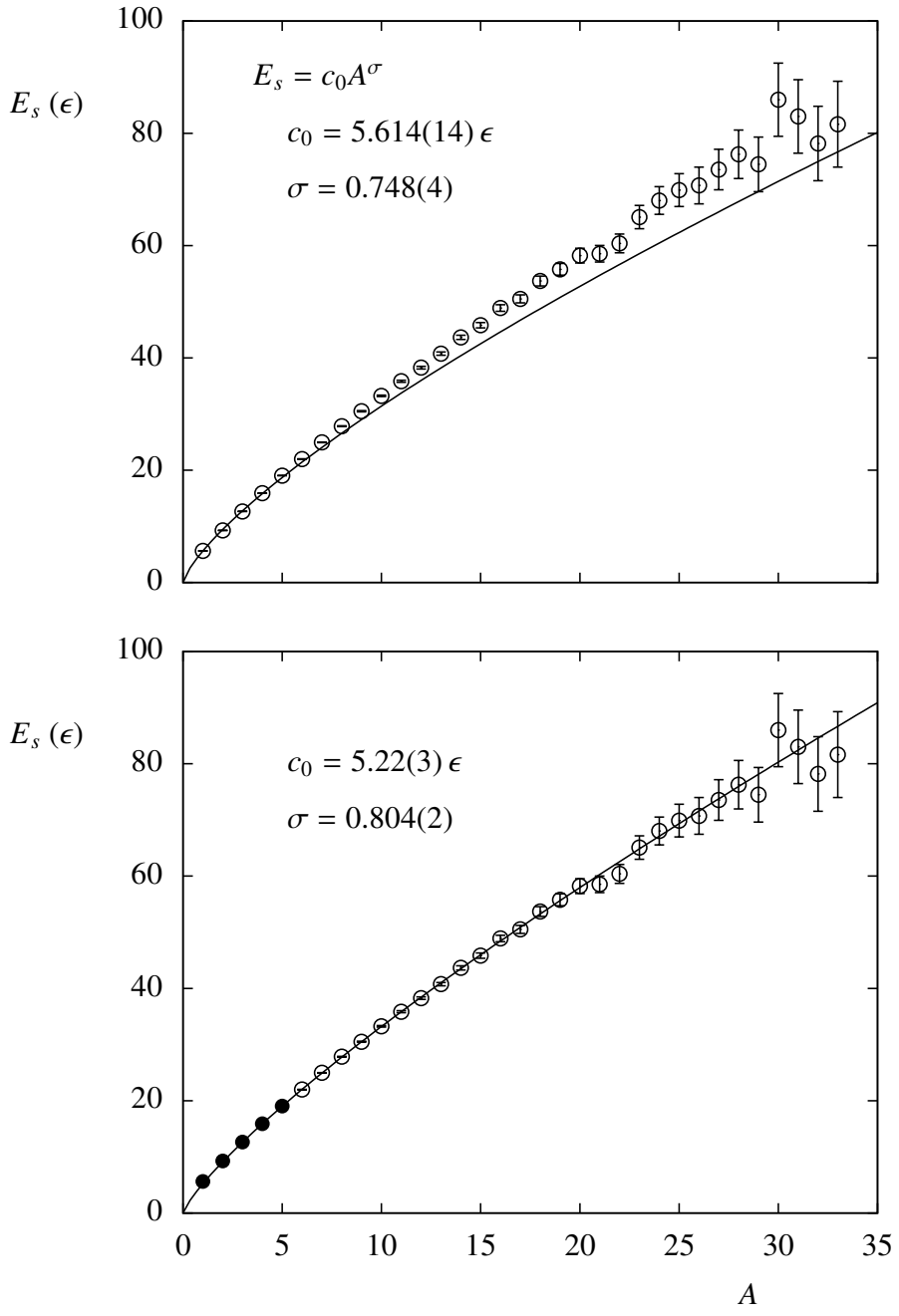

Figure 4.5: The surface energy of clusters as a function of A. The lines are fits using $E_s = c_0 A^\sigma$, the top being fit over the entire range of A and the bottom for $A > 5$.

clusters at the critical point and the validity of using this equation for clusters as small as $A = 1$ is not immediately evident. Furthermore, the dominance of the large statistics for $A = 1$ heavily weighs the fit to the small clusters. The role of the smallest cluster sizes can be removed by fitting the equation to only larger cluster sizes. The same fit of $E_s = c_0 A^\sigma$ for clusters of $A > 5$ is shown in the bottom panel of Fig. 4.5. The fit describes the larger cluster energies well, with $\widetilde{\chi}^2 = 0.4525$. What is surprising is that the fit suggests $\sigma = 0.804(2)$, a value even larger than the overpredicted value generated in the previous fit.

An alternative form of the surface energy is also considered in an attempt to improve the evaluation of the surface energy. The leptodermous expansion can be used to fit the energies, where the exponent σ is set equal to 2/3 and the curvature term is introduced,

$$E_s = a_s A^{2/3} + a_r A^{1/3}. \tag{4.6}$$

Fig. 4.6 displays the results for fitting both the entire range of cluster sizes and for $A > 5$, as was done for the previous fits. The same pathology is observed as for the previous fits; the fit is only consistent for the larger cluster sizes. The fitted parameters for the larger cluster sizes are $a_s = 9.98(6)$ and $a_r = -6.03(11)$, resulting in a fit with $\widetilde{\chi}^2 = 0.5178$.

Using the leptodermous expansion for c_0 alludes to the thermodynamic property to which it is supposedly related, the surface tension. The difference between the surface tension γ and the constant c_0 is discussed in Chapter 2, with the conclusion that there are irreconcilable differences between the two. It is still worth commenting on the relation of the two terms found in the fit of the leptodermous expansion for the case of the Lennard-Jones model.

As discussed in Chapter 2 in context of molecular fluids, the surface tension, converted to units of per $A^{2/3}$, of the Lennard-Jones model is linear with temperature and goes to zero at the critical point [Nat12]. Interpreting c_0 as the slope of this plot yields $c_0 = 13.58(13)$. It is curious to note that the inclusion of a curvature term in the surface energy raises the value of c_0 closer to this value. Unfortunately, this interpretation is unphysical because it does not explain the scaling at the critical point which suggests a value of $c_0 \simeq 4.29$. The critical scaling is unchanged by the presence of a curvature term.

It is also interesting to consider the value of the curvature term and its relation to the Tolman length [Tol49]. The surface energy is written in terms of a droplet's radius R as

$$E_s = \gamma \left(1 - \frac{2\delta}{R}\right) R^2, \tag{4.7}$$

where γ is the surface tension and δ is the Tolman length. The curvature term is related to the Tolman parameter as

$$\delta = -\frac{a_r}{2a_s} \left[\frac{3}{4\pi\rho_\ell}\right]^{1/3}. \tag{4.8}$$

Using a coexistence liquid density found at $T = 1.00\epsilon$, the observed curvature coefficient gives a Tolman length of $\delta = 0.211(4)\sigma$. There is no general consensus on what the Tolman length in the Lennard-Jones system should be and is an area of current research [GB09; GB02;

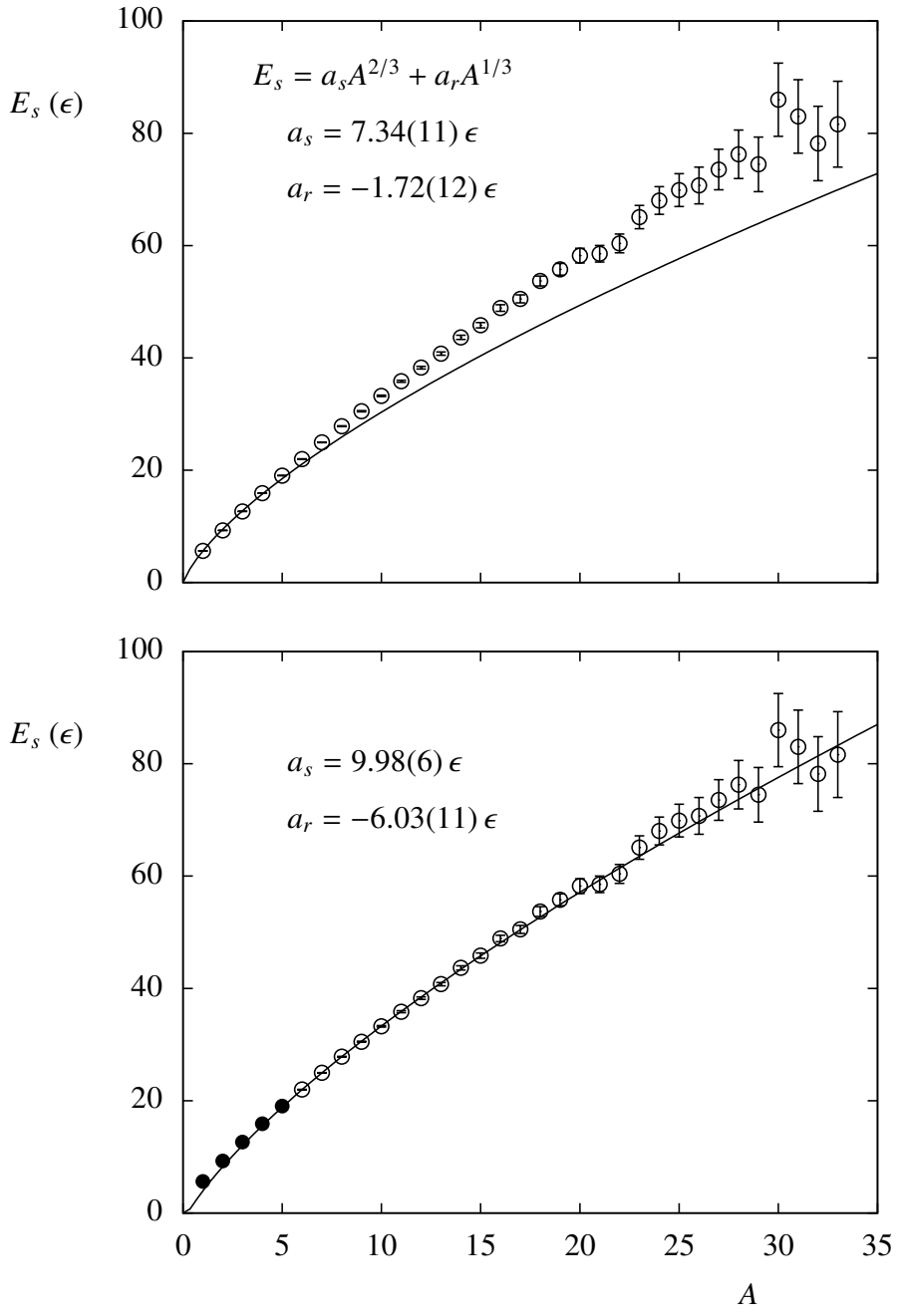

Figure 4.6: The surface energy of clusters as a function of A. The lines are fits using $E_s = a_s A^{2/3} + a_r A^{1/3}$, the top being fit over the entire range of A and the bottom for $A > 5$.

WF98]. The sign of the Tolman length is even debated. The value found here is consistent with many published values, being positive and a few tenths of a particle's diameter. The questionable connection between the surface tension and these surface energies makes the significance of this extracted Tolman length unclear.

The surface energy for the small clusters eludes being simply parametrized. Furthermore, the disconnect between the notions of surface tension and the role of the term $c_0 A^\sigma$ in the Fisher theory makes it difficult to determine what is expected for these values. The use of $c_0 A^\sigma$ in the Fisher theory is found to be the largest source of error in describing the physical cluster concentrations.

4.3.3 Cluster surface entropy

It is the relation of the surface entropy and the critical temperature that makes the Fisher theory useful in determining the limits of phase coexistence. Also, the relation of the surface energy and entropy is an assumption used in developing the Fisher theory. These aspects of the surface entropy can be studied through considering the Arrhenius trends in the limit of $1/T = 0$.

In the Fisher theory, the surface entropy is expected to be

$$S_s = \ln q_0 - \tau \ln A + \frac{c_0 A^\sigma}{T_c}. \tag{4.9}$$

The validity of this relation relies on three things. First, the surface entropy includes a term proportional to the surface energy. Second, the proportionality constant between this term and the energy is related to the critical temperature. Third, the cluster concentration follows a power law at the critical point.

The previous section revealed the difficulty of determining a consistent description of the surface energy and the same difficulty would be expected in defining the surface entropy. The analysis would be simple if the higher order terms associated with the surface energy are equivalent to those associated with the surface entropy. The slope and intercept of the Arrhenius trends can be plotted together to determine if there is a connection between the two. The expected relation is

$$S_s = \ln q_0 - \tau \ln A + \frac{E_s}{T_c}. \tag{4.10}$$

Fig. 4.7 is a plot of these two values along with a fit of the above equation. Not only is the fit good with a $\widetilde{\chi}^2 = 2.261$, the fit parameters are similar to the expected values. The critical exponent τ is found to be $\tau = 2.2935(14)$ and the critical temperature is $T_c = 1.3432(4)$. This fit is done for all cluster sizes and correctly relates the slope and intercept of the Arrhenius trends for all cluster sizes. This result indicates that the higher order terms that describe the cluster energies are the same in the cluster entropy.

There may be higher order terms associated with τ that affect the cluster concentrations at the critical point. These terms would explain why the extracted values of τ and T_c from

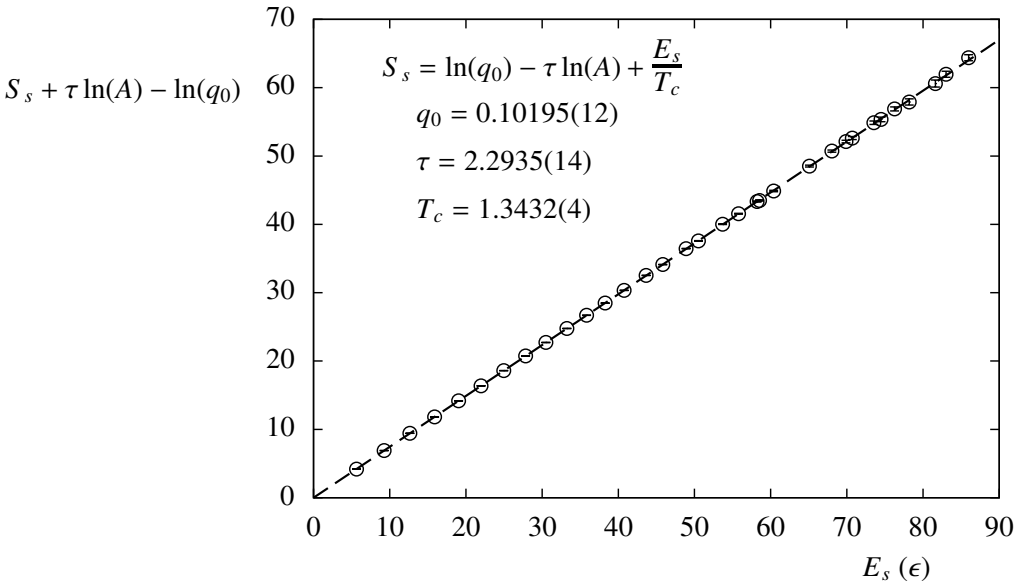

Figure 4.7: A plot of the cluster surface entropy versus the cluster surface energy.

the fit are not exactly the nominal values. The accuracy of these two constants indicate that these higher order terms are not as significant as those associated with the surface energy.

These considerations demonstrate the reliability of using the Fisher droplet model to extract the critical temperature on the basis of cluster concentrations. Even though the higher order terms are important in describing a cluster's surface energy, the same terms are found in the surface entropy. The relation of the surface energy and entropy is seen to hold even for the smallest clusters. Furthermore, the higher order terms are not as important for the cluster concentrations at the critical point and, as a result, the critical temperature is accurately predicted.

4.4 Constructing Phase Diagrams

4.4.1 The vapor phase and Fisher scaling

As discussed previously, the implication of the Fisher droplet model goes beyond describing the cluster concentrations and the critical temperature, it also allows for predicting the liquid-vapor phase diagrams at all temperatures. Using the ideal cluster theory in conjunction with

the Fisher droplet model gives the coexistence densities and pressures,

$$\frac{p}{T} = \sum_{A=1}^{\infty} q_0 A^{-\tau} \exp\left[-c_0 A^{\sigma}\left(\frac{1}{T} - \frac{1}{T_c}\right)\right], \tag{4.11a}$$

$$\rho = \sum_{A=1}^{\infty} q_0 A^{1-\tau} \exp\left[-c_0 A^{\sigma}\left(\frac{1}{T} - \frac{1}{T_c}\right)\right]. \tag{4.11b}$$

The five parameters found from fitting the cluster concentrations are used to generate the phase diagrams shown in Fig. 4.8. Also shown are the phase diagrams of the Lennard-Jones system as reported in the literature [Nat12; JZG93] and the directly measured properties from the simulations. Notice how the phase coexistence is properly described in the temperature range of the simulations performed in this study. This agreement is due to the success of the physical cluster theory, as discussed in Chapter 3. The slight overprediction of the pressure is a result of the ideal cluster law overpredicting the pressure.

The agreement at low temperatures stems from the Clausius-Clapeyron equation and the validity of assuming the vapor is ideal. The high statistics of the monomers in the simulation give rise to an accurate description of the smallest clusters. Furthermore, the monomers dominate the sums in Eq. 4.11 at low temperatures and create an accurate extrapolation of the phase diagram in this region.

The extrapolation of the phase diagrams to the critical point is less accurate than for low temperatures. The Fisher theory predicts higher densities and pressures than are actually observed beyond the highest temperature studied in the simulations. The highest deviations occur at the critical temperature itself, where the predicted critical density and pressure are double the expected value, with $\rho_c = 0.644(12)\sigma^{-3}$ and $p_c = 0.2254(11)\epsilon\sigma^{-3}$. These discrepancies stem from the inability of the Fisher theory to consistently describe the larger cluster sizes simultaneously with the small. The critical scaling is also incorrect since the critical exponent σ differs from the nominal value.

Fig. 4.9 shows the constructed phase diagrams plotted in their reduced units. This representation is important in the context of the nuclear phase diagram, where the absolute concentrations are not directly measured. Instead, the relative yields of isotopes are related to relative concentrations. As discussed in the previous paragraph, the inaccuracy of the critical density and pressure give rise to the discrepancies found in the reduced phase diagrams.

4.4.2 The liquid phase and Guggenheim scaling

As discussed in Chapter 2, Guggenheim scaling can be used to predict the liquid coexistence densities when given the vapor densities. Furthermore, a more accurate measure of the critical density and pressure can be predicted if a liquid density for a single temperature is known. This method is the only way to construct the absolute phase diagram of nuclear matter by using the density of nuclei in their ground states.

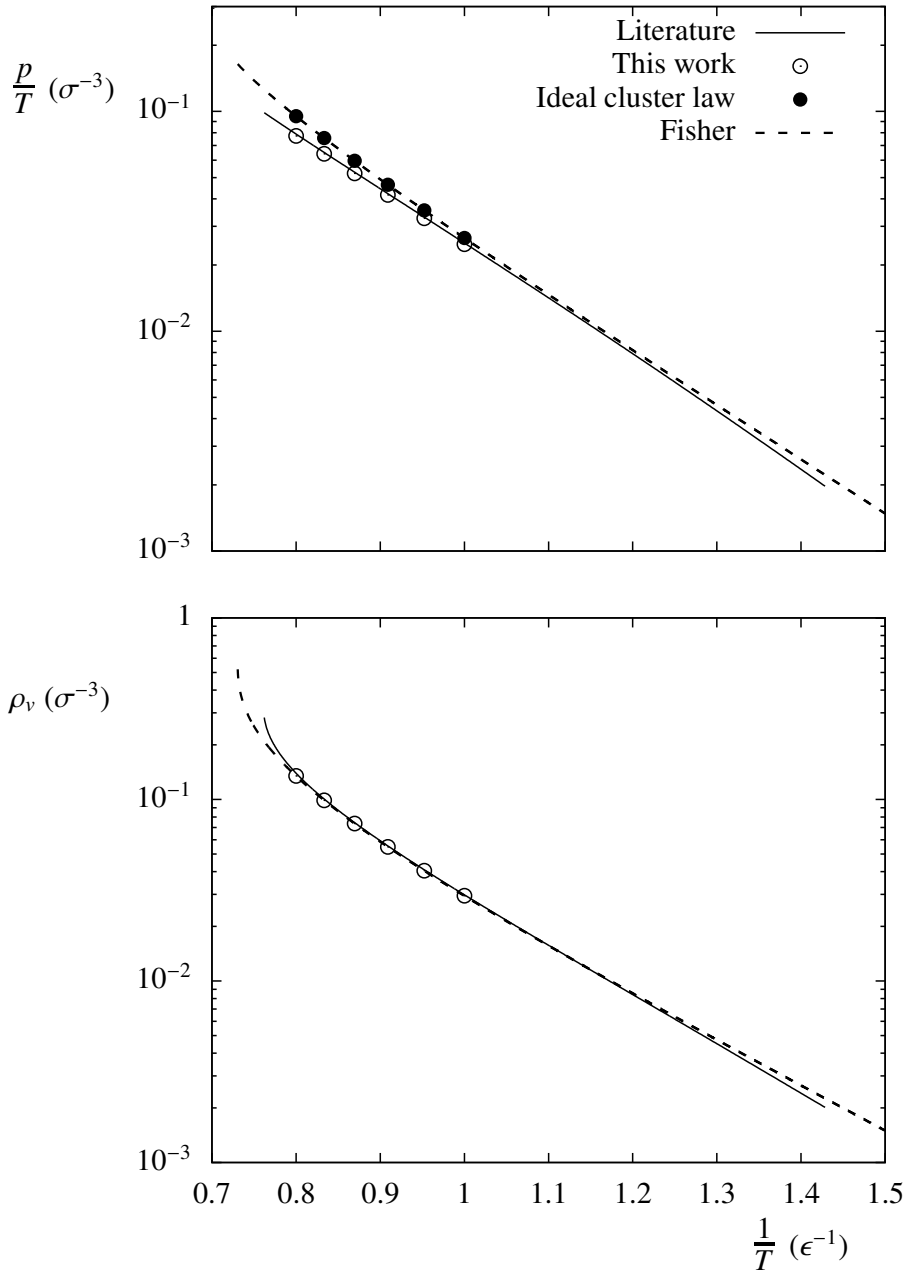

Figure 4.8: Phase diagrams of the Lennard-Jones fluid compared to those generated from the fits to the Fisher equation. The points are measurements from the simulations. There are two measurements in the case of the pressure based upon the thermodynamic definition of the pressure and the sum of cluster concentrations.

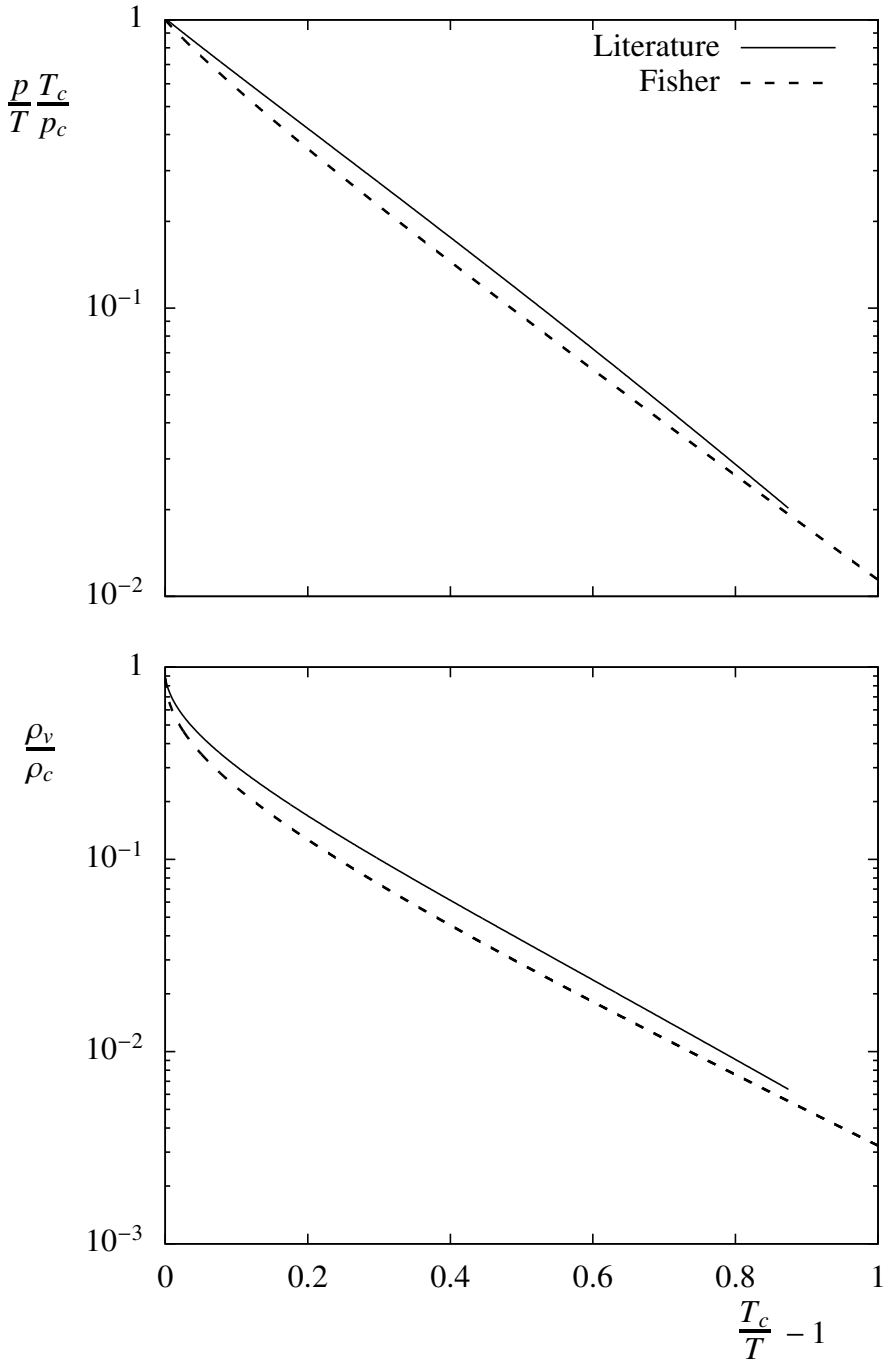

Figure 4.9: Reduced phase diagrams of the Lennard-Jones fluid compared to those generated from the fits to the Fisher equation.

The premise of this method uses the scaling result suggested by Guggenheim [Gug45; Gug93],

$$\frac{\rho_{\ell,v}}{\rho_c} = 1 + b_1\left(1 - \frac{T}{T_c}\right) \pm b_\beta\left(1 - \frac{T}{T_c}\right)^\beta, \tag{4.12}$$

where the top sign is for the liquid and the bottom is for the vapor. The critical exponent β is related to the two critical exponents of the Fisher theory by

$$\beta = \frac{\tau - 2}{\sigma}, \tag{4.13}$$

and is experimentally measured to be 0.3265(3) [PV02; Cam02]. If the constants b_1 and b_β are the same for the two phases, then the parameters can be fit to the vapor densities to predict the liquid densities as

$$\frac{\rho_\ell}{\rho_c} = \frac{\rho_v}{\rho_c} + 2b_\beta\left(1 - \frac{T}{T_c}\right)^\beta. \tag{4.14}$$

It should be noted that this method does not predict the triple point for the system since it does not consider the solid phase. To mock the presence of the triple point, the fit of the vapor densities is in the temperature range $0.65 < T/T_c < 1$.

A fit of Eq. 4.12 to the predicted vapor densities gives $b_1 = 0.6516(10)$, $b_\beta = 1.5754(7)$, and $\beta = 0.25354(14)$. These values can also be predicted by considering the critical scaling of the Fisher theory, as done in Chapter 2, and yields comparable results. The low value of β is a direct consequence of having a large value of σ in Eq. 4.13. Given these fitted values, the reduced temperature-density phase diagram is shown in Fig. 4.10.

The construction of the nuclear phase diagram in absolute units requires the use of Guggenheim scaling. The absolute scale of the cluster concentrations are not known from experiment, which amounts to not being able to predict q_0 in the Fisher theory. This problem is resolved by taking the known value of the nuclear saturation density and scaling the predicted phase diagrams to this value. This procedure can be tested in the present case of the Lennard-Jones system by considering the liquid density at the triple point, $T_0 \simeq 0.694\epsilon$ and $\rho_0 \simeq 0.84\sigma^{-3}$ [MP07]. The critical density is predicted by using Eq. 4.14 to be

$$\rho_c = \rho_0 \frac{1}{2b_\beta}\left(1 - \frac{T_0}{T_c}\right)^{-\beta}, \tag{4.15}$$

presuming the vapor density is negligible. The value of the triple point liquid density leads to predicting a critical density of $\rho_c \simeq 0.319\sigma^{-3}$, and, upon rescaling the pressures, a critical pressure of $p_c \simeq 0.112\epsilon\sigma^{-3}$. These values are significantly more accurate compared to those measured from the Fisher scaling fit parameters.

The reason for the success of this procedure is due to the robustness of the Guggenheim scaling and the accuracy of the Fisher scaling at low temperatures. As an analogy, consider how the critical densities of molecular systems are measured. The direct observation of

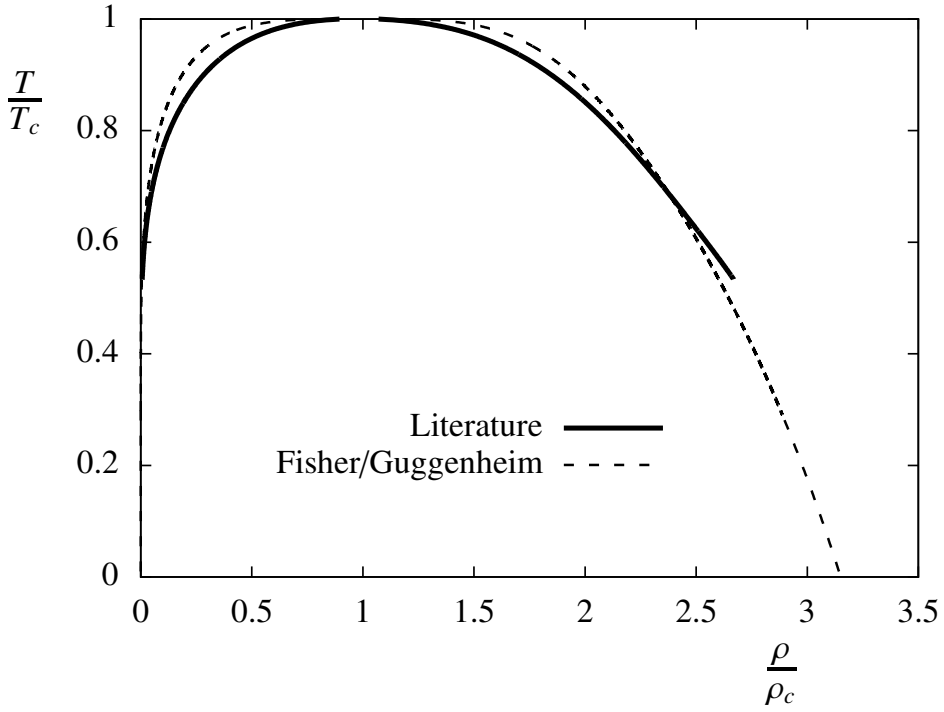

Figure 4.10: The temperature-density phase diagrams of the Lennard-Jones fluid compared to those generated from the fits to the Fisher equation, including the liquid phase determined from Guggenheim scaling.

the critical point is nearly impossible due to the fluctuations of the density near criticality. Instead, the critical temperature is determined and the low temperature behavior of the coexistence is used to extrapolate to the critical point via Guggenheim scaling. In effect, the same is done in this procedure, resulting in a measure of the critical density and pressure within 12% of the literature values.

4.5 Conclusion

The Fisher droplet model offers means of studying phase coexistence via the physical clusters observed in a vapor at coexistence. The observation of Fisher scaling in the cluster concentrations demonstrates the predictive power of the Fisher theory. The precision by which the critical temperature can be extracted from studying the system well removed from the critical point is an important result.

Many assumptions made in the Fisher droplet model are directly tested by considering the physical cluster concentrations. For example, the presumed Arrhenius nature of the concentrations is demonstrated to describe the data to a high precision. Also, the connection

between the cluster entropy and critical temperature is confirmed. The one assumption that appears to be questionable is the assignment of $c_0 A^\sigma$ to the surface energy of a cluster. This one problem explains the discrepancies between the fitted values in the Fisher equation compared to the nominal values.

The phase diagrams are effectively constructed by extrapolating the resulting fit of the Fisher equations. The largest deviations in the predicted phase coexistence are found near the critical point, where both the critical density and pressure are over twice the known values. Guggenheim scaling can be used to predict the behavior of the liquid phase at coexistence and also gives a prediction of the critical point properties within 12% of those in the literature. The considerations reveal the reliability of the reported nuclear phase diagram.

Chapter 5

Concluding Remarks

Current studies of the nuclear phase diagram have shown a new application of cluster theories. This newly found practical use of cluster theories calls for a more thorough study of the accuracy of these models. This thesis addresses this question using a study of the Fisher droplet model and the ideal cluster law and how they are observed in molecular fluids and model systems.

The nuclear system is a specific instance of the general theory of liquid-vapor phase coexistence. If the Fisher droplet model is to be used to construct the nuclear phase diagram, then the theory can also be studied in molecular phase diagrams. In this work I first discussed the Fisher droplet model as an equation of state. This equation of state can be studied in molecular fluids without any direct reference to the clusters themselves. The equation of state is consistent with an extended principle of corresponding states and I showed that the phase diagrams of molecular fluids scale together using the theory. This demonstrates the physical relevancy of the Fisher droplet model.

The role of physical clusters in describing the bulk thermodynamics of a system is also important in the construction of the nuclear phase diagram. I next used computer simulations to directly study the physical clusters of the Lennard-Jones model. The ideal cluster law is confirmed from these simulations through considering both the relation of the clusters to the thermodynamics of the bulk and the physical nature of the clusters themselves. Then, I demonstrate that the cluster concentrations exhibit Fisher scaling. The implication of the Fisher scaling is that the cluster concentrations are directly related to the critical point. Furthermore, I show that the phase diagrams of the Lennard-Jones model are effectively predicted.

The success of the Fisher droplet model to describe and predict the nature of phase coexistence of systems that have previously been studied by more traditional means demonstrate the predictive power of the theory. Experimental observation of Fisher scaling in nuclear collisions thus lead to an accurate prediction of the nuclear phase diagram. The systematic errors found in using this theory are the same order of magnitude as the experimental errors, further supporting the reliability of the reported phase diagram of nuclear matter.

The conclusions are not without their caveats and leave questions unanswered. The errors

generated in constructing the phase diagrams from physical clusters can be separated into two categories. One is the Fisher equation of state and the approximations found therein. An example of an error associated with the Fisher theory is the inconsistent scaling of the molecular phase diagrams at low temperatures. The second is the definition of physical clusters and how they relate to the system's thermodynamics. An example of an error of this type is how the ideal cluster law is not exact and there is no obvious choice for an appropriate cluster algorithm.

Future work will focus on differentiating the errors brought on by these two problems. For example, the surface energy is seen to be improperly defined in the Fisher theory. Is this a result of an incorrect cluster definition or is it an intrinsic property of the system's equation of state? I believe the study of the clusters as independent mathematical entities will shed light on these types of questions.

The work herein further validates the technique of constructing the experimental nuclear phase diagram. At the same time, it demonstrates the predictive nature of cluster theories beyond application to the nuclear system.

Bibliography

[Ban39a] W. Band, "Dissociation treatment of condensing systems", *The Journal of Chemical Physics* **7**, 324–326 (1939).
DOI: 10.1063/1.1750444

[Ban39b] W. Band, "Dissociation treatment of condensing systems, II", *The Journal of Chemical Physics* **7**, 927–931 (1939).
DOI: 10.1063/1.1750346

[Bij38] A. Bijl, "Discontinuities in the energy and specific heat", Ph.D. Thesis, Universiteit Leiden, 1938.

[BR08] B. Borderie and M.F. Rivet, "Nuclear multifragmentation and phase transition for hot nuclei", *Progress in Particle and Nuclear Physics* **61**, 551–601 (2008).
DOI: 10.1016/j.ppnp.2008.01.003

[Bre05] D.E. Breus, "I. Excluded volume effects in Ising cluster distributions and nuclear fragmentation, II. Multiple-chance effects in α-particle evaporation", Ph.D. Thesis, University of California at Berkeley, 2005.

[Cam02] M. Campostrini, A. Pelissetto, P. Rossi, and E. Vicari, "25th-order high temperature expansion results for three-dimensional Ising-like systems on the simple-cubic lattice", *Physical Review E* **65**, 066127 (2002).
DOI: 10.1103/PhysRevE.65.066127

[CK80] A. Coniglio and W. Klein, "Clusters and ising critical droplets: a renormalization group-approach", *Journal of Physics A - Mathematical and General* **13**, 2775–2780 (1980).
DOI: 10.1088/0305-4470/13/8/025

[DR93] C. Dorso and J. Randrup, "Early recognition of clusters in molecular dynamics", *Physics Letters B* **301**, 328–333 (1993).
DOI: 10.1016/0370-2693(93)91158-J

[Ell13] J.B. Elliott, P.T. Lake, L.G. Moretto, and L. Phair, "Determination of the coexistence curve, critical temperature, density, and pressure of bulk nuclear matter from fragment emission data", *Physical Review C* **87**, 054622 (2013).
DOI: 10.1103/PhysRevC.87.054622

[Fis67a] M.E. Fisher, "Theory of condensation and critical point", *Physics-New York* **3**, 255 (1967).

[Fis67b] M.E. Fisher, "Theory of equilibrium critical phenomena", *Reports on Progress in Physics* **30**, 615–730 (1967).
DOI: 10.1088/0034-4885/30/2/306

[Fre39a] J. Frenkel, "A general theory of heterophase fluctuations and pretransition phenomena", *The Journal of Chemical Physics* **7**, 538–547 (1939).
DOI: 10.1063/1.1750484

[Fre39b] J. Frenkel, "Statistical theory of condensation phenomena", *The Journal of Chemical Physics* **7**, 200–201 (1939).
DOI: 10.1063/1.1750413

[GB02] A.E. van Giessen and E.M. Blokhuis, "Determination of curvature corrections to the surface tension of a liquidvapor interface through molecular dynamics simulations", *The Journal of Chemical Physics* **116**, 302–310 (2002).
DOI: 10.1063/1.1423617

[GB09] A.E. van Giessen and E.M. Blokhuis, "Direct determination of the Tolman length from the bulk pressures of liquid drops via molecular dynamics simulations", *Journal of Chemical Physics* **131**, 164705 (2009).
DOI: 10.1063/1.3253685

[GCP09] S. Goriely, N. Chamel, and J.M. Pearson, "Skyrme-Hartree-Fock-Bogoliubov nuclear mass formulas: Crossing the 0.6 MeV accuracy threshold with microscopically deduced pairing", *Physical Review Letters* **102**, 152503 (2009).
DOI: 10.1103/PhysRevLett.102.152503

[Gro97] D.H.E. Gross, "Microcanonical thermodynamics and statistical fragmentation of dissipative systems. The topological structure of the N-body phase space", *Physics Reports* **279**, 119–201 (1997).
DOI: 10.1016/S0370-1573(96)00024-5

[Gug45] E.A. Guggenheim, "The principle of corresponding states", *The Journal of Chemical Physics* **13**, 253–261 (1945).
DOI: 10.1063/1.1724033

[Gug93] E.A. Guggenheim, *Thermodynamics: An Advanced Treatment for Chemists and Physicists*, 4th ed. (North-Holland Pub. Co., Amsterdam, 1993).

[Hil55] T.L. Hill, "Molecular clusters in imperfect gases", *Journal of Chemical Physics* **23**, 617–622 (1955).
DOI: 10.1063/1.1742067

[JZG93] J.K. Johnson, J.A. Zollweg, and K.E. Gubbins, "The Lennard-Jones equation of state revisited", *Molecular Physics* **78**, 591–618 (1993).
DOI: 10.1080/00268979300100411

[Kir08] M.W. Kirson, "Mutual influence of terms in a semi-empirical mass formula", *Nuclear Physics A* **798**, 29–60 (2008).
DOI: 10.1016/j.nuclphysa.2007.10.011

[LMF11] E.W. Lemmon, M.O. McLinden, and D.G. Friend, "Thermophysical Properties of Fluid Systems", in: *NIST Standard Reference Database Number 69*, ed. by P.J. Linstrom and W.G. Mallard, (National Institute of Standards and Technology, Gaithersburg, 2011).

[MP07] E.A. Mastny and J.J. de Pablo, "Melting line of the Lennard-Jones system, infinite size, and full potential", *Journal of Chemical Physics* **127**, 104504 (2007).
DOI: 10.1063/1.2753149

[MM40] J.E. Mayer and M.G. Mayer, *Statistical Mechanics*, (W.H. Freeman, New York, 1940).

[MEP03] L.G. Moretto, J.B. Elliott, and L. Phair, "Resistible effects of Coulomb interaction on nucleus-vapor phase coexistence", *Physical Review C* **68**, 061602 (2003).
DOI: 10.1103/PhysRevC.68.061602

[MEP05] L.G. Moretto, J.B. Elliott, and L. Phair, "Compound nuclear decay and the liquid-vapor phase transition: A physical picture", *Physical Review C* **72**, 064605 (2005).
DOI: 10.1103/PhysRevC.72.064605

[Mor97] L.G. Moretto, R. Ghetti, L. Phair, K. Tso, and G.J. Wozniak, "Reducibility and thermal scaling in nuclear multifragmentation", *Physics Reports* **287**, 249–336 (1997).
DOI: 10.1016/S0370-1573(97)00007-0

[Mor05] L.G. Moretto, K.A. Bugaev, J.B. Elliott, R. Ghetti, J. Helgesson, and L. Phair, "The complement: A solution to liquid drop finite size effects in phase transitions", *Physical Review Letters* **94**, 202701 (2005).
DOI: 10.1103/PhysRevLett.94.202701

[Mor11] L.G. Moretto, J.B. Elliott, L. Phair, and P.T. Lake, "The experimental liquid-vapor phase diagram of bulk nuclear matter", *Journal of Physics G-Nuclear and Particle Physics* **38**, 113101 (2011).
DOI: 10.1088/0954-3899/38/11/113101

[Mor12] L.G. Moretto, P.T. Lake, L. Phair, and J.B. Elliott, "Reexamination and extension of the liquid drop model: Correlation between liquid drop parameters and curvature term", *Physical Review C* **86**, 021303 (2012).
DOI: 10.1103/PhysRevC.86.021303

[MS69] W.D. Myers and W.J. Swiatecki, "Average nuclear properties", *Annals of Physics* **55**, 395–505 (1969).
DOI: 10.1016/0003-4916(69)90202-4

[Nat12] National Institute of Standards and Technology, *Lennard-Jones Fluid Properties*, (2012). URL: `http://www.nist.gov/mml/csd/informatics_research/lj_pure.cfm` (visited on 08/15/2014).

[NF00] M.G. Noro and D. Frenkel, "Extended corresponding-states behavior for particles with variable range attractions", *The Journal of Chemical Physics* **113**, 2941–2944 (2000).
DOI: 10.1063/1.1288684

[Pan87] A.Z. Panagiotopoulos, "Direct determination of phase coexistence properties of fluids by Monte-Carlo simulation in a new ensemble", *Molecular Physics* **61**, 813–826 (1987).
DOI: 10.1080/00268978700101491

[Pan88] A.Z. Panagiotopoulos, N. Quirke, M. Stapleton, and D.J. Tildesley, "Phase equilibria by simulation in the Gibbs ensemble: alternative derivation, generalization and application to mixture and membrane equilibria", *Molecular Physics* **63**, 527–545 (1988).
DOI: 10.1080/00268978800100361

[PV02] A. Pelissetto and E. Vicari, "Critical phenomena and renormalization-group theory", *Physics Reports-Review Section of Physics Letters* **368**, 549–727 (2002).
DOI: 10.1016/S0370-1573(02)00219-3

[Pit39] K.S. Pitzer, "Corresponding states for perfect liquids", *The Journal of Chemical Physics* **7**, 583–590 (1939).
DOI: 10.1063/1.1750496

[Pit55] K.S. Pitzer, D.Z. Lippmann, R.F. Curl, C.M. Huggins, and D.E. Petersen, "The volumetric and thermodynamic properties of fluids. II. Compressibility factor, vapor pressure and entropy of vaporization", *Journal of the American Chemical Society* **77**, 3433–3440 (1955).
DOI: 10.1021/ja01618a002

[PP98] J.J. Potoff and A.Z. Panagiotopoulos, "Critical point and phase behavior of the pure fluid and a Lennard-Jones mixture", *Journal of Chemical Physics* **109**, 10914–10920 (1998).
DOI: 10.1063/1.477787

[RW01] J. Richert and P. Wagner, "Microscopic model approaches to fragmentation of nuclei and phase transitions in nuclear matter", *Physics Reports* **350**, 1–92 (2001).
DOI: 10.1016/S0370-1573(00)00120-4

[RS04] P. Ring and P. Schuck, *The Nuclear Many-Body Problem*, (Springer, Verlag, 2004).

[RW82] J.S. Rowlinson and B. Widom, *Molecular Theory of Capillarity*, (Clarendon Press, Oxford, 1982).

[RG06] G. Royer and C. Gautier, "Coefficients and terms of the liquid drop model and mass formula", *Physical Review C* **73**, 067302 (2006).
DOI: 10.1103/PhysRevC.73.067302

[Sat00] N. Sator, "Lignes de percolation dans un fluide supercritique", Ph.D. Thesis, Université de Paris-Sud U.F.R. Scientifique d'Orsay, 2000.

[Sat03] N. Sator, "Clusters in simple fluids", *Physics Reports-Review Section of Physics Letters* **376**, 1–39 (2003).
DOI: 10.1016/S0370-1573(02)00583-5

[SP90] R.R. Singh and K.S. Pitzer, "Rectilinear diameters and extended corresponding states theory", *The Journal of Chemical Physics* **92**, 3096–3099 (1990).
DOI: 10.1063/1.457908

[Smi92] B. Smit, "Phase diagrams of LennardJones fluids", *The Journal of Chemical Physics* **96**, 8639–8640 (1992).
DOI: 10.1063/1.462271

[Str67] V.M. Strutinsky, "Shell effects in nuclear masses and deformation energies", *Nuclear Physics A* **95**, 420–442 (1967).
DOI: 10.1016/0375-9474(67)90510-6

[SG76] M.F. Sykes and D.S. Gaunt, "Note on mean size of clusters in Ising model", *Journal of Physics A - Mathematical and General* **9**, 2131–2137 (1976).
DOI: 10.1088/0305-4470/9/12/017

[Tol49] R.C. Tolman, "The effect of droplet size on surface tension", *The Journal of Chemical Physics* **17**, 333–337 (1949).
DOI: 10.1063/1.1747247

[Wei35] C.F. von Weizsäcker, "Zur Theorie der Kernmassen", *Zeitschrift für Physik* **96**, 431–458 (1935).
DOI: 10.1007/BF01337700

[Wid63] B. Widom, "Some topics in theory of fluids", *Journal of Chemical Physics* **39**, 2808–2812 (1963).
DOI: 10.1063/1.1734110

[WF98] P.R. ten Wolde and D. Frenkel, "Computer simulation study of gasliquid nucleation in a Lennard-Jones system", *The Journal of Chemical Physics* **109**, 9901–9918 (1998).
DOI: 10.1063/1.477658

[ZM72] J.A. Zollweg and G.W. Mulholland, "On the law of the rectilinear diameter", *The Journal of Chemical Physics* **57**, 1021–1025 (1972).
DOI: 10.1063/1.1678352

Appendix A

List of Fluids in the NIST Chemistry WebBook

Data for the phase coexistence of 73 molecular fluids are reported in [LMF11]. Tab. A.1 is a list of these chemicals. The same symbols are used in every plot pertaining to these fluids, and are listed in Fig. A.1.

Table A.1: List of the 73 chemicals whose phase coexistence data are available in [LMF11]. The ISO designation is a shorthand name for organic refrigerants.

Index	Name	Chemical Equation	ISO designation
1	Water	H_2O	
2	Nitrogen	N_2	
3	Hydrogen	H_2	
4	Parahydrogen	pH_2	
5	Oxygen	O_2	
6	Fluorine	F_2	
7	Carbon monoxide	CO	
8	Carbon dioxide	CO_2	
9	Nitrous oxide	N_2O	
10	Heavy water	D_2O	
11	Methanol	CH_3OH	
12	Methane	CH_4	
13	Ethane	C_2H_6	
14	Ethene	C_2H_4	
15	Propane	C_3H_8	
16	Propene	C_3H_6	
17	Propyne	C_3H_4	
18	Cyclopropane	C_3H_4	
19	Butane	C_4H_{10}	
20	Isobutane	C_4H_{10}	
21	Pentane	C_5H_{12}	
22	2-Methylbutane	C_5H_{12}	
23	2,2-Dimethylpropane	C_5H_{12}	
24	Hexane	C_6H_{14}	
25	2-Methylpentane	C_6H_{14}	
26	Cyclohexane	C_6H_{12}	
27	Heptane	C_7H_{16}	
28	Octane	C_8H_{18}	
29	Nonane	C_9H_{20}	
30	Decane	$C_{10}H_{22}$	
31	Dodecane	$C_{12}H_{26}$	
32	Helium	He	
33	Neon	Ne	
34	Argon	Ar	
35	Krypton	Kr	
36	Xenon	Xe	

Continued on next page

Table A.1 – continued from previous page

Index	Name	Chemical Equation	ISO designation
37	Ammonia	NH_3	
38	Nitrogen trifluoride	NF_3	
39	Trichlorofluoromethane	CCl_3F	R11
40	Dichlorodifluoromethane	CCl_2F_2	R12
41	Chlorotrifluoromethane	$CClF_3$	R13
42	Tetrafluoromethane	CF_4	R14
43	Dichlorofluoromethane	$CHCl_2F$	R21
44	Methane, chlorodifluoro-	$CHClF_2$	R22
45	Trifluoromethane	CHF_3	R23
46	Methane, difluoro-	CH_2F_2	R32
47	Fluoromethane	CH_3F	R41
48	1,1,2-Trichloro-1,2,2-trifluoroethane	$C_2F_3Cl_3$	R113
49	1,2-Dichloro-1,1,2,2-tetrafluoroethane	$C_2F_4Cl_2$	R114
50	Chloropentafluoroethane	C_2F_5Cl	R115
51	Hexafluoroethane	C_2F_6	R116
52	Ethane, 2,2-dichloro-1,1,1-trifluoro-	$C_2HF_3Cl_2$	R123
53	Ethane, 1-chloro-1,2,2,2-tetrafluoro-	C_2HF_4Cl	R124
54	Ethane, pentafluoro-	C_2HF_5	R125
55	Ethane, 1,1,1,2-tetrafluoro-	$C_2H_2F_4$	R134a
56	1,1-Dichloro-1-fluoroethane	$C_2H_3FCl_2$	R141b
57	1-Chloro-1,1-difluoroethane	$C_2H_3F_2Cl$	R142b
58	Ethane, 1,1,1-trifluoro-	$C_2H_3F_3$	R143a
59	Ethane, 1,1-difluoro-	$C_2H_4F_2$	R152a
60	Octafluoropropane	C_3F_8	R218
61	1,1,1,2,3,3,3-Heptafluoropropane	C_3HF_7	R227ea
62	1,1,1,3,3,3-Hexafluoropropane	$C_3H_2F_6$	R236fa
63	1,1,2,2,3-Pentafluoropropane	$C_3H_3F_5$	R245ca
64	1,1,1,3,3-Pentafluoropropane	$C_3H_3F_5$	R245fa
65	Octafluorocyclobutane	C_4F_8	RC318
66	Benzene	C_6H_6	
67	Toluene	C_6H_5OH	
68	Decafluorobutane	C_4F_{10}	
69	Dodecafluoropentane	C_5F_{12}	
70	Sulfur dioxide	SO_2	
71	Hydrogen sulfide	H_2S	
72	Sulfur hexafluoride	SF_6	
73	Carbonyl sulfide	COS	

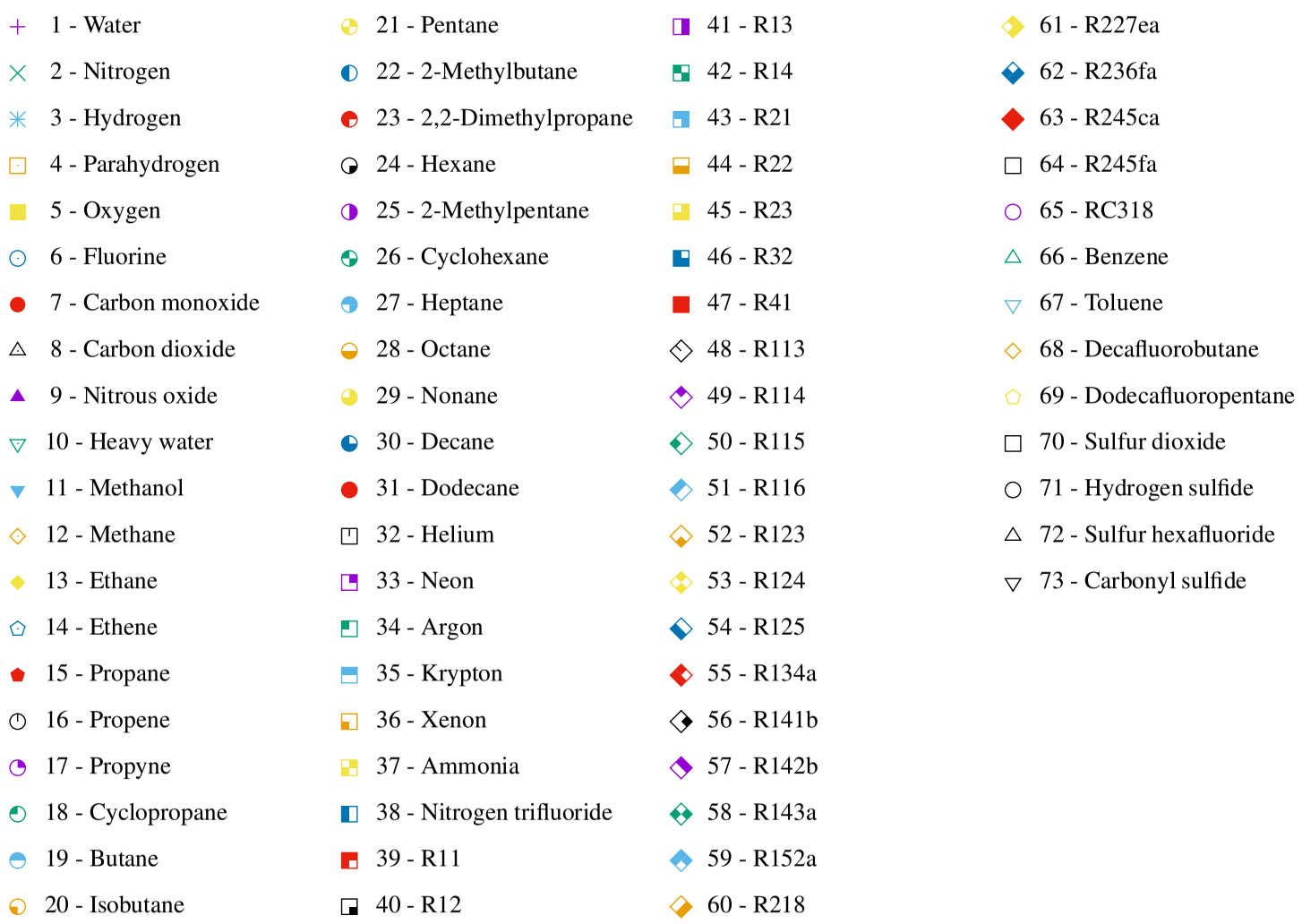

Figure A.1: List of the 73 fluids in the NIST Chemistry WebBook with the corresponding symbol used in the figures of Chapter 2. The numbers are the same as the indices in Tab. A.1.